COAL PYROLYSIS AT HIGH TEMPERATURE*

P. R. Solomon and D. G. Hamblen

Advanced Fuel Research, Inc.
87 Church Street, East Hartford, CT 06108
and
G. J. Goetz and N. Y. Nsakala

Kreisinger Development Laboratory
Combustion Engineering, Inc., Windsor, CT 06095

INTRODUCTION

This paper considers the application of a recently developed pyrolysis model to the high temperature rapid pyrolysis of coal in an entrained flow reactor. The model is based on experiments using a heated grid pyrolysis apparatus, which have helped to establish a relationship between the chemical structure of a coal and its pyrolysis products (1-9). The relationship has been incorporated into a kinetic model of thermal decomposition (1-6) which has the following general features: 1) The time and temperature dependent evolution of the products of thermal decomposition are predicted using a general set of kinetic parameters and a knowledge of the coal's structural composition; 2) the evolution of a species results from the thermal decomposition of a particular structural element within the coal at a kinetic rate which depends on the type of element but which is relatively insensitive to coal rank; 3) much of the needed structural information can be obtained from quantitative Fourier Transform Infrared (FTIR) analysis of the coal and pyrolysis products. The model has proved successful in simulating the results of vacuum thermal decomposition experiments in a heated grid for a variety of bituminous coals and lignites.

The heated grid experiment has advantages over other pyrolysis experiments in achieving good mass and elemental balances and in allowing the primary pyrolysis products to be observed with minimal secondary reactions. It has the distinct disadvantage, however, that the heating of the coal is slower than in practical devices and it is very difficult to measure or estimate the time-temperature history of the coal. While the general concepts of the thermal decomposition model and the relative magnitude of kinetic rates appear to be valid, the exact kinetic rates especially at high temperatures are uncertain. To improve the kinetic data, other experiments are needed. In one approach which has recently been reported, coal is dropped into a hot furnace and the evolving gases are monitored in-situ with a FTIR (10). This experiment verified the general features of the model but yielded higher kinetic rates. The experiment could only follow events on a time scale longer than a few hundred milliseconds due to the limit imposed by the FTIR scanning rate. Data was presented for temperatures between 500° and 800° C.

In the present investigation, results are extended to temperatures up to 1470° C and higher rates using pyrolysis experiments performed in an entrained flow reactor at Combustion Engineering. In this experiment coal is injected into a hot gas stream and after a variable residence time of 0 to 450 milliseconds, the reaction is quenched. The pyrolysis gas compositions were determined and the chars were analyzed by FTIR, elemental analysis and optical microscopy to determine the changes in char chemistry and physical appearance. The time-temperature histories of the solid particles have been calculated to provide input to the pyrolysis model. The pyrolysis model was successful in simulating the reactor data after adjustment to the kinetic rates at high temperatures.

EXPERIMENTAL

Combustion Engineering's Drop Tube Furnace System (DTFS) is similar in design to the reactors described by Nsakala et. al. (11) and Badzioch and Hawksley (12). The DTFS (Fig. 1) is comprised of a 2.54 cm inner diameter preheater, a 5.08 cm inner diameter test furnace, a fuel feeding system, and a gas analysis system. Both furnaces are powered with silicon carbide (SiC) heating elements.

The conditions of this particular experiment were as follows follows: 1) A 200 x 400 mesh size fraction of Pittsburgh seam coal was introduced by screw feeding through a water-cooled probe into the test furnace reaction zone; 2) The primary stream (comprised of the fuel fed at a rate of 1 gram/min and 15% CO_2/85% N_2 carrier gas fed at 2 liters/min) was allowed to mix rapidly with a preheated down-flowing secondary gas (15% CO_2/85% N_2) stream (fed at 28 liters/min); 3) After a variable distance (zero to 40.6 cm) the pyrolysis products were aspirated in a water-cooled probe to quench all the reactions; 4) The solids were separated from gaseous products in a small cyclone; 5) A portion of the gas sample was analyzed on-line to determine NO_x, O_2, CO, CO_2 and SO_2 concentrations; and 6) Solid samples were analyzed by FTIR, ultimate analysis and optical microscopy. Experiments were performed with furnace wall temperatures of 1370 and 1470°C. Free fall velocities of particles in these experiments were small compared with gas velocities; hence it was assumed that the particles traveled at the same velocities as the gas. Maximum residence times in the reaction zone varied from 0.342 to 0.453 sec for the higher and lower temperature, respectively.

PYROLYSIS RESULTS

The physical and chemical changes occurring during pyrolysis are characterized by the data illustrated in Figs. 2, 3, 5 and 6. Figure 2 follows the infrared spectra of solid samples collected at various positions in the reactor. The techniques for preparing and analyzing the FTIR spectra have been presented previously (2). The figure presents the absorbance from 1 mg of sample in a KBr pellet or 1 mg/1.33 cm^2. The data are for a wall temperature of 1370°C. The results indicate that no changes occur for the first 5 cm in the reactor. Between 5 and 10 cm the absorbance in the aliphatic stretch region at 2900 cm^{-1} decreases, indicating a decreasing concentration of aliphatic C-H bonds which goes to zero at 20 cm. The behavior of the aromatic stretch region at 3050 cm^{-1} indicates that the aromatic C-H concentration starts to decrease between 10 and 20 cm. The behavior of the region near 1200 cm^{-1} indicates that the density of O-C bonds is not decreased during the initial stage of pyrolysis. The FTIR spectra for the 1470°C wall temperature are similar except that the aliphatic C-H concentration goes to zero at 10 cm and the aromatic C-H concentration at 10 cm is about the same as it is for 20 cm in the lower temperature run.

The samples were examined optically to determine physical change occurring during pyrolysis. In agreement with the FTIR results, little happens to the samples collected at 5 cm or less. At 10 cm however, the particles are observed to have become substantially swollen. By 20 cm they are well formed structures which look like foamy soap bubbles. The wall thickness in these bubbles appears to be about 1 micron. At 30 and 40 cm the bubbles appear to be more opaque and have shrunk slightly. Results for the 1370°C run showing samples collected at zero and 20 cm are presented in Fig. 3. The long dimension of the photomicrograph is 1.9 mm. The swelling increases the diameter by a factor of about 4.

CALCULATION OF TIME-TEMPERATURE HISTORIES

Calculations were made of the following quantities: 1) the average gas temperatures in the preheater, the experimental section and the collection probe; 2) the radially dependent gas temperature in the experimental section; 3) the coal particle temperatures and 4) the temperature of a thermocouple at positions along the reactor

center line. The calculations include a model for the particle swelling which is found to produce a rapid temperature rise because of the increase in surface area for absorbing radiation.

To determine both radial and longitudinal temperature profiles, calculations were performed numerically on a PDP/11 computer by considering tubular shells at progressive cross sections of the flow path. The radial gas temperatures are calculated for the primary gas core, and for n concentric rings of gas. The total calculation proceeds as follows: starting at the inlet, with the particle temperature set equal to the primary gas temperature, n-1 concentric gas rings set equal to the secondary gas temperature, and the outer ring fixed at the wall temperature, a system of differential equations are integrated using a Runga-Kutta integration scheme to determine the temperature of each element at the next time increment. (Note-The differential equations include: a) radiative heat transfer between the coal particles and the wall including the effects of the cold injector and collector; b) convective heat transfer between the coal and the core gas c) conductive heat transfer within the gas; and d) the heat capacities of the coal and gas). Using these new temperatures, an average temperature for the gas is calculated (the temperature after complete mixing), and this average temperature is used to calculate an average velocity, which in turn is used to calculate the axial position of the particles and the gas. The results of the calculations were compared with standard predictions for heat transfer in a pipe (13) and it was found that under the particular conditions of the experiment the additional heat transfer due to convection and turbulence (even in the collection tube) could be neglected. The general conclusion from these calculations is that the particle temperature is dominated by radiation from the hot furnace walls. The particles heat rapidly and achieve temperatures close to the wall temperatures. The local gas around the particles (e.g. the primary gas stream) is heated by conduction from the particles but the secondary gas stream is not well coupled to the particles. For this reason mixing effects appeared to be of minor importance for calculating particle temperatures in the reactor section.

The results of the calculation for the collection probe at 5 and 10 cm are shown in Fig. 4. For the 5 cm case the particle temperature rises rapidly, driven by radiative heating. The primary gas temperature also rises rapidly (much faster than in the absence of the coal) due to heat transfer from the coal. The average gas temperature is dominated by the secondary gas which is not well coupled to the coal particles and thus heats as in the case for no coal. The temperature for the coal and the gas is assumed to fall in the smaller diameter collection probe at a uniform temperature due to turbulent mixing. To cool below reaction temperatures takes about 20 milliseconds.

The particle volume is assumed to increase with the volume of evolved gases until it has reached four times its original diameter, which appeared to be the experimentally observed limit. According to the prediction at the 5 cm collection point the particle diameter starts to change slightly for the higher wall temperature experiment but not for the lower wall temperature. The volatile yield corresponding to this change would be less than 1%. These results are in agreement with the chemical and FTIR measurements of the samples for 5 cm and less which show no measurable change from the raw coal and with the visual observation of the 5 cm sample which shows some slight particle swelling for small particles in the high temperature wall case.

By 10 cm the coal for both wall temperatures has come to within 100 kelvins of the wall temperature. The coal temperature exceeds the average gas temperature because of the better radiation coupling to the wall. The particle swelling is complete for both wall temperatures in agreement with the visual observation of the samples for 10 cm and greater.

PYROLYSIS MODEL

The pyrolysis model assumes a coal structure consisting of highly substituted
aromatic ring clusters containing heteroatoms linked by relatively weak aliphatic
bridges. Evidence suggests that during thermal decomposition these weak links
break, releasing the clusters and attached bridge fragment which comprise the tar.
Simultaneous with the evolution of tar molecules is the competitive cracking of
bridge fragments, substituted groups and ring clusters to form the light molecular
species of the gas. The quantity of each gas species depends on the functional
group distribution in the original coal. At low temperatures there is very little
rearrangement of the aromatic ring structure. There is, however, decomposition of
the substituted groups and aliphatic (or hydroaromatic) structures resulting in CO_2
release from the carboxyl, H_2O from hydroxyl, hydrocarbon gases from aliphatics, H_2S
from mercaptans and some HCN and CO from weakly bound nitrogen and oxygen groups.
At high temperature there is breaking and rearrangement of the aromatic rings. In
this process, H_2 is released from the aromatic hydrogen, CS_2 from the thiophenes,
HCN from ring nitrogen and additional CO from tightly bound ether linkages. As this
process continues the char becomes more graphitic.

A striking feature of thermal decomposition which was observed for a variety of
coals is that the temperature dependent evolution rate of a particular species is
similar for all coals. This is true even though the amount of the species may vary
substantially from one coal to another. These rates characterize the thermal
decomposition of the various functional groups. They depend on the nature of the
functional group but appear insensitive to coal rank. The differences between coals
may be attributed to differences in the mix of functional groups.

The mathematical description of the pyrolysis model has been presented previously
(1-6). The evolution of tar and light species provide two different mechanisms for
removal of a functional group from the coal; evolution as a part of a tar molecule
and evolution as a distinct species with cracking of the molecule. To model these
two paths with one path yielding a product which is similar in composition to the
parent coal, the coal is represented as a rectangular area with X and Y dimensions.
The Y dimension is divided into fractions according to the chemical composition of
the coal. $Y^°_i$ represents the initial fraction of a particular component (carboxyl,
aromatic hydrogen, etc) and $\sum Y^°_i = 1$. The evolution of each component into the gas
(carboxyl into CO_2, aromatic hydrogen into H_2, etc) is represented by the first
order diminishing of the Y_i dimension, $Y_i = Y^°_i \exp(-k_i t)$. The X dimension is divided
into a potential tar forming fraction $X^°$ and a non-tar forming fraction $1-X^°$ with
the evolution of the tar being represented by the first order diminishing of the X
dimension $X = X^° \exp(-k_t t)$. The amount of a particular component in the char is
$(1-X^°+X)Y_i$ and the amounts in the gas and tar may be obtained by integration.
In the heated grid experiment the products cool upon evolution so they undergo no
further reactions. In the present experiment, the evolved products continue to
react. Under these conditions it has been assumed that the decomposition of a
component occurs at the same rate in the evolved product as it does in the char.

The coal compositional parameters for the Pittsburgh seam coal and the kinetic rates
used in the simulation are presented in Table I. Most of the composition parameters
have been obtained from elemental and FTIR analysis. The carboxyl, CO-loose and
N-loose have been estimated from the parameters of a previously run Pittsburgh seam
coal (5) by assuming that these components represented the same fraction of the
oxygen and nitrogen in both coals. The split of the N and CO into loose and tight
groups conforms to the experimental observation that these components have at least
two distinct evolution rates which presumably indicate distinct chemical species.
The tar was estimated from the previously measured coal, but decreased by 30% to

account for the decrease in going from vacuum to 1 atmosphere (see Ref. 9). The kinetic rates have been modified from those most recently presented (5). 1) The H_2 and CO-tight rates have been increased at high temperature to match the new experimental data. 2) The rates for the other species appeared to be adequate at high temperature. However, the recent experiments by Freihaut et al (10) suggest that they are low in the range 500-800°C. The rates of Table I are a compromise between these observations and the heated grid data. 3) The rates have also been simplified by using the same rate for tar, N-loose, CO-loose, carboxyl and hydroxyl instead of 5 slightly different rates.

RESULTS

The theory and experiment are compared in Figs. 5 and 6 for the two temperatures (1370°C and 1470°C) which were measured. Fig. 5a and 5b illustrate the char composition. The model predicts that little happens for the first 5 cm for both temperatures. At 10 cm and longer there are substantial changes especially in the hydrogen and oxygen. The model predicts a rapid decrease in the aliphatic hydrogen followed by a slower decrease in the aromatic hydrogen. This behavior is confirmed by the FTIR spectra. The model prediction for oxygen indicates an initial rapid evolution of CO_2, H_2O and CO-loose and a slower evolution of CO-tight from ether groups. The FTIR spectra (Fig. 2) show a rapid decrease in the OH concentration indicated by the decrease in the broad peak between 3600 and 2200 cm^{-1} and the sharp peak at 1600 cm^{-1} which is attributed to an aromatic ring stretch enhanced by attached hydroxyl groups (2). (Note- The decrease in the broad band is confused by the persistence of a narrower KBr-H_2O peak at 3400 cm^{-1}. This occurs because much less sample is used for the high carbon content chars so that scaling the spectra to 1 mg/1.33 cm^2 enhances the contribution from the KBr.) As the char oxygen decreases, the CO concentration increases in agreement with the data in Figs. 5c, and 5d. Predictions for CO_2 and H_2O produced in pyrolysis are also presented. These predictions do not inclue secondary gas-char reactions.

Figures 6a and 6b show predictions for four additional evolved species. The stable products from the evolution of the hydrocarbons are H_2 and soot. This was observed in the heated grid experiments (3,5). The methane and acetylene are predicted to be short lived due to thermal cracking to soot and hydrogen.

Figures 6c and 6d show the overall product distribution. The experimental points are obtained using the ash tracer method (14). Unfortunately, soot may be included in varying amounts with the char. This would tend to underestimate the char concentration by a varying amount.

CONCLUSION

A pyrolysis model which was developed to simulate coal pyrolysis in a heated grid appears to be successful in simulating the high temperature pyrolysis of coal in an entrained flow reactor. The model relates evolved products to the coal structure. The structure parameters for the coal were input on the basis of the parameters obtained for a similar coal in the heated grid. No adjustments of these structure parameters were made in making the simulation. The kinetic parameters were modifications of the parameters derived from the heated grid experiments. Major changes were made in the aromatic hydrogen and CO-tight rates at high temperatures. The exponential and preexponential factors for these two components were adjusted to increase the rate in the range 1370-1470°C but hold its value close to the original rates at lower temperature so that a fit is still obtained for the heated grid data.

The rates for aliphatics, tar, hydroxyl, CO-loose, N-loose and carboxyl received minor adjustments and so still fit the heated grid data.

The rates with the greatest uncertainty are those for olefin, acetylene and soot for which there is no data from the present experiment. The soot rate (the rate for

10

conversion of aliphatic to soot) is the highest rate in the simulation. It dominates the initial fast change in the coal. Additional experimental work is needed to sort out the effects of the aliphatic evolution and subsequent cracking to olefins, acetylene and soot.

ACKNOWLEDGEMENT

<div align="center">REFERENCES</div>

1. Solomon, P. R. and Colket, M. B., Fuel, 57, 749, (1978),.

2. Solomon, P. R., ACS Div. of Fuel Chemistry, Preprints, 24, #2, 184 and Advances in Chemistry, to be published, (1979),.

3. Solomon, P. R., ACS Div. of Fuel Chemistry Preprints, 24, #3, 154, (1979a),.

4. Solomon, P. R. and Colket, M. B., 17th Symposium (International) on Combustion, P. 131, the Combustion Institute, Pittsburgh, PA, (1979).

5. Solomon, P. R. and Hamblen, D. G., Understanding Coal Using Thermal Decomposition and Fourier Transform Infrared Spectroscopy, Presented at the Conference on the Chemistry and Physics of Coal Utilization, Morgantown, West Virginia, June 2-4, (1980) .

6. Solomon, P. R., Fuel, 60, 3, (1981),.

7. Suuberg, E. M. et al, Ind. Eng. Chem. Process Design Develop. 17,37, (1978),.

8. Suuberg, E. M., Peters, W. A. and Howard, J. B., Seventeenth Symposium (International) on Combustion, p. 117, The Combustion Institute, Pittsburgh, PA, (1979).

9. Suuberg, E. M., Peters, W. A. and Howard, J. B., Am. Chem. Soc. Dir. Petrol. Chem. Preprints, 23, (1), 175, (1977).

10. Freihaut, J. D., Solomon, P. R. and Seery, D. J., ACS, Division of Fuel Chemistry Preprints, 25, Sept., (1980).

11. Nsakala, N.-Y., Essenhigh, R. H. and Walker, P. L., Jr., Combustion Sci. Technol., 16, 153, (1977).

12. Badzioch, S. and Hawksley, P. G., W. Ind. Eng. Chem. Process Des. Dev., 9, 521, (1970).

13. Heat Transfer, Alan J. Chapman, Macmillan Publish. Co., (1980).

14. Kobayashi, H., Howard, J. B. and Sarofim, A. F., Sixteenth Symposium (International) on Combustion, The Combustion Institute, Pittsburgh, PA, 411, (1971).

TABLE I

Kinetic Rates and
Functional Group Composition for a Pittsburgh Seam Bituminous

| Composition Parameter (dmmf)	Pittsburgh Seam Bituminous	Kinetic Rates		
C	.853			
H	.057			
N	.017			
S(organic)	.021			
O	.052			
S(mineral)	.014*			
CO_2 – Carboxyl	.006	$k_1 = 5400$		exp $(-8850/T)$
H_2O – 9/17 Hydroxyl	.010	$k_2 = 5400$		exp $(-8550/T)$
CO – Ether Loose	.006	$k_3 = 5400$		exp $(-8850/T)$
CO – Ether Tight	.062	$K_4 = 2.15 \times 10^{16}$		exp $(-57000/T)$
N – Nitrogen Loose	.003	$k_5 = 5400$		exp $(-8850/T)$
N – Nitrogen Tight	.014	$k_6 = 290$		exp $(-13000/T)$
$CH_{1.8}$ – Aliphatic	.276	$k_7 = 19000$		exp $(-11000/T)$
H – Aromatic H	.020	$K_8 = 40644$		exp $(-14085/T)$
C – Non Volatile	.582	$K_9 = 0$		
S – Organic	.021			
Total	1.000			
Tar	.30	$K_t = 5400$		exp $(-8850/T)$
Olefins		$K_o = 2 \times 10^9$		exp $(-24000/T)$
Acetylene		$K_a = 1 \times 10^{16}$		exp $(-50000/T)$
Soot		$K_s = 4 \times 10^{19}$		exp $(-60000/T)$

*Dry

12
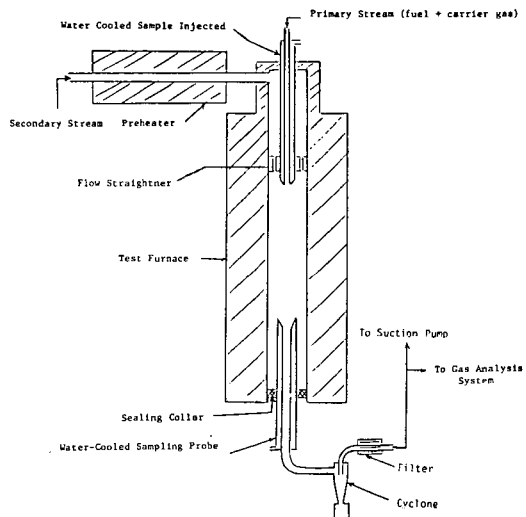
FIGURE 1   SCHEMATIC OF THE COMBUSTION ENGINEERING DROP TUBE FURNACE SYSTEM.
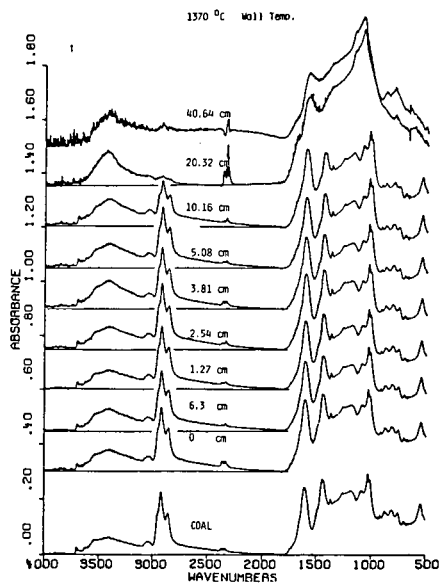
FIGURE 2.   INFRARED SPECTRA OF CHARS COLLECTED IN THE DTFS

13

a), Char Samples at 0 cm.

|←————— 1 mm —————→|
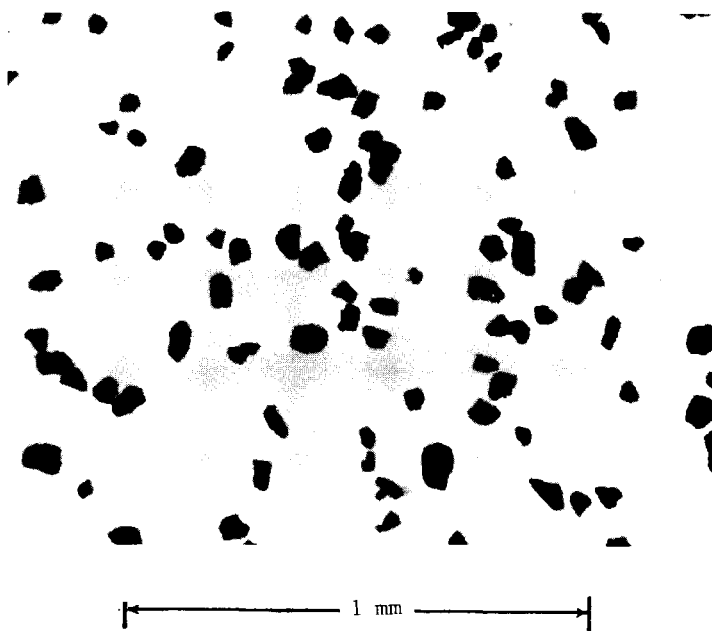
b), Char Samples at 20 cm.
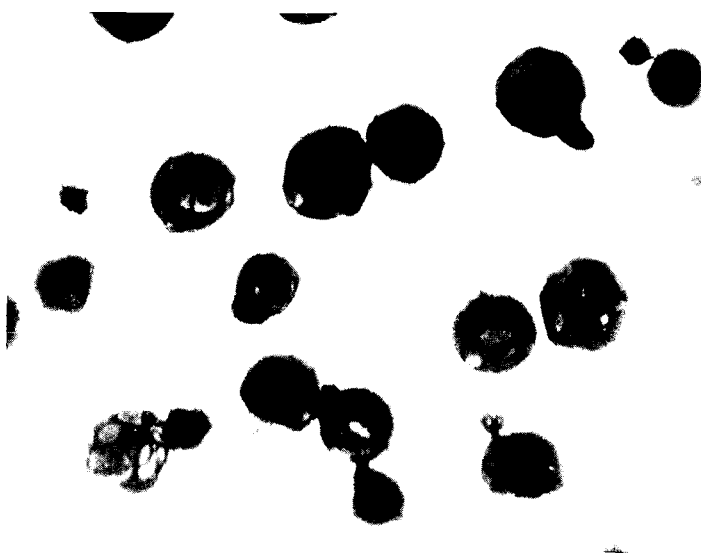
FIGURE 3. PHOTOMICROGRAPHS OF CHAR SAMPLES FROM THE DTFS
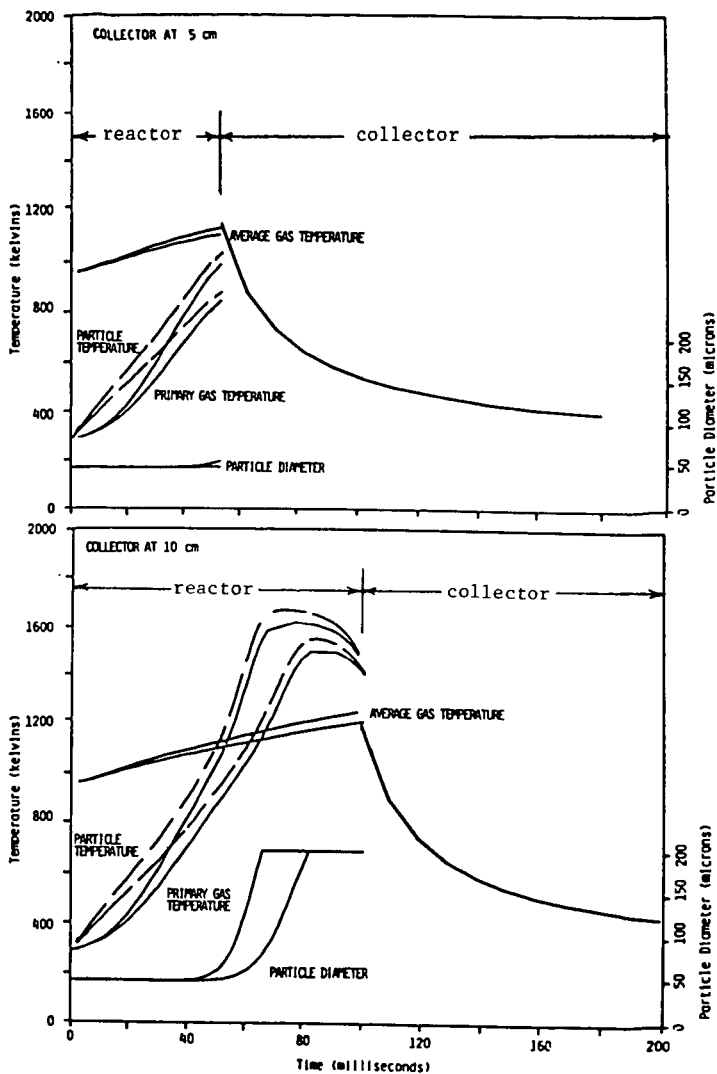
FIGURE 4.

TIME HISTORY OF TEMPERATURE AND PARTICLE DIAMETERS IN THE DTFS. Dashed lines are particle temperatures. Solid lines are the primary gas temperatures, average gas temperatures and particle diameter. A pair of curves is presented for each property. The upper curve is for a 1744 K wall temperature and the lower curve is for 1644 K.

15

FIGURE 5. PYROLYSIS PRODUCT DISTRIBUTION. Lines are predictions, symbols are experimental data. In a and b the char composition is normalized by the composition of the parent coal.

16

1744K

1644K

FIGURE 6. PYROLYSIS PRODUCT DISTRIBUTION. Lines are predictions, symbols are experimental data. In c and d the symbols are for 100% - % char to correspond to the upper line.
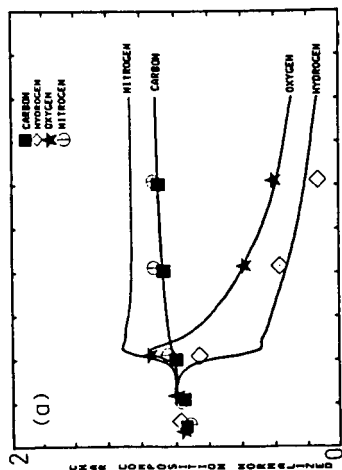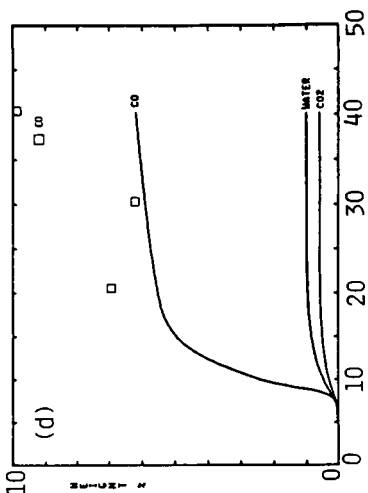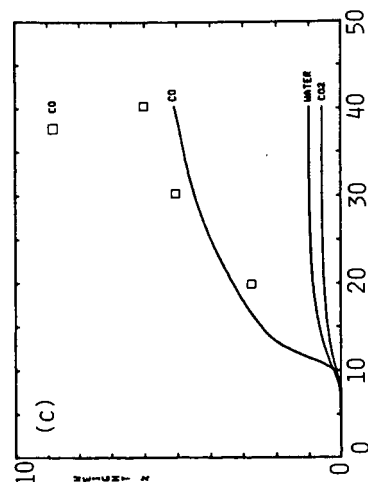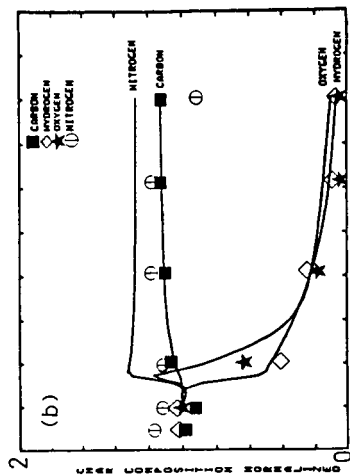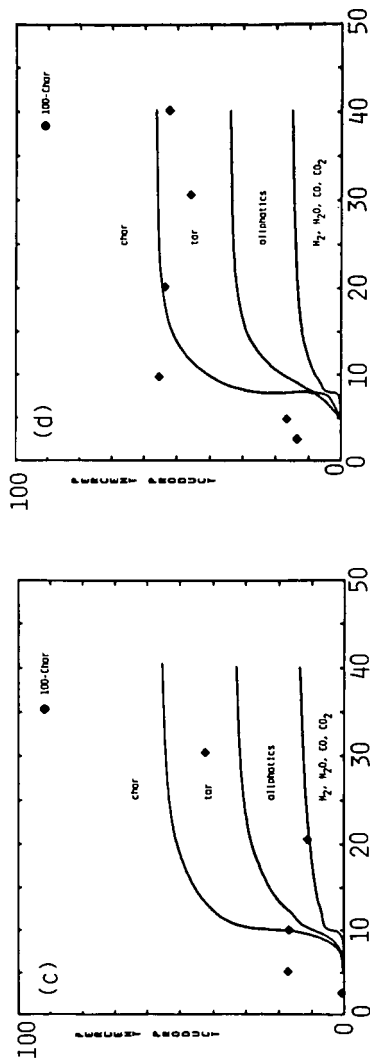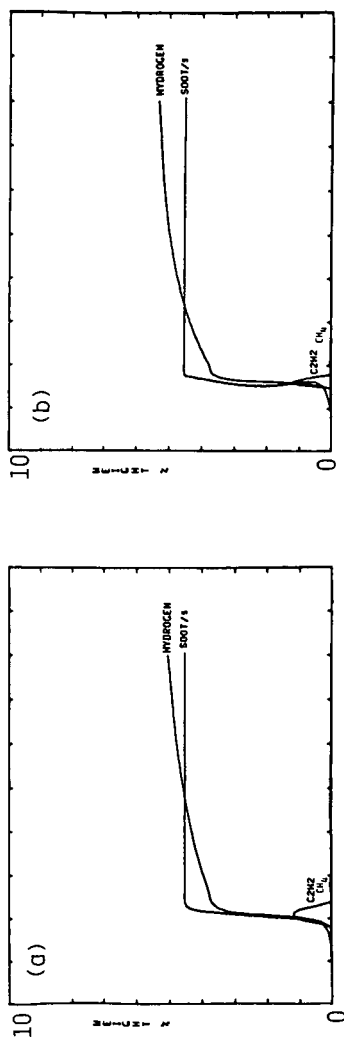
Distance into Reactor (cm)

EVOLUTION OF FUEL NITROGEN DURING
THE VACUUM THERMAL DEVOLATILIZATION OF COAL

J. D. Freihaut and D. J. Seery

United Technologies Research Center
East Hartford, CT   06108

Introduction

The fate of fuel nitrogen during the combustion or gasification of coal is a matter of practical and fundamental concern. During coal combustion, NO_x is known to form via HCN species released from the nitrogen-containing molecular components of the coal. During gasification processes, the release of nitrogen-containing fused ring compounds in evolved tar species is a matter of environmental concern. Since the thermal decomposition of the parent coal is an initial phase in both com-bustion and gasification, it is necessary to develop a knowledge of the fate of fuel nitrogen during thermal decomposition.

This study contains results of an investigation of the evolution of fuel nitrogen during the vacuum thermal decomposition of coal. Results are shown for variations with coal characteristics and apparent thermal history. Apparent heating rates of 75 C/sec to 2000 C/sec and final temperatures of 500 C to 1780 C were utilized. A variety of coals were investigated ranging in rank from a lignite to an anthracite.

The results indicate that nitrogen distribution in the volatiles is a sensitive function of the chemical characteristics of the parent coal. This distribution of nitrogen in the light gas, tar and char products of vacuum devolatilized coal is highly dependent on rank of the parent coal. Variations in nitrogen evolution with coal characteristics are most readily apparent in several aspects: (1) the coal nitrogen released with the tar species; (2) the release of nitrogen contained in primary tars as HCN upon secondary thermal decomposition reactions of the primary tars; (3) the retention of nitrogen in the char species.

Experimental Design

Figure 1 represents schematically the apparatus employed to perform the thermal decomposition experiments. The procedure involves placing small samples (20-50 mg) of finely ground coal (-100+325 mesh) between the folds of a fine mesh screen.

18

Stainless steel is used for final temperatures between 500 C and 1000 C. Tungsten
is used for temperatures between 1000 C and 1780 C. The grid is driven to a pre-
determined temperature via the preset control circuitry. The apparent heating rate
is monitored by a thermocouple bead placed between the folds of the screen.

Light gases are immediately vented through a glass wool filter into a 61 cm
long infrared cell in a Fourier Transform Infrared Spectrometer. The cell was cal-
ibrated for mixtures of HCN (200, 100, 50 and 25 ppm) diluted in N_2 to a total
pressure of 400 torr to avoid the uncertainties of pressure broadening by mixtures.
At the end of a devolatilization run the cell and reactor chamber are filled with
nitrogen to give a total pressure of 400 torr and simulate the calibration.

The control circuit in this investigation operated a Harrison power supply
Model 6269A in the current program mode. In this mode heating rate and final
temperature are coupled over the entire final temperature range. The coupling
between heating rate and final temperature for the two screen materials can be de-
scribed by a simple equation of the form log $(\dot{T})$=m T + B, where the parameters for
each screen are given in Table I. The coupling between heating rate and final
temperature is logarithmic in a manner analogous to Newton's law of heating/cooling.
For the stainless steel screen the final temperature of 530 C is associated with a
heating rate of ~ 100 C/sec while a final temperature of 1000 C is associated with
a heating rate of 600 C/sec. The maximum heating rate obtained for the tungsten
screen was ~ 2000 C/sec for a final temperature of 1780 C.

Chemical Structure Characteristics of the Coals

The coals examined in this investigation are the same as those previously
reported in an investigation of tar yields and characteristics obtained from the
devolatilization of the coal.[1] Detailed elemental analyses for the coals are given
in Table II. Figure 2 represents the location of the coals on the coalification
band as revealed by H/C and O/C values. The position of the Western bituminous
coals relative to the Eastern bituminous coals reflects the differences in rank and,
indirectly, geologic sources. This figure also reveals the maximum tar yields
obtained from these coals. These yields are important characteristics of the
devolatilization behavior of a coal as is the variation in tar yield with apparent
thermal drive.[1]

Figure 3 illustrates the infrared structural characteristics of the coals.
Variations in infrared structural characteristics of a coal with its elemental

19

composition (position on the coalification band) have been previously discussed.[2,3,4,5] The relationship of the tar yields and temperature sensitivity of tar yields to infrared structural characteristics of the parent coal has also been previously discussed.[1] Proceeding from the low rank side of the coalification band to the high rank side there is an apparent maximum in aliphatic hydrogen absorption ($\sim$ 3000 – 2750 cm^{-1}) around the location of the Utah bituminous coal (H/C = 0.85, O/C = 0.13). Such an apparent maximum is indirectly observed in the spectra of Fig. 3, normalized with respect to 1 mg of coal in a KBr pellet. It is more directly observable in plots of integrated absorbance versus sample size for each of the coals. The slopes of such plots give apparent extinction of coefficients for each coal. The aliphatic extinction coefficient for the Utah coal is about 24% greater than that of the Pittsburgh seam bituminous coal. Its total hydrogen content is only about 3% greater. The greater apparent aliphatic hydrogen in the Utah bituminous coal reflects not only a difference in the amount of hydrogen present as aliphatic hydrogen, but also the nature and distribution of the molecular species to which the aliphatic hydrogen functional groups are attached.[6]

In proceeding through the coalification band it is also noted that the resolution of the aromatic hydrogen peaks ($\sim$ 3040 cm^{-1}, 680-920 cm^{-1}) increases with rank. This increase in resolution is reflected in the apparent aromatic hydrogen absorption coefficients of the coals. The integrated area absorption coefficients for aromatic hydrogen generally increase with rank for these coals. If the strength of the bands associated with aromatic hydrogen absorption is an indication of the aromaticity of the coal, then the spectra of these coals indicate a consistent increase in aromaticity with rank as reflected by the position on the coalification band diagram (Fig. 2).

These structural considerations are important because they lead to general understanding of the relationship between chemical structural characteristics of a coal and its primary devolatilization behavior. A previous report demonstrated that the influence of chemical structure on devolatilization for subbituminous and bituminous coals is most clearly reflected in the primary (vacuum, disperse phase, small particle size) tar yields and tar characteristics.[1] This report demonstrates that the nitrogen distribution in the primary volatiles and char residual can also be related to structural characteristics of the parent coal.

20

Nitrogen Distribution in the Devolatilization Products
Coal Nitrogen in the Char, Tar, Light Gas Species

Typical mass fraction distributions of the coal nitrogen in the devolatiliza-
tion products are listed in Table III. Typical distributions are illustrated in
Figs. 4-7. The data indicates that little (< 5%) of the coal nitrogen is evolved as
HCN in those runs characterized by final temperatures of 700 C and below. In the
500 C to 700 C final temperature runs, most of the volatile nitrogen is in the tar
species. As the thermal drive is increased (final temperatures ~ 700 C to ~ 950 C)
HCN becomes a greater component in the volatiles nitrogen. The temperature de-
pendence of the HCN evolution in this temperature range is coal dependent. The
subbituminous and Western bituminous coals, for example, give sharper increases in
HCN evolution with respect to final temperature than the Pittsburgh bituminous or
Alabama bituminous.

For all of the samples examined except the anrthracite, more of the coal nitro-
gen is evolved as an element of the tar species than as HCN in the < 1000 C runs.
In the range of conditions, the retention of coal nitrogen in the char residue is
similar for the subbituminous and Western bituminous coals. The fraction of coal
nitrogen retained in the char is approximately the same for the same final temper-
ature. The temperature dependent nitrogen retention in the chars of the Eastern
bitiminous coals (high volatile A Pittsburgh seam, Alabama medium volatile) is
appreciably different than those of the subbituminous and Western bituminous coals.
The chars of the Pittsburgh seam show less nitrogen variations with final temper-
ture. The medium volatile bituminous chars show nitrogen variation with temperature
similar to that of the Western bituminous but at higher levels of mass fraction
retention.

Mass Fractions of Coal Nitrogen in Tar

All of the coals show substantial increases in nitrogen evolved as HCN for final
temperatures above 950 C. A portion of this increase is the result of secondary
cracking reactions of primary tar vapors under the conditions of increased thermal
drive. As noted above, a previous study[1] on tar yields revealed that tar yields
can be substantially modified by increasing the heating rate of the coal. Reduction
in the tar yields by an increase in thermal drive results in a corresponding reduc-
tion in the coal nitrogen evolved in the tar. Cracking of the nitrogen – containing
tar species results in the evolution of the nitrogen as HCN. The relationship
between the coal nitrogen and the evolved tar species is illustrated in Figs. 8-10.

21

Figure 8 shows the fractions of Utah bituminous coal mass and coal nitrogen evolved as tar and as an element of the tar species for various final temperatures. Figure 9 shows plots of the mass fraction of coal evolved at tar versus the mass fraction of coal nitrogen evolved as tar, irrespective of thermal drive conditions. As the tar species are reduced by increasing the thermal drive, nitrogen is released as HCN from the tar cracking process.

Mass Fractions as CHAR

Figures 10 and 11 plot the mass fraction of the coal evolved as char versus the mass fraction of the coal nitrogen evolved as char nitrogen. As with the tar plots, upon elemination of the thermal history parameter, there is an obvious similarity in the nitrogen evolution of the subbituminous and bituminous coals. The plots indicate that the main phase of the devolatilization process is characterized by nitrogen retention in the char in proportion to the fraction of coal mass evolved as char. At mass fractions of char greater than - 0.5 (characterized by runs of 950 C final temperature and less) all of the chars lost retained nitrogen at a rate much greater than additional mass loss.

Phenomenological Description of Nitrogen Evolution

A phenomenological description of the evolution of coal nitrogen during vacuum devolatilization emerges from the investigation. For final temperatures of 950 C and less and apparent heating rates of 600 C/sec and less, the tar and char species generally contain 0.7 or more of the coal nitrogen. In this range of conditions, tar removes coal nitrogen in proportion to the mass fraction of coal evolved as tar. Char retains nitrogen in proportion to the mass fraction of coal evolved as char. The balance of the coal nitrogen evolves predominantly as HCN. Small but observable amounts of NH_3 are produced at low final temperatures. More NH_3 appears to be formed from low rank coals.

The distribution of the coal nitrogen in the tar, char or light gases produced during devolatilization is dependent on the rank of the parent coal in a manner analogous to the distribution of coal mass as tar, char or light gases. An increase in the fraction of volatiles evolved as tar with increase in rank results in a proportionate increase in nitrogen evolution as an element of the tar species. A decrease in tar yield with increase in thermal drive, results in a proportionate decrease in coal nitrogen evolved as tar. As the tar yield decreases, the tar nitrogen is evolved as HCN. Higher rank coals appear to produce tars more thermally stable than lower rank coals (See Reference 1).

22

For final temperatures greater than 950 C and heating rates in excess of 600 C/sec, Western bituminous and subbituminous coals display tar yield reductions as great as 50-60% of the maximum tar yield. The coal nitrogen evolved as tar is proportionately reduced. At volatile yields greater than ~ 0.5 of the parent coal the primary form of nitrogen evolution from the char is HCN. At these levels of conversion little increase in total volatiles by mass is observed while substantial reductions in char nitrogen levels are observed.

Relationship of Nitrogen Devolatilization Behavior to Coal Structural Characteristics, Structural Models

The chemical nature of the nitrogen distribution in the mix of molecular species present in the parent coal is indicated by the following phenomenlogical observations: (1) non-preferential evolution of coal nitrogen as char, tar or light gas during the devolatilization process; (2) the nitrogen distribution in the devolatilization products (tar, char, light gas) varies with rank and thermal drive as does the distribution of coal mass as char, tar and light gas; (3) HCN is the dominant nitrogen-containing light gas observed in rapid-heating; disperse phase devolatilization.

In the context of related investigations and a previous report on tar yields/characteristics, the observations indicate: (1) nitrogen is uniformly distributed throughout the mix of molecular species present in the parent coal, irrespective of rank; (2) the primary type of nitrogen-bonding present in the parent coal is as a heteroatom in an aromatic ring system, i.e., pyridine-type; (3) variations with rank in the nitrogen distributions in the devolatilization products can be understood on the basis of a shift with rank in a condensation frequency function (the distribution of molecular species as characterized by the number of fused rings/structure).

This devolatilization study as well as others indicate[7,8] that HCN is the principal nitrogen-containing light gas evolved during disperse phase, rapid-heating coal devolatilization. Studies performed by Houser,[9] et. al. and Axworthy,[10] et. al. indicate HCN is the principal light gas evolved from the thermal decomposition of pyridine-type nitrogen compounds. In addition, recent studies performed by Deno, et. al.[11] indicate that the nitrogen present in the parent coal is found as an heteroatom in aromatic ring structures. Taking into account the known highly aromatic nature of coals, the data of this study indicate that the primary form of nitrogen appears to be as a heteroatom in aromatic ring structures.

23

As noted in an earlier report,[1] distinguishing features of the devolatilization behavior of a coal are its maximum tar yield and the sensitivity of tar yield to the conditions of thermal drive. It was shown, for example, that the Pittsburgh seam bituminous coal gave a maximum tar yield ~ 40% greater than the Utah bituminous coal, ~ 50% greater than either the Colorado bituminous or Alabama bituminous coals, ~ 85% greater than the two subbituminous coals. Only a small fraction of the lignite was evolved as tar and the anthracite gave only light gases. The Pittsburgh seam coal (HVA) and Alabama bituminous coal (MVB) gave tar yields which were relatively insensitive to changes in thermal drive by comparison to the Western bituminous and subbituminous coals. Total vacuum volatile yields do not vary significantly with rank until coals with characteristics of the medium volatile bituminous coal. This report indicates that the nitrogen distribution in the devolatilization products reflects these patterns.

Thus moving along the coalification band from the low rank to the high rank side, the tar yield becomes a greater fraction of the total volatiles evolved and the primary tars formed appear to be more thermally·stable. Correspondingly, more of the parent coal nitrogen is evolved as tar and is retained by the thermally stable tars of these coals.

The devolatilization data, indicate that an increase in a condensation index (shift to a higher average number of the frequency function describing #fused rings/molecular species) and aromaticity of coal with position on the coalification band provides a reasonable explanation of changes in behavior with rank. The chemical nature of the nitrogen distribution in the parent coal forces the coal nitrogen devolatilization behavior to reflect the coal mass devolatilization behavior.

The variation in devolatilization behavior with rank appears to support some earlier attempts to develop a model of coal constitution based on the average number of fused rings in a molecular unit (lamella) of the coal. A model such as suggested by Ayre and Essenhigh[12] and latter modified by Scaroni and Essenhigh[13] appears able to provide a reasonable explanation of behavior with some qualifications. The data of this study indicate a change in devolatilization behavior with respect to total yield at a carbon content lower than 90%. The data also indicates a change in devolatilization behavior with respect to the yields and characteristics much lower than 90%. It is believed that a statistical function of the type described above showing a pronounced shift in characteristics in the 82-85% carbon level would more adequately reflect behavior observed in these studies.

The devolatilization data of this study and the previous tar study indicate that coal does behave as if it devolatilizes in two stages. The main stage (mass fraction conversions of ~ .4-.5) of volatile evolution requires relatively low final temperatures and is followed by a second stage of volatile evolution requiring temperatures in excess of 1000 C for appreciable rates. The coal nitrogen does evolve as if it were contained in two components. The two-component hypothesis of coal constitution was first noted by Clark and Wheeler[14] and later emphasized by Essenhigh and Howard[15] to explain devolatilization behavior.

However, rather than identifying the easily evolved volatile matter as being generated by the weakly bonded amorphous material associated with stacked ring structures, the data suggest the easily evolved nitrogen to be associated with ring structures susceptible to thermal cracking and/or volatilization at temperatures of 950 C or below. Variations with rank in easily evolved nitrogen expelled as tar or HCN reflect variations in the ring size distribution function with rank characteristics. The Pittsburgh seam bituminous coal evolves more coal nitrogen as tar than the Utah bituminous coal because its parent nitrogen is contained in ring structures more thermally stable, that is, of greater degree of ring condensation and having fewer associated functional groups. For the same reason, the Alabama bituminous (medium volatile) coal initially expels most of its nitrogen as tar. The Alabama bituminous yields less total volatiles than the high volatile bituminous coals because a greater fraction of its nitrogen is associated with non-volatile ring structures. That is it contains a large fraction of structures too large to be volatilized before char-incorporating secondary reactions "polymerize" the species in the char matrix.

This study on nitrogen evolution and the previous study dealing with tar yields and characteristics obtained from a variety of coals indicates:

1. In vacuum devolatilization conditions, coal behaves as if it contains two volatile components, as previously noted.

2. Lignite to high volatile bituminous coals can be differentiated with respect to devolatilization yields, primarily tar yield and characteristics.

3. Coal nitrogen distribution in the volatile products for subbituminous coals and higher ranks reflects the coal mass distribution in the volatile products.

4. Coal nitrogen for subbituminous and higher rank coals behaves as if it were incorporated as an heteroatom in the aromatic ring system of the parent coal.

5. As previously noted, variations in devolatilization behavior with rank appear to reflect a variation in the degree of ring condensation present in the coal matrix.

6. Variations in devolatilization behavior (more specifically, tar and nitrogen evolution) with rank reflect a shift in the characteristics of a ring-size distribution function with rank.

TABLE I

COUPLING BETWEEN FINAL TEMPERATURE AND HEATING RATE

Screen Material	m	b	T Range, ^{o}C
Stainless steel	1.96×10^{-3}	0.92	530 - 950
Tungsten	6.50×10^{-4}	2.16	1000 - 1750

REFERENCES

1. Freihaut, J. D. and Seery, D. J., Amer. Chem. Soc. Div. of Fuel Chem. Preprints, 26, No. 2, 133 (1981).

2. Brown, J. K. and Hirsch, P. B., Nature, 175, 229 (1955).

3. Fujii, S., Osawa, Y, and Sugimura, H., Fuel, 49, 68 (1970).

4. Solomon, P. R., Amer. Chem. Soc. Div. of Fuel Chem. Preprints, 24, No. 3, 184 (1979) and Advances in Chemistry (to be published).

5. Painter, P. C., et. al. Applied Spectroscopy (to be published).

6. Bellamy, L. J. The Infrared Spectra of Complex Molecules, John Wiley & Sons, New York (1975).

7. Pohl, J. H. and Sarofim, A. F., Sixteenth Symp (Intern) on Combustion, The Combustion Institute, Pittsburgh, 491 (1979).

8. Blair, D. W., Wendt, J. D. L, and Bartok, N., Sixteenth Symp (Intern) on Combustion, The Combustion Institute, Pittsburgh, 475 (1977).

9. Houser, T. J., et. al., Int. Jr. of Chem. Kinetics, XII, 555 (1980).

10. Axworthy, A.E., et. al., Fuel, 57, 29 (1978).

11. Deno, N. C., Pennsylvania State U., Dept. of Chem, Private Communication.

12. Ayre, J. L. and Essenhigh, R. H. Sheffield Univ. Fuel Soc. Jr., 8, 44 (1957).

13. Scaroni, A. W. and Essenhigh, R. H., Amer. Chem. Soc. Div. of Fuel Chem.. Preprints, 23, No. 4, 124 (1978).

14. Clark, A. H. and Wheeler, R. V., Trans. Chem. Soc., 103, 1754 (1913).

15. Essenhigh, R. H. and Howard, J. B., The Pennsylvania State U., Studies, 31 (1971).

TABLE II

ELEMENTAL ANALYSIS (DMMF)

	Mon Lig(L)	WY Sub(S1)	WY Sub(S2)	Utah Bit(UB)	Col Bit(CB)	Pitt Bit(PB)	Ala Bit(AB)	Anth. (AN)
C	0.6827	0.7540	0.7550	0.7818	0.8100	0.8197	0.8497	0.9369
H	0.0457	0.0490	0.0517	0.0552	0.0553	0.0536	0.0463	0.0259
O	0.2547	0.1807	0.1699	0.1386	0.1119	0.0936	0.0818	0.0189
N	0.0102	0.0128	0.0171	0.0169	0.0163	0.0142	0.0173	0.0108
S_o	0.0067	0.0035	0.0063	0.0076	0.0064	0.0109	0.0052	0.0072
H/C	0.803	0.780	0.822	0.847	0.819	0.785	0.654	0.332
O/C	0.280	0.180	0.169	0.133	0.104	0.086	0.072	0.015

TABLE III - 1

NITROGEN DISTRIBUTIONS IN DEVOLATILIZATION PRODUCTS

Subbituminous 2 (SUB B)

$T_f(^oC)$	f^N_{CHAR}	f^N_{tar}	f^N_{HCN}	Σf^N
520	0.99	0.05	---	1.04
600	0.76	0.24	0.01	1.01
745	0.67	0.19	0.10	0.96
820	0.63	0.28	0.17	1.00
890	0.57	0.22	0.21	1.00
945	0.57	0.12	0.20	0.89
950	0.53	0.11	0.30	0.94
1040	0.48	0.17	0.30	0.95
1090	0.40	0.14	0.40	0.94
1160	0.31	0.07	0.63	1.01
1240	0.28	0.06	0.65	0.99
1365	0.17	0.06	0.66	0.89
1390	0.08	0.04	0.61	0.73
1600	0.10	0.04	0.54	0.68
1700	0.08	0.04	0.92	1.03
1780	---	0.03	0.87	0.90

TABLE III - 2

NITROGEN DISTRIBUTIONS IN DEVOLATILIZATION PRODUCTS

Utah Bituminous (HVB)

$T_f(^oC)$	f^N_{CHAR}	f^N_{tar}	f^N_{HCN}	Σf^N
530	0.81	0.04	0.01	0.86
595	0.66	0.22	0.01	0.89
745	0.58	0.26	0.08	0.92
790	0.57	0.27	0.09	0.93
880	0.49	0.25	0.17	0.91
915	0.48	0.24	0.17	0.89
935	0.51	0.30	0.13	0.94
1020	0.42	0.29	0.16	0.87
1090	0.40	0.24	0.25	0.89
1160	0.44	0.22	0.38	1.04
1240	0.30	0.21	0.51	1.02
1390	0.20	---	0.61	0.81
1600	0.20	0.10	0.67	0.97
1700	0.13	0.06	0.72	0.91
1780	0.10	0.05	0.96	1.11

TABLE III - 3

NITROGEN DISTRIBUTIONS IN DEVOLATILIZATION PRODUCTS

Pittsburgh Bituminous (HVA)

$T_f(^{\circ}C)$	f^N_{CHAR}	f^N_{tar}	f^N_{HCN}	Σf^N
565	0.61	0.49	0.01	1.11
585	0.61	0.38	0.01	1.00
618	0.58	0.45	0.00	1.03
735	0.55	0.41	0.05	1.01
745	0.59	0.41	0.05	1.05
775	0.52	0.41	0.06	0.99
830	0.53	0.39	0.09	1.01
855	0.54	0.43	0.10	1.07
915	0.46	0.36	0.10	0.96
935	0.55	0.36	0.08	1.09
1040	0.44	0.40	0.10	0.94
1090	0.50	0.60	0.12	1.21
1107	0.41	0.40	0.24	1.04
1125	0.39	0.39	0.17	0.95
1165	0.46	0.43	0.22	1.11
1220	0.32	0.28	0.20	0.80
1220	0.39	0.36	0.33	1.08
1300	0.29	0.54	0.30	1.13
1450	0.33	0.19	0.33	0.85
1450	0.26	0.30	0.37	0.93
1700	0.04	---	0.43	0.47
1780	0.06	0.15	0.28	0.49
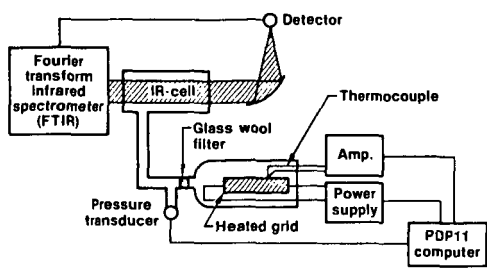
Fig. 1   Heated Grid Apparatus
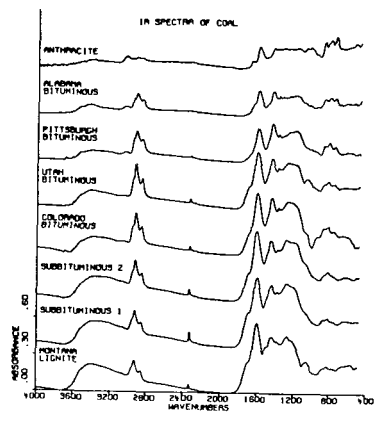
Fig. 3   IR Spectra of Coals
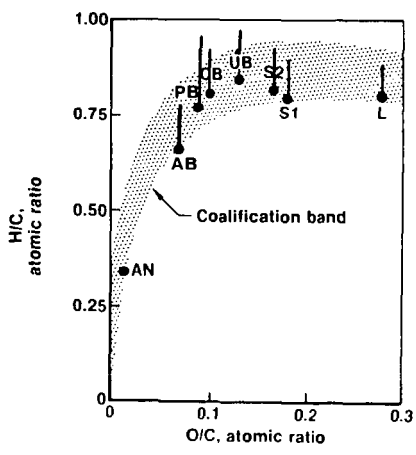
Fig. 2   Coal Band Location
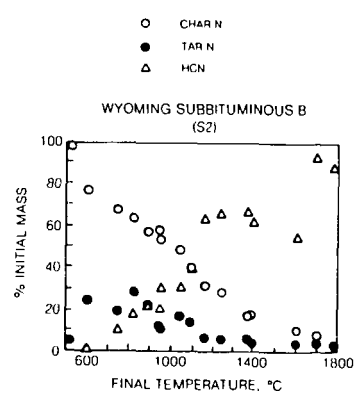
Fig. 4   Nitrogen Distribution:
          Subbituminous Coal
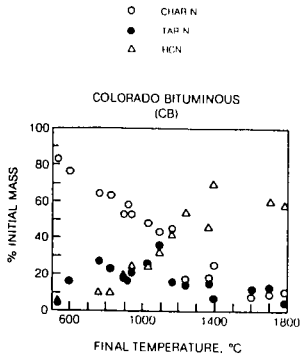
Fig. 5 Nitrogen Distribution:
Colorado Bituminous Coal
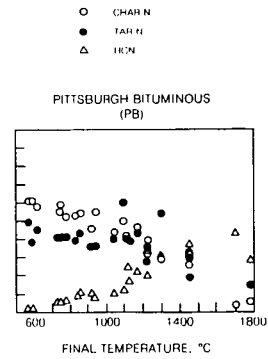
Fig. 7 Nitrogen Distribution in
Pittsburgh Bituminous Coal
Devolatilization Products
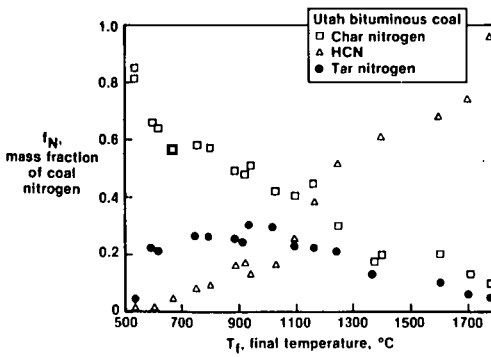
Fig. 6 Nitrogen Distribution:
Utah Bituminous Coal
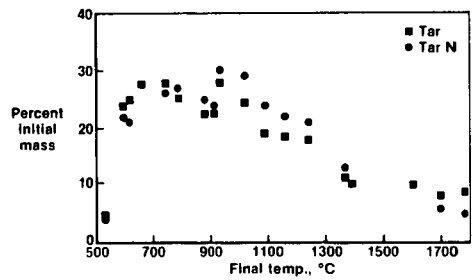
Fig. 8 Mass Fraction of Coal Mass and
Coal Nitrogen vs. Final Temperature for
Utah Bituminous Coal

33
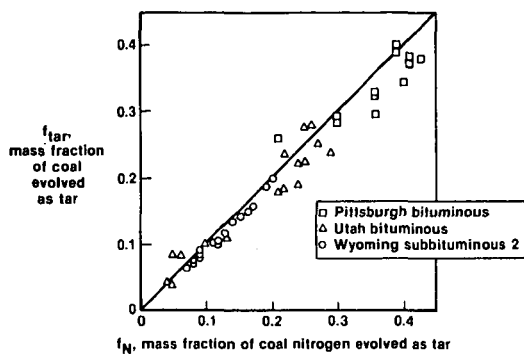
Fig. 9   Mass Fraction of Coal as Tar vs. Fraction of Coal Nitrogen as Tar
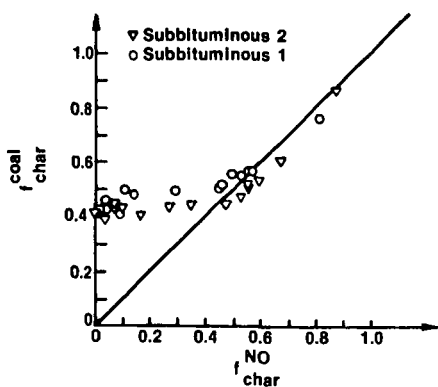
Fig. 10   Mass Fraction of Coal as Char vs. Fraction of Coal Nitrogen as Char
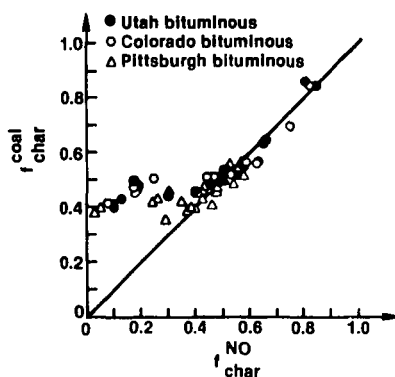
Fig. 11   Mass Fraction of Coal as Char vs. Fraction of Coal Nitrogen as Char

34

MINERAL MATTER EFFECTS ON THE RAPID PYROLYSIS AND HYDROPYROLYSIS OF A BITUMINOUS COAL

Howard D. Franklin, William A. Peters, Jack B. Howard

Department of Chemical Engineering and Energy Laboratory,
Massachusetts Institute of Technology, Cambridge, Mass. 02139

Previous research at M.I.T. on rapid coal pyrolysis has dealt with the kinetics of evolution of individual products as a function of temperature, pressure, particle size, reactive gas, and coal type (1-5). Studies elsewhere have shown that constituents of coal mineral matter affect significantly other types of coal conversion reactions (6-14). Specifically, clays found in coal have been shown to affect coal carbonization (6), and to catalyze H_2 transfer to coal and coal model compounds (7,8). Pyrite, an important mineral in Eastern U.S. coals, is a strong catalyst for coal hydroliquefaction (7-11), while calcite promotes steam and CO_2 gasification of coal (12,13). Even quartz, though chemically inert, affects hydroliquefaction by acting as a diluent to agglomeration (14). Despite this importance of mineral content in coal thermochemistry, little work has been done on additive effects on rapid coal pyrolysis. Therefore this study was conducted to determine systematically how the important minerals present in coal influence the yields of individual devolatilization products.

EXPERIMENTAL

The coal used, described in Table 1, was a Pittsburgh No. 8 Seam bituminous coal from the Ireland Mine of the Consolidation Coal Company. Mineralogical analysis was by Fourier Transform Infrared Analysis (FTIR) of the low temperature ash of the coal (15). Pyrite content was not measured directly, but the pyrite-by-difference value agrees well with measured pyritic sulfur values for other samples from the same mine (16). The coal was ground to -270+325 US mesh (45-53μm) and a fraction of this raw sample was retained to obtain pyrolysis data on whole coal. The remainder of the sample was extracted with concentrated HF and HCl to remove its native clays, calcite, and quartz, and was then subjected to float-sink separation in a 2.50 specific gravity fluid to remove pyrite. The resulting demineralized coal contained 4.3% by weight mineral matter, most of it pyrite.

Mineral additives representing each of the major mineral constituents of this coal were studied. These are listed in Table 2. Acid-treated montmorillonite, prepared by extracting with HCl a portion of the montmorillonite sample, was used to study the effect of solid acidity on possible clay catalysis of pyrolysis. Shale was obtained from the Pittsburgh No. 8 Seam, and is representative of the native clays found in this coal. All mineral additives were ground to 2-40 μm grain size, and added to the coal by co-slurrying with water in concentrated suspension for 24 hours.

At high temperatures and under the reducing conditions of coal pyrolysis, calcite and pyrite will decompose to CaO and pyrrhotite (FeS_{1+x}, $0<x<0.3$) respectively. In order to determine whether the extent of contact with the coal affects the catalytic properties of these particular minerals, additional sources of CaO and pyrrhotite were tried as well. $FeSO_4$, which is completely water

soluble, was added to the coal by impregnation from solution. Under pyrolysis conditions it should decompose to pyrrhotite. CaO was added in a manner similar to that for the mineral additives.

The pyrolysis apparatus and procedures have been described previously (2,17,18). Briefly, a thin horizontal layer of coal is sandwiched between the folds of a 325 US mesh stainless steel screen and held between two electrodes in either a length of glass pipe or a stainless steel pressure vessel. The coal is heated by electrically heating the screen. The vessel and its gaseous contents remain close to room temperature throughout the run and thus the volatiles are quenched almost instantaneously on escape from the coal particles. The entire time-temperature history of the sample is recorded by use of a chromel-alumel thermocouple (75 μm bead diameter) positioned within the folds of the screen alongside the coal particles. Heat transfer calculations show that at pressures of 1 atm and heating rates of 1000 K/s or less, coal particles and thermocouple beads 80 μm or less in diameter closely follow the temperature of the screen and are spatially isothermal.

All the reaction products were collected. Gases and low boiling liquids were trapped on lipophilic sorbents and subsequently analyzed by gas chromatography. Char was determined gravimetrically, and was further characterized by elemental analysis. Tar (room temperature condensibles) was collected on a filter at the reactor outlet and by a methylene chloride wash of the reactor internals, and its yield was determined gravimetrically. Total material balances usually exceeded 95%.

All runs were preformed at heating rates of about 1000 K/s with holding times of 0 or 5 s at the maximum temperature attained, and cooling rates of about 200 K/s. These elements of the time-temperature history pertain only to the parent sample since the volatiles, once formed, rapidly escape the sample and are quenched as mentioned above. Demineralized, calcite-pretreated, and CaO-pretreated samples were heated in 1 atm He to temperatures in the range 800 to 1400 K for both 0 and 5 s holding times. Other samples were pyrolyzed in helium at temperatures near 1300 K for 5 s holding times, and at temperatures near 1000 K for 0 s holding times. In hydropyrolysis runs, samples were heated in 69 atm H_2 to temperatures between 800 and 1400 K for the demineralized coal, and to one temperature, generally near 1100 K, for the pretreated samples. Only 0 s holding times were used in hydropyrolysis runs.

RESULTS

Pyrolysis in Helium

The total yield of volatiles and the yield of tar obtained from pyrolysis of the demineralized coal to different temperatures in 5 s holding time runs are shown in Fig. 1. Each data point represents the cumulative yield from one experimental run and is associated with a specific time-temperature history. The curves represent simple first-order reaction models fitted to the data, and are used to indicate trends in the data. The error bars represent +1 standard deviation from the yield calculated by the fitted model. Heating and cooling rates did not exactly reproduce from run to run, and thus the holding or peak temperature obtained is not necessarily a good representation of the entire time-temperature history of a run. Therefore the fitted models

were used to generate equivalent peak or holding temperatures for each run. The model parameters were used to determine a calculated yield of a given product for each actual time-temperature history. These yields were then compared with yields calculated using the same parameters and idealized (linear 1000 K/s heatup, 0 or 5 s hold time, linear 200 K/s cooldown) time-temperature histories. The peak or holding temperature of the idealized history having the same calculated yield as that of the actual history was picked as the temperature representative of the run. As a rule equivalent temperatures for different products were within 30 K of the corresponding observed peak or holding temperature.

Results for raw coal and for clay-, quartz-, and iron-pretreated samples are shown in Figs. 2-5. The curves and error bars plotted on all these graphs indicate demineralized coal yields, while each letter represents one run with a sample pretreated with a particular mineral or compound as specified in Table 2. Points labelled "W" represent runs with raw (undemineralized) coal.

There are in general few effects on pyrolysis due to any of these minerals. Figures 2 and 3 show that the total yield of volatiles and the yield of tar are unaffected by these additives. While there are no points in Fig. 3 for pyrite or $FeSO_4$, other runs not plotted showed these additives to have no effect on tar yields. Data for most other products show similar trends. Methane yields (Fig. 4) are, however, significantly reduced by pyrite and $FeSO_4$ ("P" and "F" points). Kaolinite suppresses the yield of light liquid hydrocarbons (Fig. 5, "K" points), which consist mostly of BTX range compounds.

Results for calcium minerals have been reported previously (19). To summarize them, both CaO and $CaCO_3$ increase char yields, while strongly decreasing tar yields and slightly reducing yields of other hydrocarbon volatiles. Evolution of CO is enhanced by these additives by an amount approximately proportional to calcium loading. Comparison of CO_2 yields from $CaCO_3$ pretreated coal with those from demineralized coal and pure calcite indicates that calcite in the presence of coal decomposes yielding CO_2 at lower temperatures than it does when pyrolyzed alone.

Pyrolysis in Hydrogen

Effects of minerals in hydropyrolysis were determined in a similar manner to that used for pyrolysis. Simple first-order models were fitted to hydropyrolysis data from demineralized coal, and the resulting curves with error bars served as a basis of comparison for the data from hydropyrolysis of mineral-treated coals.

Few of the minerals were found to influence hydropyrolysis behavior to any significant extent. Total yield of volatiles (Fig. 6) is not affected by any of the additives tried, although tar yields are reduced slightly by addition of shale or calcite, and reduced strongly by addition of CaO, kaolinite, or acid-treated montmorillonite (17). Methane (Fig. 7) and ethane, the most important hydropyrolysis products after tar, are suppressed by addition of calcite or shale. Carbon dioxide yields are strongly enhanced by the calcium minerals (Fig. 8). The calcite-pretreated sample in this case was different from the one used for pyrolysis in He, and contained only 14.55% by weight $CaCO_3$.

DISCUSSION

The most striking point brought out in this study is the variation in catalytic activity exhibited by the different minerals present in coal. The clays, which might be expected to show hydrocarbon cracking activity due to their solid acidity, have virtually no effect on the pyrolysis yield structure. The reduction in liquid hydrocarbon yields by kaolinite (Fig. 5) might be attributable to secondary cracking of these compounds by this clay. The degree of reduction is, however, too small to determine the products of this postulated cracking. It is not immediately clear why kaolinite would crack light liquids and not crack tar (Fig. 3). One possible explanation is the relative ease of accesibility of the lighter liquids to the pore structure of the clay where most of its active surface area lies. The reduction in methane yields by shale in hydropyrolysis (Fig. 7) is not easily explained. Clays have been shown to retard the rate of CH_4 production in slow hydrogasification of chars (20). While the reactions in that system are substantially different from those of rapid hydropyrolysis, a common underlying mechanism for CH_4 yield suppression might be present. Kaolinite and acid-treated montmorillonite reduce tar yields in hydropyrolysis (17), while montmorillonite does not. The clays thus seem to show some hydrocracking activity, which is possibly dependent on their solid activity.

Iron-sulfur minerals, pyrite and $FeSO_4$, also have little influence on pyrolysis behavior. Their only significant effect on pyrolysis in He is to reduce CH_4 yields (Fig. 4). This phenomenon is difficult to explain as none of the other light hydrocarbon products are affected by iron-sulfur mineral addition. The lack of effects of iron-sulfur minerals on hydropyrolysis product yields is very surprising given the known activity of these minerals for hydroliquefaction. Weller et al. (21) did show that a pyrite sample that strongly enhanced liquefaction at 250 atm H_2 pressure had no effect on liquefaction at 69 atm H_2, the pressure used in the present study. A pressure effect for iron-sulfur catalysis of coal hydrogenation might thus be indicated. The postulated active species for coal hydrogenation in the presence of iron-sulfur minerals is pyrrhotite. The precise stoichiometry of the pyrrhotite formed will be a function of the hydrogen pressure (22), and this stoichiometry will affect the subsequent activity of the pyrrhotite (23). Further study of pyrrhotite stoichiometry and activity as a function of hydrogen pressure is clearly needed.

The strong effects of calcium minerals on coal pryolysis are in striking contrast to the comparative lack of activity of the other coal minerals. While the solid-acid clays show little cracking activity, calcium minerals reduce the yield of volatile hydrocarbon products (19). In addition, CaO and $CaCO_3$ are especially active in cracking oxygen functional groups to CO (19). A large portion of bituminous coal oxygen occurs in acidic functional groups such as phenols or carboxylic acids, and the strongly basic CaO might react with these groups. In addition, we have pointed out previously (19) that the reactions by which phenol decomposes homogeneously to CO would be catalyzed by a solid base. Non-acidic oxygen functional groups such as furans have also been shown to crack over CaO (24). Thus strong bases would seem to influence the decomposition of coal oxygen to a greater degree than would other additives. It also appears that solid bases, or at least CaO, are good catalysts for cracking aromatics or other coal hydrocarbon volatile products (19, 24). Since $CaCO_3$, which decomposes to CaO during pyrolysis, is the only coal mineral which generates a solid base, it is the coal mineral with the strongest influence on coal pyrolytic behavior.

The effects of calcium minerals on hydropyrolysis are less easily explained. Calcite suppresses CH_4 yields (Fig. 7) in hydropyrolysis to about the same extent as do the clays. The same study (20) that showed clays to reduce char hydrogasification rates also showed calcite to reduce those rates. Why these two groups of minerals should have the same effects on coal hydrogen reactions is unclear. It is noteworthy that while calcite suppresses CH_4 yields, CaO does not. As discussed below, the $CaCO_3$ present in calcite-pretreated coal did not decompose to CaO under hydropyrolysis conditions, and its effects need not therefore parallel those of lime.

Carbon dioxide yields from CaO-pretreated coals hydropyrolyzed in 69 atm H_2 (Fig. 8) are almost identical to those from the same sample pyrolyzed in 1 atm He at similar time-temperature histories (17), and in both cases the CO_2 yields are considerably higher than those from demineralized coal. Since the carbonate content of the CaO-pretreated sample was small, this excess CO_2 probably results from accelerated decomposition of an as yet undetermined coal oxygen functional group. Carbon dioxide yields from calcite-pretreated coal under 69 atm H_2 are very similar to those from CaO-pretreated coal. This strongly contrasts with the pyrolysis behavior of this sample under 1 atm He (19) where, at similar time-temperature histories, the calcite itself had started to decompose. It is interesting to note that the calcite-pretreated sample gave CO_2 yields that were no larger than those from the CaO-pretreated sample, despite having 2.75 times as much Ca. A saturation effect is probably present.

There is no difference between pyrolysis yields of the raw coal and the demineralized coal. Since 90% of the native mineral matter of the coal used consisted of clays, pyrite, and quartz (Table 1) this result agrees with the other findings of this study as to the relative lack of activity of these minerals. It also implies, however, that the demineralization technique itself has no effect on the subsequent pyrolysis behavior of this bituminous coal.

CONCLUSIONS

Clays and iron-sulfur minerals have few effects on the pyrolytic behavior of this bituminous coal. Calcium minerals reduce yields of volatile hydrocarbon products, and enhance CO formation. Calcite and shale reduce yields of CH_4 in coal-hydrogen reactions, while acid-treated montmorillonite, kaolinite, and CaO reduce yields of tar under these conditions. Iron-sulfur minerals have few catalytic effects on coal hydropyrolysis at H_2 pressures of 69 atm.

ACKNOWLEDGEMENTS

REFERENCES

1. Anthony D.B., Howard, J.B., AIChE J 22, 625 (1976).

2. Suuberg E.M., Peters W.A., Howard J.B., Ind. and Eng. Chem. Proc. Des. and Dev. 17, 37 (1978).

3. Suuberg E.M., Peters W.A., Howard J.B., Proc. 17th Symp. (International) on Combustion 1979 p. 117, The Combustion Institute, Pittsburgh, Pa.

4. Suuberg E.M., Peters W.A., Howard J.B., <u>Amer. Chem. Soc. Adv. in Chem. Ser.</u> <u>183</u>, 239 (1979).

5. Suuberg E.M., Peters W.A., Howard J.B., Fuel <u>59</u>, 405 (1980).

6. Howard H.C., <u>Chemistry of Coal Utilization, Supplemental Volume</u>, 1963, p.340 Wiley, New York.

7. Given P.H., EPRI Report No. 207-0-0, 1974 p. A-122.

8. Mukherjee D.K., Choudhury P.B., Fuel <u>55</u>, 4 (1976).

9. Guin J.A., Tarrer A.P., Prather J.W., Johnson D.R., Lee J.M., Ind. and Eng. Chem. Proc. Des. and Dev. <u>17</u>, 118 (1978).

10. Granoff B., Thomas M.G., Baca P.M., Noles G.T., Amer. Chem. Soc. Div. of Fuel Chem. Prepr. <u>23</u> (1), 23 (1978).

11. Gangwer J.E., Prasad H., Fuel <u>58</u>, 577 (1979).

12. Feldmann H.F., Chauhan S.P., Longanbach J.R., Hissong D.W., Conkle H.N., Curran L.M., Jenkins D.M., Battelle Columbus Laboratories Report BM1-1986,1977.

13. Sears, J.T, Muralidhara H.S., Wen C.Y., Ind. and Eng. Chem. Proc. Des. and Dev., <u>19</u>, 358 (1980).

14. Gray, D., Fuel <u>57</u>, 213 (1978).

15. Painter P.C., Coleman M.M., Jenkins R.G., Whang P.W., Fuel <u>57</u>, 337 (1978).

16. Padia A.S., ScD Thesis, MIT Dept. of Chem. Eng. 1976.

17. Franklin H.D. PhD Thesis, MIT Dept. of Chem. Eng. 1980.

18. Anthony D.B., Howard J.B., Meissner H.P., Hottel H.C., Rev. Sci. Instrum. <u>45</u>, 992 (1974).

19. Franklin, H.D., Peters W.A., Howard J.B., Amer. Chem. Soc. Div. of Fuel Chem. Prepr. <u>26</u> (2), 121 (1981).

20. Tomita A., Mahajan O.P., Walker P.L., Amer. Chem. Soc. Div. of Fuel Chem. Prepr. <u>22</u> (1), 4 (1977).

21. Weller S., Pelipetz M.G., Friedman S., Storch H.H., Ind. and Eng. Chem. <u>43</u>, 1243 (1950).

22. Richey W.D., 12th Central Regional Meeting Amer. Chem. Soc., Pittsburgh, Pa., Nov. 1980.

23. Montano P.A., Granoff B., Fuel <u>59</u>, 214 (1980).

24. Mead D.W., M.S. Thesis, MIT Dept. of Chem. Eng. 1979.

TABLE 1

CHARACTERISTICS OF COAL EXAMINED

Proximate Analysis		Ultimate Analysis		
Wt.% (as received)		Wt.% (dry)		Wt.% (dmmf)
Moisture	2.0	Carbon	71.74	82.91
Volatile Matter	36.2	Hydrogen	4.84	5.65
Fixed Carbon*	51.0	Oxygen*	6.22	7.19
Ash	10.8	Nitrogen	1.14	1.32
	100.0	Organic Sulfur**	2.54	2.94
		Mineral Matter	13.47	
			100.00	100.00

Petrographic Analysis		Mineral Matter Analysis	
Wt.% mineral matter free		Wt.%	
Vitrinite	81.5	Kaolinite	13
Semi-Fusinite	6.0	Calcite	10
Fusinite	2.5	Quartz	7
Micrinite	3.0	Montmorillonite	14
Macrinite	1.2	Illite	9
Exinite	5.2	Pyrite*	45
Resinite	0.6		100
	100.0		

* by difference

**calculated from total sulfur (5.77% by weight dry coal) and measured pyrite content

TABLE 2

MINERAL MATTER ADDITIVES STUDIED

MINERAL	PLOTTING SYMBOL	SOURCE	OBTAINED FROM	WT. % MINERAL IN PRE-TREATED SAMPLE*
Kaolinite	K	Mesa Alta N.Mex. (API REF CLAY)	Ward's Natural Science Estab.	11.9
Montmorillonite	M	Belle Fourche N.D. (API REF CLAY)	Ward's Natural Science Estab.	8.8
Acid-Treated Montmorillonite	A	Made in house from above		10.2
Shale	S	Moundsville W. VA	U.S.G.S.	9.6
Pyrite	P	Moundsville W. VA	U.S.G.S.	17.1
Calcite	C	Sumterville FLA	Dixie Lime & Stone	20.2
Quartz	Q	not known	Harvard Mineralogy Museum	18.0

CHEMICAL			OBTAINED FROM	
CaO	L	-	Fisher Scientific	5.9**
FeSO$_4$	F	-	Fisher Scientific	6.7

* Does not include 4.3% mineral matter content of demineralized coal

** Actual mineral in coal was mixture of 74% Ca(OH)$_2$ - 26% CaCO$_3$

41
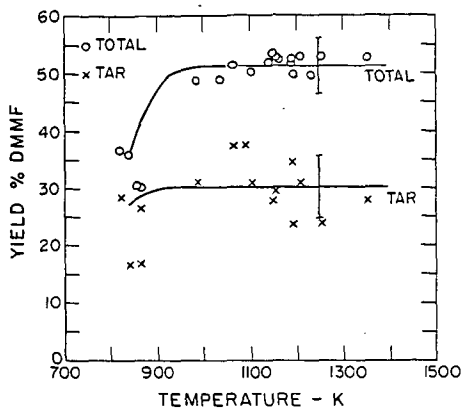
Figure 1   Total Yield of Volatiles and Yield of tar from Demineralized Coal Pyrolysis in 1 atm He, 5 s Holding-Time Runs.
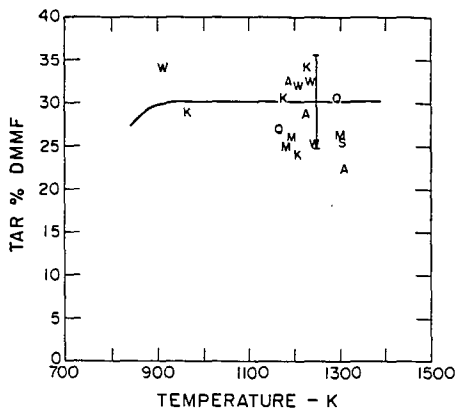
Figure 3   Yield of Tar from Pyrolysis of Pretreated Coal in 1 atm He, 5 s Holding-Time Runs.
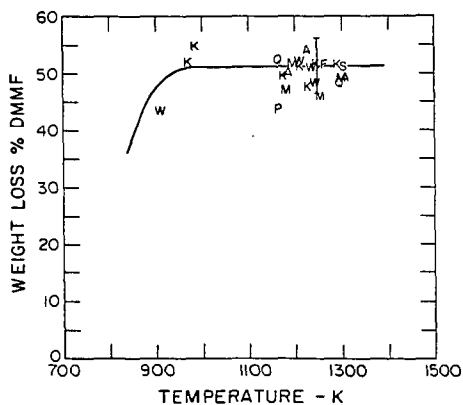
Figure 2   Total Yield of Volatiles from Pyrolysis of Pretreated Coal in 1 atm He, 5 s Holding-Time Runs.
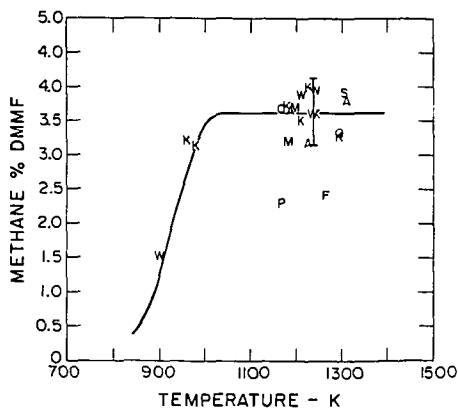
Figure 4   Yield of Methane from Pyrolysis of Pretreated Coal in 1 atm He, 5 s Holding-Time Runs.

42
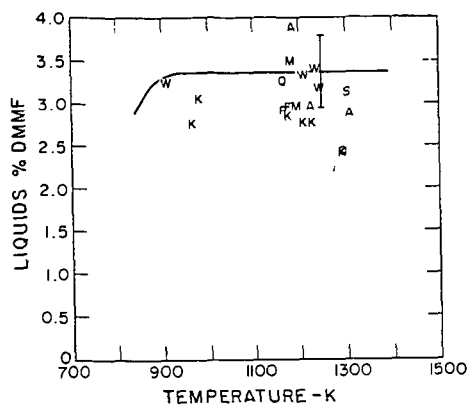
Figure 5   Yield of Light Liquid Hydrocarbons from
            Pyrolysis of Pretreated Coal in 1 atm He,
            5 s Holding-Time Runs.
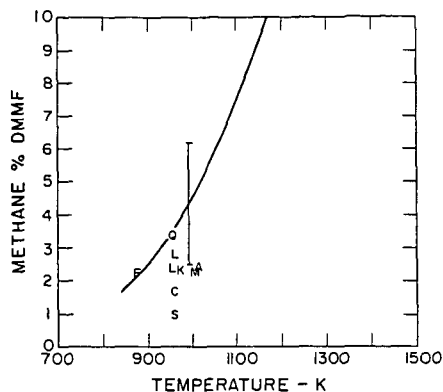
Figure 7   Yield of Methane from Pyrolysis of Pre-
            treated Coal in 69 atm H₂, 0 s Holding-
            Time Runs.
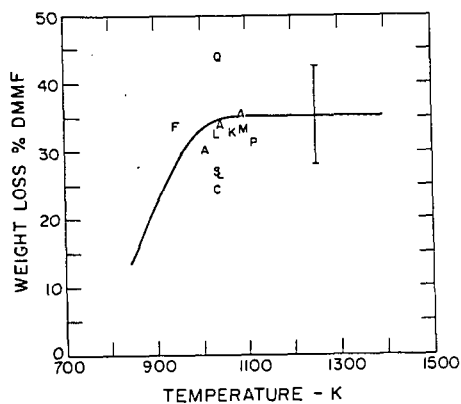
Figure 6   Total Yield of Volatiles from Pyrolysis of
            Pretreated Coal in 69 atm H₂, 0 s Holding-
            Time Runs.
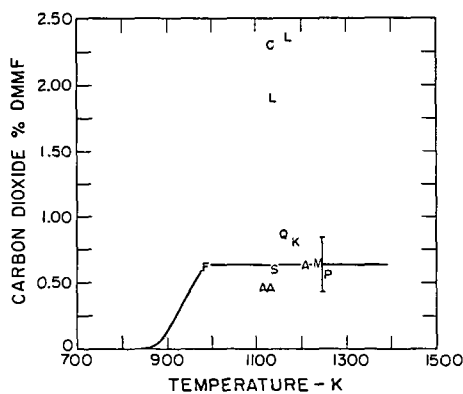
Figure 8   Yield of Carbon Dioxide from Pyrolysis of
            Pretreated Coal in 69 atm H₂, 0 s Holding-
            Time Runs.

43

HYDROGENOPYROLYSIS OF COAL AND COAL DERIVATIVES

R. Cyprès

Faculty of Applied Sciences
Department of General Chemistry
and Carbochemistry
Université Libre de Bruxelles
BELGIUM

1. INTRODUCTION

Coal hydropyrolysis is now developping as one of the third gene-
ration processes for coal gasification or partial liquefaction.
The advantages of coal hydropyrolysis are : rapid primary devola-
tilisation of the coal, with production of more volatile matter
than what is determined by standard methods; desulfurization of
the char; simultaneous hydrocracking of the primary tar. General
reviews on the subject have been published recently (1)(2)(3)(4)
Present paper deals with three aspects of fixed bed hydropyroly-
sis : the increased formation of methane and light monocyclic aro-
matics and phenols; the desulfurization process and yield, with
regard to the composition of the mineral constituents of the coal;
the mechanism of thermal cracking of hydro- and perhydropolycyclic
hydrocarbons.

2. POSTCRACKING OF THE PRIMARY VOLATILE MATTER

During pyrolysis of coal under H_2 pressure, the primary volatile
matter are submitted to hydrocracking. This postcracking is shown
by the variation, compared to what happens in inert atmosphere,
of the methane concentration in the gas and of the light aromatics
(B.T.X. : benzene, toluene and xylene) and phenols (P.C.X. : phe-
nol, cresols and xylenols) in the liquid phase.

Experiments have been made with a 32,8% V.M. coal from Beringen,
sized < 500 µm, between 480 and 850°C at a fixed H_2 pressure of
30 bar. One run was made with 30 bar He pressure at 580°C. Residen-
ce time of carrier gas was about 60 s. Yields in gas, oil, water
and char are given in table I.

T (°C)	H_2					He
	485	580	650	780	850	580
Char	75.7	70.9	66.7	61.6	60.6	75.0
Oil	9.5	9.2	8.8	6.4	5.5	6.4
Gas	9.1	10.2	15.1	24.2	28.3	7.9
Water	4.4	6.9	8.9	10.1	9.2	4.7

Table I : Yields (% maf) (30 bar H_2 pressure)

Above 700°C, coal devolatilisation is higher than the volatile
matter content, determined following standard methods.

Hydrogen pressure influence at 580°C between 1 and 50 bar has
been studied on the same coal. Yields obtained are given in
table II.

44

H₂ pressure-bar	H_2					He
	0	10	20	30	50	30
Char	76.6	72.4	70.6	70.9	69.0	75.0
Oil	7.4	10.3	9.8	9.2	8.9	6.4
Gas	5.3	10.0	10.3	10.2	9.9	7.9
Water	5.3	6.0	7.0	6.9	6.1	4.7

Table II : Yields (% maf) at 580°C.

Fig. 1 gives the variation of CH_4 and C_2H_6 content in the gas at 30 bar H_2 pressure compared with conventional carbonisation, as a function of temperature. CH_4 content increases from 45% at 500°C to 80% at 850°C. Under conventional atmospheric carbonisation the known reverse evolution occurs. CH_4 formation is due to hydrodealkylation of higher hydrocarbons.

The change in composition of B.T.X., P.C.X. and naphthalenes is given on fig. 2 as a function of carbonisation temperature. Light aromatics are steadily increasing. Phenols, on the contrary, are at their highest concentration in the low temperature oil. Phenols dehydroxylation occurs only above 700°C. Water content shows an increase parallel to the decrease of P.C.X. (phenol, cresols, xylenols) content. The speed of cresols disappearance is equal to the speed of their formation by dealkylation of the xylenols. Phenol increase is a result of both processes. The optimal phenol production is at about 750°C. The dehydroxylation of P.C.X. contributes to the B.T.X. increase between 600 and 800°C.

Naphthalenes yields are increasing with temperature as a result of known formation of di- and polycyclic aromatics from cracking fragments. Under hydrogen pressure these reactions are markedly slowed down but nevertheless still present.

Fig. 3 shows that, for the light aromatics, hydrogen pressure influence at 580°C is important between 1 and 20 bar. This is not the case for the phenols. Naphthalenes increase with the pressure from 1,2% at 1 bar to 3,6% at 50 bar.

3. DESULFURIZATION OF THE COAL DURING HYDROGENOPYROLYSIS

It is known that high temperature hydropyrolysis leads to partially desulfurized char. In this paper, this hydrodesulfurization was considered regarding the nature of the sulfurous minerals present in the coal.As an exemple a high S containing italian coal was submitted to a fixed bed hydrocarbonisation at 30 bar H_2 pressure. Experiments were performed at 580°C, 700° and 850°C. Pyrite is reduced by H_2 to an extent depending mainly upon pyrolysis temperature. The reduction of pure pyrite and mixtures of pyrite and pitch coke under hydrogen pressure has been studied by thermogravimetry between 1 and 50 bar up to 950°C. It can be seen on fig. 4 that the first loss of S, corresponding to the conversion of FeS_2 to FeS_x (pyrrhotite) is complete around 500°C.

The reduction to Fe is only complete at much higher temperature. At 950°C, under 50 bar, total reduction is achieved within 10 minutes, whereas at 1 bar, it needs 40 minutes. The same behaviour is observed for pyrite in the coal. The higher the pyrolysis temperature is, the more important is the pyritic sulfur elimination.

Scanning electron microscopy photographies show the distribution of S, Ca and Fe in the coal and in the char. The pyritic sulfur

is well localised in the coal, whereas the organic sulfur is uni-
formely distributed in the bulk of the sample. The calcium con-
tent of this italian coal is high, mostly as $CaCO_3$ but also some
$CaSO_4$ (Fig.5).

In the char, after hydrogen treatment, it can be observed on
Fig.6 that FeS_2 has been reduced. At low temperature, reduction
is limited to pyrrhotite (FeS_x), at high temperature, to iron.
But where Ca is detected it is associated with S, probably in
the form of CaS and some unreduced $CaSO_4$. The experimental re-
sults are summarized in table III. They show in this case of a
high calcium containing coal, that the higher the pyrolysis tem-
perature is, the more sulfur remains in the char. It seems to be
due to increased decomposition of $CaCO_3$ into CaO, which is more
active to fix the volatile sulfur compounds. $CaCO_3$ from the ash
would have the same effect under hydrocarbonisation conditions,
as limestone or dolomite, added to coal, in combustion, as to
reduce atmospheric SO_2 pollution. As a conclusion of this, it
can be said that high calcium containing coals, will not be de-
sulfurized in the same ratio as pyritic coals and that an in-
crease of their hydrocarbonisation temperature will leave more
sulfur in the char.

SULCIS COAL					
Proximate analysis		Ultimate analysis (Mf)			
Moisture	6,0	C	63,24	S, pyritic	0,83
Ash (Mf)	12,9	H	3,71	sulfate	0,05
Volatile Matter	56,4	O	14,11	organic	3,57
(% Maf)		N	1,77		
		S	4,45		
		Ash	12,9		
		Total	100,28	Total	4,45
HYDROGENOPYROLYSIS pH_2 = 30 bar					
T°C		580	700	850	
Devolatilisation (% Maf)		51,6	61,1	61,9	
Gas		19,2	36,2	39,7	
Oil		14,8	10,3	8,2	
Water		16,4	18,8	14,1	
Char		48,4	38,9	38,1	
S balance in					
Char		34,1	35,6	41,9	
Oil		7,0	6,0	4,7	
Gas		59,1	58,4	53,4	

Table III : Sulcis coal and chars.

THERMAL CRACKING OF DI- AND POLYHYDROAROMATICS AT ATMOSPHERIC
PRESSURE OF INERT GAS

In connection with the high content of hydropolyaromatic compounds
present in coal liquids produced by several industrial processes,
due to partial hydrogenation, the thermal cracking in inert gas

at atmospheric pressure of di- and polycyclic compounds, partial-
ly and totally hydrogenated was studied in view of their conver-
sion to monocyclic aromatic hydrocarbons.

Korosi (5) has shown that steam cracking of decaline, with a
steam to hydrocarbon ration of 16/1 at 854°C and nearly atmosphe-
ric pressure leads to 18 W% benzene and up to 19 W% C_2H_4 in the
gas phase.

We made thermal cracking at atmospheric pressure in inert gas and
without any catalyst of the following di- and polycyclic compounds:

1,2-dihydronaphthalene, 1,2,3,4-tetrahydronaphthalene (tetraline),
decahydronaphthalene (decaline), 1- and 2-naphtols, 1,2,3,4-tetra-
hydro-1-naphtol, 5,6,7,8-tetrahydro-1-naphtol, cisdecahydro-1-
naphtol, perhydroindane, perhydrofluorene, perhydropyrene,
9,10-dihydrophenanthrene, 1,2,3,4,5,6,7,8-octahydrophenanthrene,
perhydrophenanthrene and phenanthrene.

The experimental devices and results of some of those studies were
already published (6,7,8,9).

Comparison between B.T.X. and ethylene yields obtained by thermal
cracking of tetraline and decaline is given in fig.7. It was de-
monstrated that cracking mechanism of partially hydrogenated
naphthalene is completely different of what happens with decaline.
In the first case the main cracking reaction is dehydrogenation
leading back to naphthalene (Equation 1). Two other pathways,
less important, occur at the same time. They can explain the for-
mation of indene and of the small amounts of monocyclic aromatic
(Eq. 2 and 3).
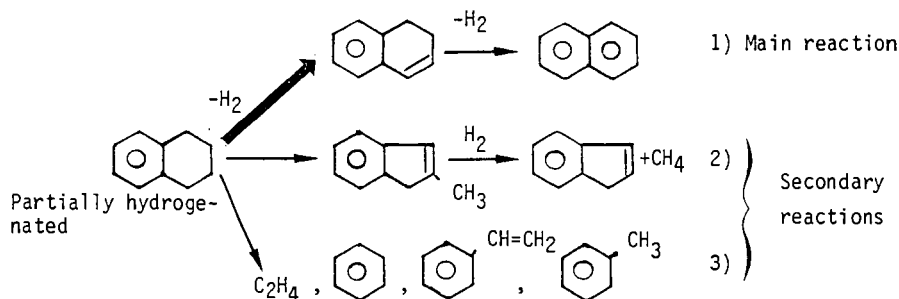
For the perhydrocompounds, on the contrary, the main reaction is
the opening of one or two cycles with formation of alkylmonocy-
clic compounds whose subsequent dehydrogenation gives the corres-
ponding aromatics. At the same time, C_2H_4 and H_2 are the major
constituents of the gas phase. Smaller amounts of $1,3-C_4H_6$,
1,7-octadiene, C_3H_6 and C_4H_8 are also observed. It was shown in
previous work that the light olefines react to give benzene and
toluene above 750°C (10,11,12).
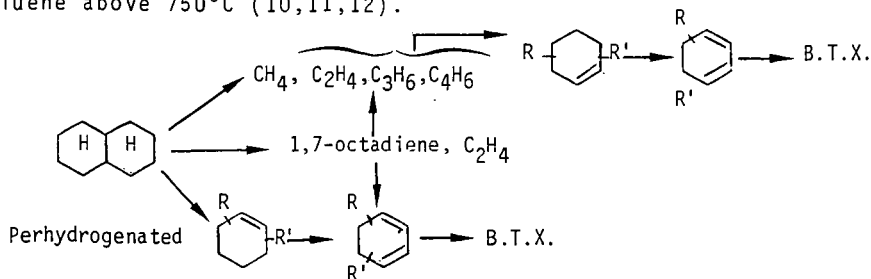
The influence of an hydroxyl group on thermal behaviour of dicyclic compounds was studied by cracking the naphtols, the tetrahydronaphtols and decahydro-1-naphtol. Rësults obtained show that two cracking mechanismes can be considered for naphtols. The first one is decarbonylation, similar to what was demonstrated to happen with phenol (13). Indene is formed. The second one is a dehydroxylation leading to naphthalene. The hydroxyl group position has a relative importance on the contribution of both of them.
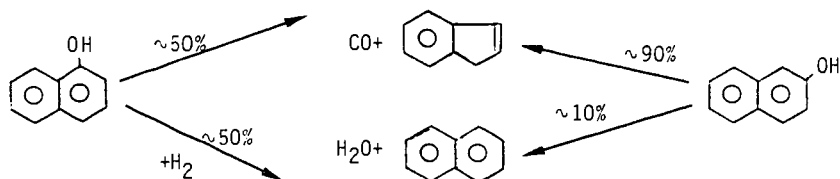
In the case of naphtol partially hydrogenated, the OH group can be located either on the aromatic ring or on the saturated one. Therefore, thermal cracking of 5,6,7,8-tetrahydro-1-naphtol and 1,2,3,4-tetrahydro-1-naphtol was performed. The main thermal degradation reaction was, in the first case, dehydrogenation into 1-naphtol, undergoing subsequently the above described reactions. B.T.X. and C_2H_4 production is low. Those different degradation pathways of 5,6,7,8-tetrahydro-1-naphtol can be summarized as follow :
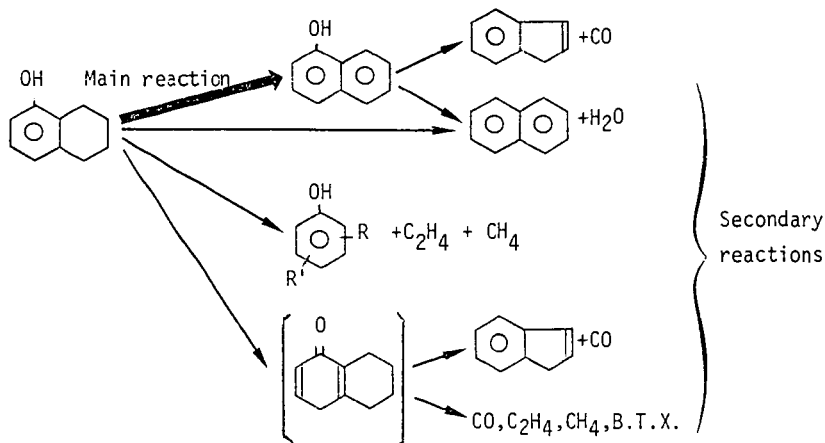
Concerning 1,2,3,4-tetrahydro-1-naphtol, the main degradation reaction is a dehydroxylation with subsequent dehydrogenation into naphthalene. The presence of an hydroxyl group located on the saturated ring makes the rupture of the C-C bond easier, increasing the B.T.X. production. The different mechanismes are summarized as follow.
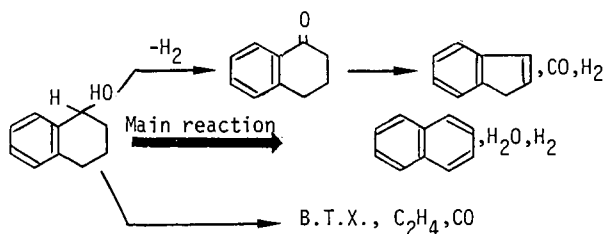
The main cracking reaction of decahydro-1-naphtol is similar to that of decahydro-naphthalene : C-C bond ruptures leading to ole-fines and cycloolefines, together, in this case, with CO elimina-tion. The obtained olefines give easily B.T.X. A secondary reac-tion of partial dehydrogenation leading to indene formation oc-curs simultaneously and explains the lower B.T.X. yield compared with decahydronaphthalene.
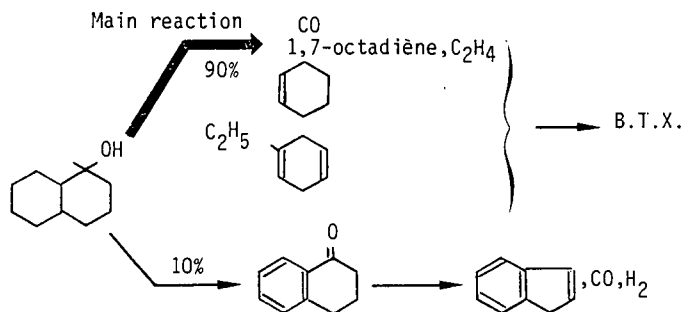
Comparison between B.T.X. and ethylene yields obtained by thermal cracking of the hydrogenated naphtols is given in fig. 8.

It can be seen that the dicyclic perhydrocompounds lead to much higher B.T.X. yields than those of the partially hydrogenated pro-ducts. The influence of the hydroxyl group is apparent when compa-ring tetrahydronaphtols and tetrahydronaphthalene. The B.T.X. yield of the two tetrahydronaphtols are higher than that of te-trahydronaphthalene. The hydroxyl position has also a marked ef-fect. Located on the saturated ring, the B.T.X. yield is higher than when the OH group is on the aromatic ring.

Decahydronaphtol gives again higher B.T.X. yield but, due to a se-condary dehydrodecarbonylation reaction, it reaches 24 W% against 34 W% for decahydronaphthalene.

As polycyclic model substances, phenanthrene and 3 hydrogenated derivatives (di-, octa- and perhydrophenanthrene), perhydrofluo-rene, perhydroindane and perhydropyrene have been cracked in the same conditions. Detailed results are available but not given in this paper for lack of time. The maximum yields of B.T.X. and ethylene are given for all of them in table IV.

It can be seen that all the perhydrocompounds give excellent yields of monocyclic aromatics and of ethylene, whereas the cor-responding partially hydrogenated compounds show predominantly dehydrogenation, leading back to the aromatic starting hydrocar-bon. The hydrogen saturation of all the polycyclic compounds men-tioned, even in the case of pyrene with his 4 condensed aromatic rings, weakens the C-C bonds. It makes possible the rupture of the cycles, with light olefines production. Above 750°C, they contribute to an additional benzene formation as demonstrated in earlier work.

B.T.X. 1,1	3,8	34,0
C_2H_4 -	2,9	18,9
B.T.X. 15,6	8,2	23,9
C_2H_4 2,6	2,5	17,6
B.T.X. 1,3	1,3	38,3
C_2H_4 0,8	3,6	18
B.T.X. -	33,6	30,2
C_2H_4 -	~ 15	33
B.T.X.	27,3	
C_2H_4	17	

Table IV : Optimum B.T.X. and C_2H_4 yields (in W% of injected compounds) obtained by thermal cracking of di- and polyhydroaromatics.

As to show in wich position of the starting molecule, cracking occurs first, polycyclic compounds labelled in specific position with ^{14}C and ^{3}H have been used. The radioactivity of the cracking products is measured by radiochromatography. Phenanthrene and perhydrophenanthrene are labelled in position 9 with $^{3}_{1}H$, and in positions 9 and 10 with $^{14}_{6}C$.

The radioactive ^{3}H or ^{14}C content in the cracking products is expressed as :

$$\frac{\text{molar specific activity of a given compound}}{\text{molar specific activity of the starting labelled compound}} \quad \text{in} \quad \left(\frac{\text{mCi/mmole}}{\text{mCi/mmole}}\right)$$

Cracking of phenanthrene 9-^{3}H and of phenanthrene -9,10 ^{14}C

Table V gives composition and tritium content of the cracking products.

Gas phase	Composition (M %)			^{3}H content		
	875°C/2s	890°C/2s	900°C/2s	875°C/2s	890°C/2s	900°C/2s
Hydrogen	92,5	92,3	93,6	0,37	0,27	0,21
Methane	6,9	7,3	6,2	1,16	0,85	0,76
Ethylene	0,4	0,3	0,2	0,82	0,51	0,39
Ethane	0,05	0,07	0,03	1,36	0,66	0,57
Acetylene	Tr.	Tr.	Tr.			
Propene	-	Tr.	Tr.			
Liquid phase	850°C/2,5s	875°C/2s		850°C/2,5s	875°C/2s	
Benzene	0,7	0,1		0,57	-	
Indene	0,5	0,3		0,99	0,47	
Naphthalene	3,6	1,6		0,77	0,90	
Fluorene	0,5	0,5		0,39	0,32	
Phenanthrene	91,6	95,0		1,02	1	
Pyrene	0,3	0,4		-	1,70	

Table V : Composition and tritium content of cracking of phenanthrene 9-^{3}H

The tritium content in hydrogen is higher for low cracking yield. This means that there is preferential rupture of C-H bond in position 9. This is in agreement with what is admitted in litterature where Beckwitt and Thompson (14) give the following reactivity position sequence in phenanthrene : $9 > 1 > 3 \simeq 2$. With increasing pyrolysis temperature the formation of 1-phenanthryl radical and even 2- and 3-phenanthryl radicals leads to a reduction of ^{3}H content in hydrogen. The ^{3}H content of methane is high, what demonstrates an important contribution of the ^{3}H located on C_9.

Cracking of phenanthrene -9,10 ^{14}C at 885°C give ^{14}C content of 0,39 in CH_4, 0,52 in naphthalene, 0,5 in fluorene and 1 for the uncracked phenanthrene.

The fluorene and methane formation, the only considered here, starts with the elimination of one C and two H in position 9. The hypothetical intermediate would be a fluorenyl biradical.

$^{14}C = 1$
$^3H = T = 1$

$^{14}C = 0,5$ $^{14}C = 0,5$ $+H_2$ (T = 0,37)
T = 0   T = 1

$+H_2$ (T = 0,37)

$^{14}C = 0,5$ +   *CH_3T
T = 0,37

$^{14}C = 0,5$
T = 1,37

Measured : $^{14}C = 0,51$ $^{14}C = 0,4$ and $0,48$
T = 0,33   T = 1,16
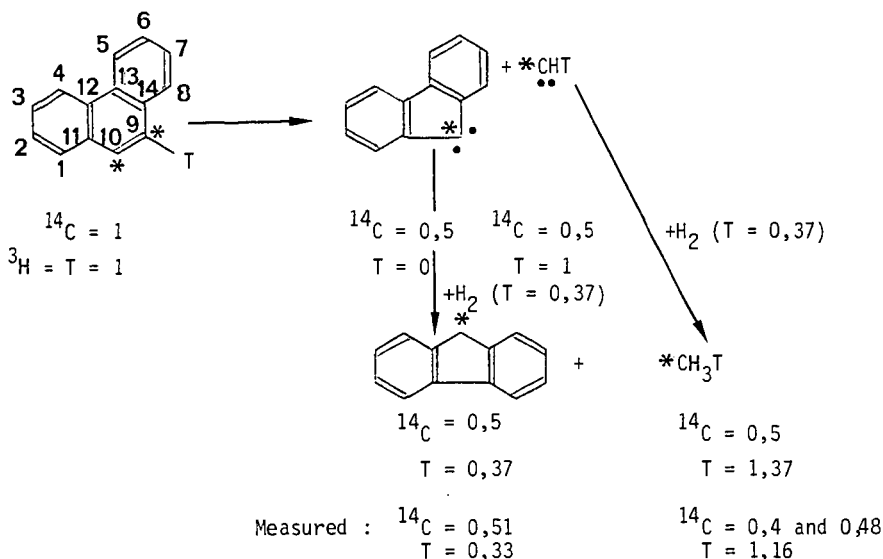
The intermediate fluorenyl biradical is hydrogenated by the hydrogen of the gas phase, whose tritium content is 0,37. Thus, the theoretical tritium content of the fluorene should be 0,37, as 1 mole H_2 is needed. The measured values are in very good agreement with this as ^3H content found was 0,33 and ^{14}C 0,51. For CH_4, measured content was 1,16 for ^3H, and 0,4-0,48 for ^{14}C. The ::CHT biradical has taken one of the two radioactive carbon and all the tritium. His ^{14}C content is 0,5 and ^3H content 1. Hydrogenation of ::CHT to ::CH_3T needs one mole H_2 whose ^3H content is again 0,37. Thus, the total content is 1,37. This value is to compare with 1,16 measured. This lower value is due to the fact that not all the CH_4 is originated in this way.

Similar mechanismes were elaborated for some of the other minor constituents of the liquid phase : naphthalene and benzene. They will be available in more detailed publications.

- Cracking of perhydrophenanthrene -9,10^{14}C

Table VI shows the composition, yields of cracking gaseous and liquid phases, and the respective ^{14}C content of the cracking compounds obtained at 750°C and 2s for perhydrophenanthrene -9,10^{14}C.

Experimental results show that no phenanthrene nor hydrophenanthrene are formed : there is no direct dehydrogenation of perhydrophenanthrene as is observed for the hydrophenanthrene. The C-C rupture happens before the C-H rupture. The H_2 production is due to subsequent dehydrogenation of the monocyclicperhydro-or hydrcaromatics.

	Composition(M%)	Yields	^{14}C content
	Gas phase	(M%)	$\left(\dfrac{mCi/mM}{mCi/mM}\right)$
H_2	25,7	103,5	-
CH_4	26,8	109,5	0,14
C_2H_4	32,1	131,1	0,12
C_2H_6	5,8	23,8	0,17
C_3H_6	5,9	24,0	0,18
C_3H_8	0,4	1,5	-
C_4H_8	3,7	15,1	-
	Liquid phase	(M%)	$\left(\dfrac{mCi/mM}{mCi/mM}\right)$
Benzene	33,4	33,8	0,36
Toluene	18,3	18,4	0,60
Ethylbenzene	0,9	0,9	0,71
m,p-xylenes	2,8	2,8	0,74
o-xylene	0,6	0,6	0,74
Styrene	6,2	6,3	0,77
Naphthalene	9,6	9,7	0,87
Perhydrophenant.	-	-	1
Other compounds	28,2	28,6	

Table VI : Composition, yields and ^{14}C content obtained by cracking of perhydrophenanthrene -9,10^{14}C (T° 750°C, t = 2s)

Considering also that C_2 and C_3 olefins are detected in the gas phase as soon as the cracking begins two possible pathways can be considered.
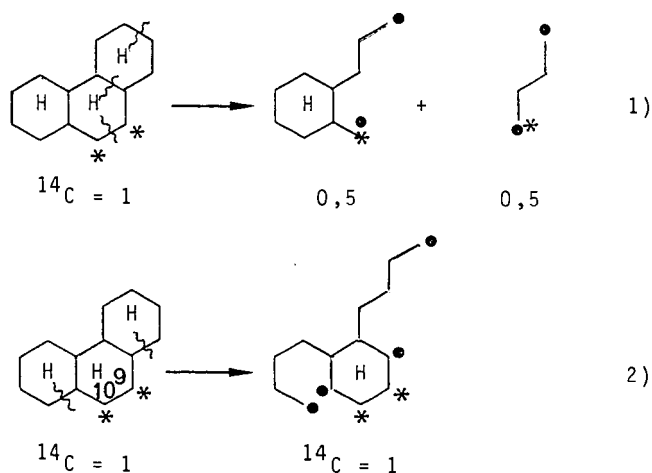
The ^{14}C contents of the intermediate species are indicated. Let us consider benzene and toluene formation. Mechanism 1), followed by dealkylation and dehydrogenation of the remaining cycle, leads to inactive benzene and active CH_4 ($^{14}C=0,5$). Mechanism 2) leads to a benzene with a ^{14}C content of 1. The benzene ^{14}C content measured was 0,36. Thus pathways 1) and 2) contribute respectively for 2/3 and 1/3 to the benzene formation. This leads to the conclusion that in this perhydrocompound there is a preferential rupture between the carbons, in 9 and 10 position.

For toluene, the ^{14}C content measured was 0,6, twice that of benzene. This is in good agreement with what was said for the benzene formation. Pathway 1) is giving toluene with ^{14}C content of 0,5, after elimination of a C_3 radical from the intermediate. Pathway 2) gives as for benzene, toluene with ^{14}C content of 1, after a C_3 and a C_4 elimination and dehydrogenation of the cycle. Considering that as found for benzene, pathway 1) contributes for 2/3 and pathway 2) for 1/3 to the first step of the reaction, the theoretical activity of toluene should be a ^{14}C content of (2/3 x 0,5) + (1/3 x 1) = 0,66. as to compare with the measured content of 0,60.

Concerning the radioactivity in ethylene which is one of the major products in the gases, the measured ^{14}C content was 0,12. This demonstrates that ethylene is not formed by preferential elimination of the carbon atom in the 9 position.

5. CONCLUSIONS

During hydrocarbonisation of coal, the main reaction below 750°C is hydrodealkylation. This makes possible to optimalize the B.T.X. and low boiling phenols formation. Dehydroxylation of the phenols is only important above 750°C giving an increase in water and additionnal light aromatics. The oxygen content of the coal, corresponding to the hydroxyl group is not hydrogen consuming below 750°C, as it is the case at high temperature where conversion to methane is the goal of the process. Dealkylation of alkylphenols and alkylaromatics explains the almost linear increase with temperature of methane. Hydrogen pressure prevents reassociation of free radicals, not only in the pyrolysis of coal itself, but also in the postcracking process. Due to this fact, naphthalene and other heavy polycyclicaromatics yields remain low, compared to what is found when carbonisation is performed under pressure of an inert gas.

The sulfur elimination in the char depends of the nature of the mineral constituents of the coal. $CaCO_3$ and $MgCO_3$ under hydrogen pressure react with sulfur compounds to form CaS. Calcium is not associated with sulfur in the coal, except for some $CaSO_4$. But in the char, on the contrary, calcium is combined with the sulfur. The concentration of $CaCO_3$ is however not sufficient to fix all the sulfur. Pyritic sulfur is eliminated at high temperature. But it seems possible that this sulfur is trapped on $CaCO_3$. High sulfur containing coals will only be well desulfurized under hydropyrolysis conditions if their ashes are poor in CaO and MgO.

Thermal pyrolysis at atmospheric pressure under inert gas demonstrates that all perhydropolycyclic hydrocarbons are easily cracked into monocyclic aromatics and ethylene. The mechanism of the ring opening, in the case of perhydrophenanthrene, labelled with carbon 14 in 9 and 10 position, is a rupture of the C-C bond between 9 and 10. This conclusion is in good agreement with the perhydrocompounds cracking results. No formation of naphthalene was observed at low conversion yields of tricyclic perhydrocompounds, what would be the case if opening of the external ring would be the main reaction pathway. Hydropolycyclic aromatics

undergo mainly dehydrogenation leading back to the corresponding aromatic starting compound.

The low stability of the perhydropolycyclic compound makes possible to convert industrially the hydropolycyclic compounds, abundant in coal liquid hydrogenates, into benzene and ethylene, two compounds of major importance in industrial organic chemistry. The polycyclic aromatics have to be saturated by additional hydrogenation to the corresponding perhydrocompounds, wich can then be directly cracked at 800-850°C for 0,5s residence time, into benzene, ethylene, methane and hydrogen. The process is hydrogen self sufficient.

This work is part of the European Community Program on the "Chemical and Physical Valorisation of Coal".
Coworkers are B.BETTENS, C.BRAEKMAN-DANHEUX, P.BREDAEL, S.FURFARI, F.NINAUVE and TRAN HUU VINH.

REFERENCES

1) R.J. BELT, L.A. BISSETT, Report (1978)(DOE), MEJC/RI-79/2

2) H.D. COCHRAN, Jr
   ACS Symp.Ser. (1979), 110, 37-54

3) G. FYNES, W.R. LADNER, J.O.H. NEWMAN
   to be published in "Progress in Energy and Combustion Services"

4) R. CYPRES
   Preprints of the Contribution to the Fifth International Conference on Coal Research, Vol.II, B-2, 23-40, Düsseldorf (1980)

5) A. KOROSI, H.N. WOEBCKE and P.S. VIRK
   Am.Chem.Soc.div.Fuel Chem. (1976), 21 (6), 190-197

6) P. BREDAEL and D. RIETVELDE
   Fuel (1979), 58, 215-218

7) P. BREDAEL and TRAN HUU VINH
   Fuel (1979), 58, 211-214

8) C. DELAUNOIS
   Ann.Mines de Belgique (1972), 2, 93-107

9) R. CYPRES and P. BREDAEL
   Fuel Process.Techn. (1980), 3, 297-311

10) E. GIL-AV, J. SHABTAY and F. STECKEL
    J.Chem.Eng.Data (1960), 5, 98-105

11) P. BREDAEL
    Ann.Mines de Belgique (1974), 28, 1-6

12) R. CYPRES and C. BRAEKMAN-DANHEUX
    Ann.Mines de Belgique (1974), 11, 1109-15

13) B. BETTENS and R. CYPRES
    Tetrahedron (1974), 30, 1253-1260

14) A.L.J. BECKWITT and M.J. THOMPSON
    J.Chem.Soc. (1961), 73

Hydrogenopyrolysis at 30 bar H$_2$ pressure

1 bar conventional carbonisation

% vol.

CH$_4$

CH$_4$

C$_2$H$_6$

C$_2$H$_6$

500 600 700 800 900 1000 T°C
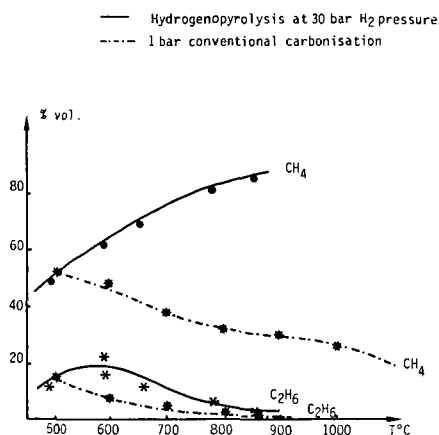
FIG. 1 : GAS COMPOSITION AS FUNCTION OF TEMPERATURE.

P$_{H_2}$ = 30 bar

W%

Light aromatics

B.T.X.

P.C.X.
Benzene

Naphthalenes

Xylenol
Cresol
Phenol

500 600 700 800 900 T°C
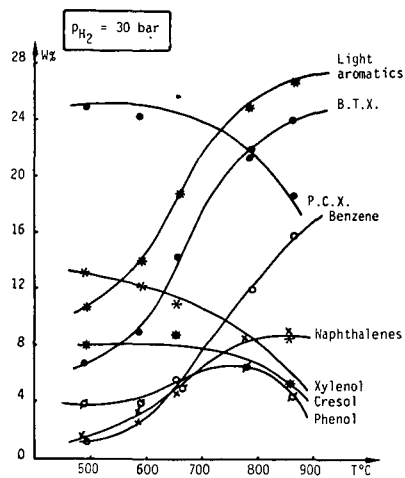
FIG. 2 : OIL COMPOSITION AS A FUNCTION OF TEMPERATURE.
τ = 60s , <500 µm

W% T° 580°C.

P.C.X.

Light aromatics

B.T.X.

Naphthalenes

0 10 20 30 40 50 60 70 80 90 100 bar H$_2$
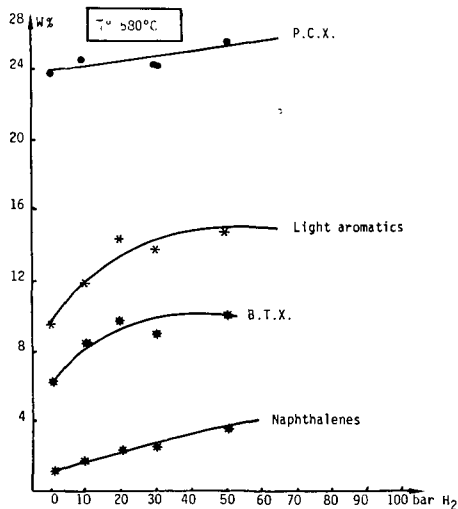
FIG. 3 : B.T.X. AND NAPHTHALENES YIELDS AS A FUNCTION OF H$_2$ PRESSURE
(W% OF DIL)
τ = 60s , <500 µm

0   30   t (min.)

% S loss

50 20   10 1 atm.

100

50

0

500   950   T°(C)
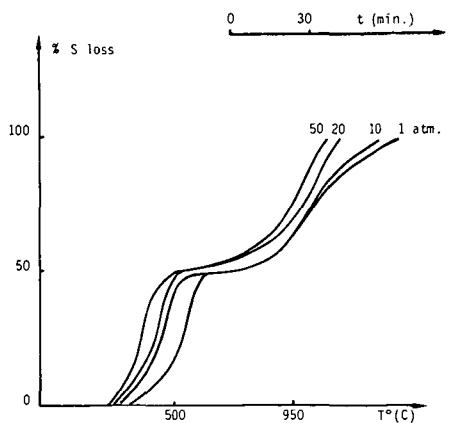
FIG. 4 : REDUCTION OF FeS$_2$ UNDER H$_2$ PRESSURE

56
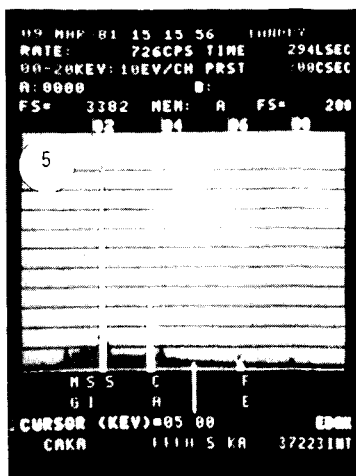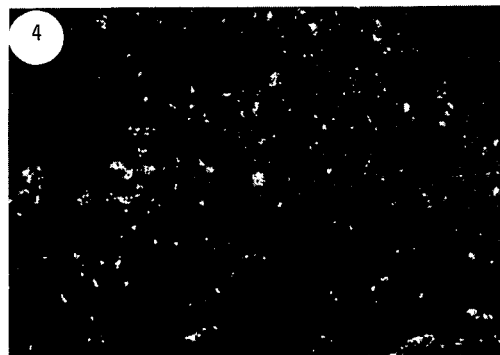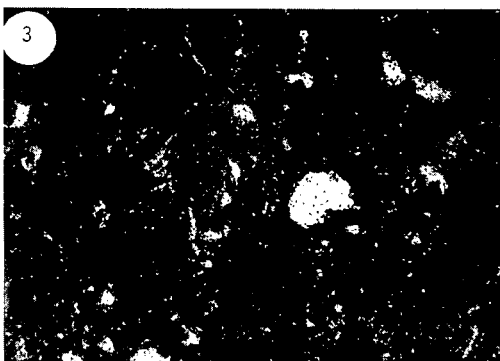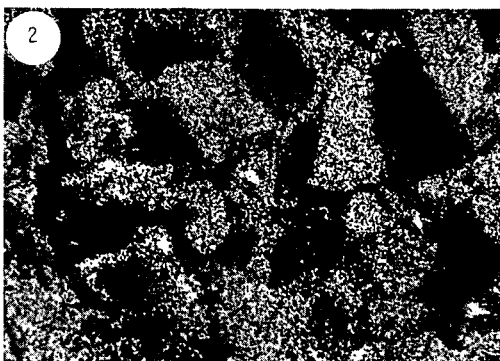
Fig.5 : SEM images

SULCIS COAL (56,4% VM, 12,9% ASH,
4,45% S_t)

before pyrolysis

1. Coal
2. S x-ray distribution image
3. Ca x-ray distribution image
4. Fe x-ray distribution image
5. x-ray spectrum

57
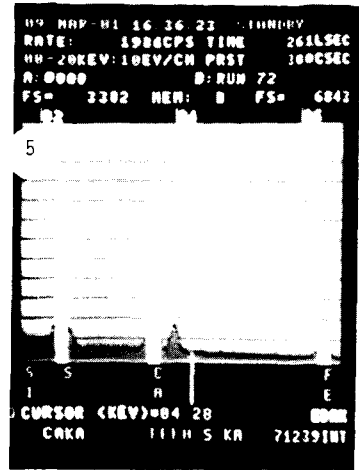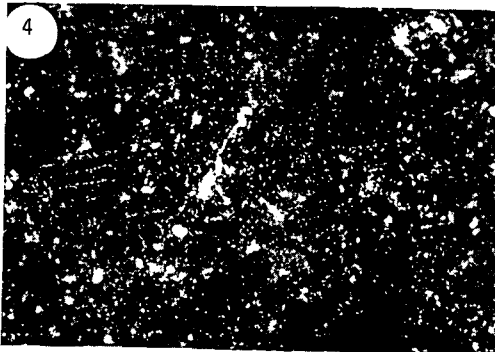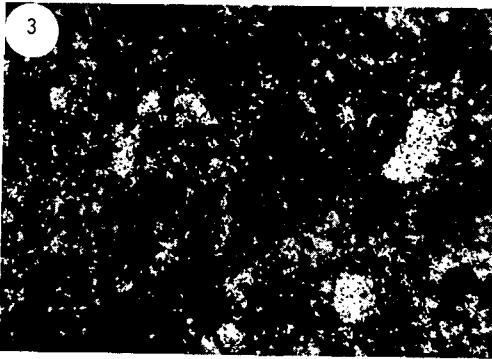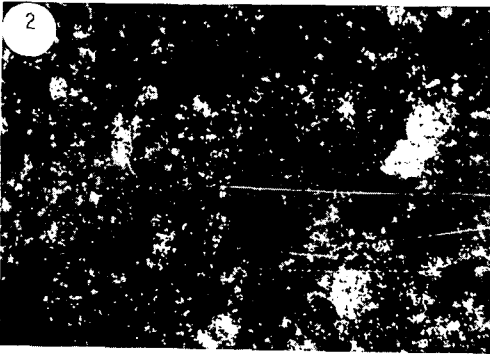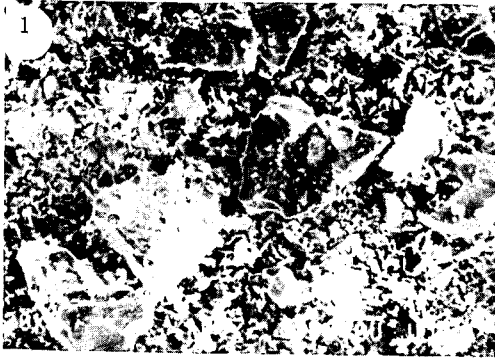
Fig. 6 : SEM images

SULCIS after Hydrogenopyrolysis
850°C - 30 bar H_2

1. Char
2. S x-ray distribution image
3. Ca x-ray distribution image
4. Fe x-ray distribution image
5. x-ray spectrum

1. B.T.X. (5,6,7,8 -tetrahydro-1-naphtol)
1'. C_2H_4 (5,6,7,8 -tetrahydro-1-naphtol)
2. B.T.X. (1,2,3,4 -tetrahydro-1-naphtol)
2'. C_2H_4 (1,2,3,4 -tetrahydro-1-naphtol)
3. B.T.X. (cis-1-decalol)
3'. C_2H_4 (cis-1-decalol)

FIG. 8 : PYROLYSIS OF HYDRONAPHTOLS
B.T.X. AND ETHYLENE YIELDS (W%)

B.T.X. (decaline)

C_2H_4 (decaline)

B.T.X. (tetraline)
C_2H_4 (tetraline)
B.T.X. (1,2-dihydro-napht.)

FIG. 7 : PYROLYSIS OF HYDRONAPHTHALENES
W% YIELDS IN B.T.X. AND ETHYLENE

AN IN-SITU EXPERIMENTAL OBSERVATION AND PREDICTIVE MODEL OF FREE RADICAL FORMATION UNDER LIQUEFACTION REGIME CONDITIONS

By

L. Petrakis, D. W. Grandy and G. L. Jones
Gulf Research & Development Company
P. O. Drawer 2038
Pittsburgh, Pennsylvania 15230

Over the past 24 years, there have been many studies of free radicals in coal by electron spin resonance (ESR) techniques directed towards learning something about coal's chemical structure, petrography and geology (1). More recently, some of the more modern and potentially useful magnetic resonance techniques such as ENDOR have been used to probe the structure of coal (2). Beyond providing structural information and being a natural product of coal metamorphosis, the free radicals in coal, especially those formed during the heating of coal, are believed to play a key role in liquefaction and pyrolysis reactions (3). Our goal is to gain a more complete understanding of the effect of liquefaction process variables on the free radicals in coal and try to find what connection free radicals have with liquefaction, i.e. to answer the question: are free radicals the key to coal liquefaction? We have used ESR spectroscopy to study the free radicals in a variety of coals and vacuum pyrolyzed coals (4), free radicals in the various product components from the solvent refined coal (SRC-I) process (5), and the free radicals in a variety of coal solvent slurries reacted under a variety of conditions (6, 7). Coal macerals, or the various organic constituents of coal analogous to minerals in rocks have also been studied by ESR spectroscopy in our laboratory after a variety of pyrolysis (6) and liquefaction treatments (9). All of these experiments were performed as most have been done in the past, i.e. at room temperature after the reactions had taken place. Recently we have developed

a high temperature, high pressure ESR cavity to study the free radicals in coal during liquefaction (10, 11, 12).

We have used this high temperature, high pressure ESR cavity for detailed study of the effects of process variables on the free radicals in Powhatan #5 coal during liquefaction. The procedure used was a 2^5 factorial design involving two levels each of temperature (400 and 460^oC), gas (H_2 and N_2), pressure (8.2 and 11 MPa), solvent (tetralin and SRC-II heavy distillate derived from Powhatan #5 coal) and heating time 3 and 15 minutes to reaction tempera- ture. Free radical spectral parameters were monitored continually from about 2 minutes after reaction temperature was reached, up to one hour. After finding, from this work, that temperature and solvent were the two most important variables, we proceeded to study these variables in more detail, using 400, 425, 400, 450, 460 and 480^oC and tetralin, naphthalene and SRC-II as liquefaction solvents. The data from the study of process variables effects and the more detailed study of temperature and solvent effects were analyzed with the aid of a regression model.

Free radical measurements on the coal solvent slurries are done under liquefaction conditions, i.e. in-situ, using a high temperature, high pressure ESR cavity. The details of the cavity and its operation have been published previously (11, 12). The cavity system is basically a cylindrical brass TE_{011} X-band cavity with internal modulation coils and internal axial heater inside a water-cooled berrylium copper pressure vessel. Samples are prepared in 4 mm OD, 2.5 mm ID quartz tubes by placing 0.5 g of Powhatan #5 coal in the bottom of the tube and injecting 0.5 g of tetralin or SRC-II heavy distillate (SHD). In the naphthalene experiments, the coal and naphthalene were premixed at 1:1 by weight and then poured into the sample tube. Temperature measurement is by a thermocouple imbedded in the sample. Typically, several spectra are recorded

before heating and then continuously from about 4 minutes after heating was begun up to one hour. Spin concentration measurements are made relative to the signal from a $CuSO_4 \cdot 5H_2O$ reference on the internal wall of the cavity. The calculations for spin concentration and its temperature correction are outlined in detail elsewhere (12, 13). Data are normally displayed as corrected (to 20^oC) spin concentration versus time plots.

About 45 experiments were done using Powhatan #5 coal to screen the major process variables, such as solvent, temperature, gas type, pressure, and heating time. The data from these experiments were used to formulate a regression model to sort out the major effects and their inter-actions (13). Table I summarizes the results of this model. Reaction time alone was found to be insignificant. Temperature was found to be the most significant variable, accounting for about half of the effects present in the model. When solvent and solvent gas interactions are added in with tempera-ture, almost 90% of the variation of the data is accounted for. Heating time, pressure and gas type alone or in combination with temperature have relatively minor effects on the data.

Based on these observations, it was decided that temperature and solvent type warranted further investigation. Experiments at 425, 440, 450 and 480^oC were added as well as a complete series of experiments with Powhatan coal using naphthalene as the liquefaction solvent. Heating time was fixed at 3 minutes, pressure at 1600 psig and hydrogen was used in all of the additional experiments. Figure 1 shows the variation of spin concentration as a function of time for the three coal-solvent systems at 400^oC. The points are experimental data and the solid lines are the spin concentrations predicted by the regression model. These are not fitted curves. At time 0,

the slurries are unheated. All points at t>0 are at the desired experimental temperature. Note that the spin concentration in the tetralin solvent experiments is essentially the same as the unheated coal and that all the SHD and naphthalene experiments are somewhat higher. Figure 2 is a similar plot of the experimental data and predicted spin concentrations at 480^OC. Here the spin concentration of all three Powhatan coal-solvent slurry systems is much higher than that of the unheated slurries. Again, the same ordering of spin concentration among the solvent systems is observed. The relative order of spin concentration in the solvents, tetralin<SHD<naphthalene, is believed to be due to the relative hydrogen donor capabilities of the three solvents. Naphthalene is a pure aromatic and should have no donatable hydrogens. Tetralin has four donatable hydrogens and SRC-II heavy distillate, although highly aromatic, would be expected to have some donatable hydrogen. Figures 3, 4 and 5 are spin concentration versus time plots displaying the data for all six temperatures used for each of the solvents. The naphthalene, Powhatan coal experimental data, shown in Figure 3, shows the general trend to higher spin concentration with increasing temperature. The data at 400, 425 and 440° fall very close. There is a similar bunching at higher values for the 450 and 460° data. The spin concentration found at 480° is considerably higher than all the other data from the lower temperatures. The SHD Powhatan coal experiments, shown in Figure 4, show a similar ordering of spin concentration among the 6 temperatures, however, the values at the corresponding temperatures are lower than in the previous figure depicting the naphthalene experimental data. Figure 5, showing plots of spin concentration versus time for the tetralin solvent experiments, has a similar trend of increasing spin concentration with temperature, however, the order of the 460 and 480^OC data are reversed compared to the other two solvents. From these data and a few data

taken under similar conditions at 470°C, there appears to be a maximum in spin concentration around 460°C in the Powhatan coal tetralin slurry system.

Discussion and Conclusions

1. In general, the coal free radicals are quenched in following the order of naphthalene<SHD<tetralin. This conclusion agrees with our expectations which are based upon the amount of donatable hydrogen present in the three solvents. The rate of free radical formation is assumed to be only temperature dependent. This is based on previous extensive pyrolysis experiments with coals and coal macerals. The observed free radical concentration depends on the competing effects of free radical formation and free radical quenching. The latter, unlike the former, is solvent dependent. The solvent dependency will be determined both by the amount of donatable hydrogen that is available as well as by the ease with which the free radical quenching hydrogen can be transferred to the coal free radicals.

2. The free radical concentration of the liquefaction slurry generally increases with increasing temperature. This is strictly true for the naphthalene and SHD experiments and is followed by the tetralin experiments up to 460°C where an apparent maximum is reached, with the spin concentration decreasing then at higher temperatures. The general increase in spin concentration with temperature is expected due to the greater thermal energy available for bond breaking. From the results of the correlative model, we find that about half of the variation in the spin concentration is due to temperature alone. Temperature and solvent interactions account for 70% of the observed effects.

3. The spin concentration is dependent upon reaction time and this dependence is also influenced by solvent and temperature. At $400^{\circ}C$, the relative slopes of the spin concentration versus time curves, from 0.1 to 1.0 hr., are 15, 5 and $0x10^{18}$ spins/g per hour for the naphthalene, SHD and tetralin experiments, respectively, demonstrating the solvent dependence. At 480°, the slopes have increased to 40, 35 and $20x10^{18}$ spins/g per hour for the same three solvents.

4. From the results of the full correlative model, we find that temperature, solvent and residence time and their interactions account for about 90% of the effects noted in the free radical concentration. Gas type has some minor significance as does pressure. Heating time has a negligible effect.

ACKNOWLEDGMENT

References

1. H. T. Schamler and E. duRutter in "Chemistry of Coal Utilization",
   Supp. Vol. (H. H. Lowry Ed.) John Wiley and Sons, Inc. New York,
   1963 pp 78-85.

2. H. L. Retcofsky, M. R. Hough and R. B. Clarkson, ACS Fuel Div. Preprints,
   Vol. 24, No. 1, 1979 p 83.

3. R. C. Neavel, Fuel 55, 237 (1976).

4. L. Petrakis and D. W. Grandy, Anal. Chem. 50, 303 (1978).

5. D. W. Grandy and L. Petrakis, Fuel, 58, 239 (1979).

6. L. Petrakis and D. W. Grandy, ACS Fuel Div. Preprints, Vol. 23, No. 4,
   1978 p. 147.

7. L. Petrakis and D. W. Grandy, Fuel, 59, 227 (1980).

8. L. Petrakis and D. W. Grandy, Fuel, 60, 115 (1981).

9. L. Petrakis and D. W. Grandy, Fuel, 60, 120 (1981).

10. L. Petrakis and D. W. Grandy, Nature

11. D. W. Grandy and L. Petrakis, J. Mag. Res. 41, 367 (1980).

12. L. Petrakis, D. W. Grandy, R. G. Ruberto and N. L. Carr, "Fundamentals
    of Coal Depolymerization", Quarterly Report, DOE/ET/14940-2, NTIS,
    Springfield, VA 1980.

13. L. Petrakis and D. W. Grandy, submitted to Fuel.

TABLE I

GENERAL CORRELATION MODEL

Variables Effects*	Sum of Square of Each Term	Fractional Contribution of Each Term		Fractional** Probability of Null Hypothesis (i.e., term not significant)
C_1•time•temperature	119455	.480		.0001
C_3•time•temperature•solvent	51511	.207	.897	.0001
C_2•time•temperature•solvent•gas	52284	.210		.0001
C_4•time•pressure	8025	.032		.0001
C_5•time•temperature•heating rate	6556	.026	.094	.0001
C_6•time•temperature•gas	4739	.019		.0001
C_7•time•temperature•pressure•gas	4355	.017		.0001
C_8•time•pressure•heating rate	652	.003		.0129
C_9•time•temperature•pressure	565	.002		.0205
C_{10}•time•heating rate	358	.001		.0649
C_{11}•time	256	.001		.1184

Total Number of Points = 773; Total Data Sum of Squares = 328302; Total Model Sum of Squares = 248755; Error = 79548; R-Square (Model SOS/Total SOS) = 0.758

* Corrected Spin Concentration = Intercept + Sum of Terms.

** The lower the number, the higher the probability that the variable effects are real.

SPIN CONCENTRATION VS. ELAPSED TIME
POWHATAN #5 COAL, 1600 psig H_2, 400°C 3 min HT.
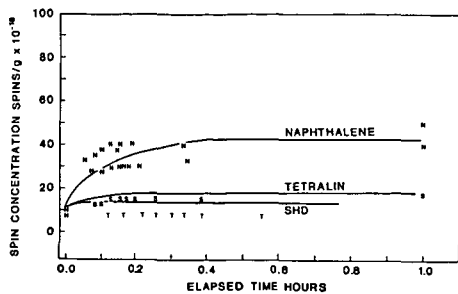
FIGURE 1

SPIN CONCENTRATION VS. ELAPSED TIME
POWHATAN #5 COAL, 1600 psig, 480 °C 3 min HT.
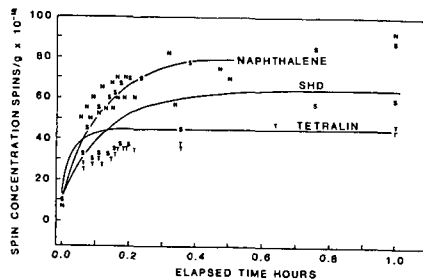
FIGURE 2

SPIN CONCENTRATION VERSUS ELAPSED TIME
POWHATAN #5 COAL AND NAPHTHALENE
1600 psig (11.0 MPa) H_2 3 min HT
AVERAGE VALUES
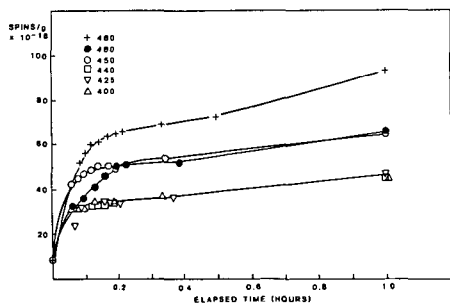
FIGURE 3

SPIN CONCENTRATION VERSUS ELAPSED TIME
POWHATAN #5 COAL AND SRC II HEAVY DISTILLATE
1600 psig (11.0 MPa) H_2 3 min HT
AVERAGE VALUES
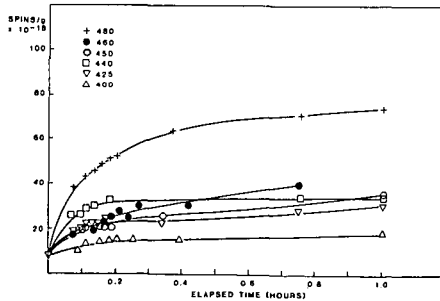
FIGURE 4

SPIN CONCENTRATION VERSUS ELAPSED TIME
POWHATAN #5 COAL AND TETRALIN
1600 psig (11.0 MPa) H_2 3 min HT
AVERAGE VALUES

FIGURE 5

68
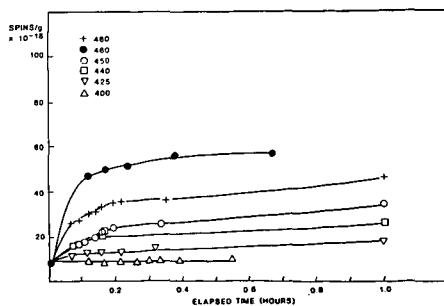
The Catalysis of the Exchange Reactions Between Tetralin-d_{12} and Diphenylmethane by Inorganic Compounds

C.B. Huang, H.-H. King and L.M. Stock

Department of Chemistry
University of Chicago
Chicago, Illinois 60637

Introduction

An array of inorganic compounds have been investigated as catalysts for coal gasification reactions (1,2). The pathways by which these compounds alter the rate and the product distributions in the gasification reaction have not been fully resolved. Whether the most effective catalysts promote the initiation reactions which occur at the threshhold temperatures or the rapid gas forming reactions at the higher ultimate temperatures has not been established. We sought to resolve this point by an investigation of the influence of inorganic substances on the exchange reactions between the hydrogen atoms in the benzylic positions and the hydrogen atoms in the

$$C_6H_5CH_2C_6H_5 + \text{Tetralin-}d_{12} \rightarrow C_6H_5CHDC_6H_5 + \text{Tetralin-}d_{11}$$
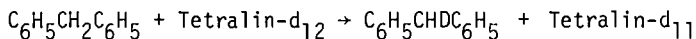
aromatic positions. These exchange reactions proceed slowly at 400°C in the

$$C_5H_5CH_2C_6H_5 + \text{Tetralin-}d_{12} \rightarrow C_6H_5CH_2C_6H_4D + \text{Tetralin-}d_{11}$$
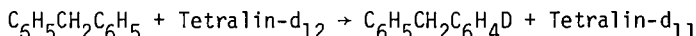
absence of catalysts (3). Both of these reactions may contribute in an important way to the breakup of the coal structure during the gasification reactions shown for the radical initiated decomposition of a 1,3-diphenylpropane:

$$C_6H_5CH_2CH_2CH_2C_6H_5 + R\cdot \rightarrow RH + C_6H_5\dot{C}HCH_2CH_2C_6H_5$$

$$C_6H_5\dot{C}HCH_2CH_2C_6H_5 \rightarrow C_6H_5CH=CH_2 + C_6H_5CH_2\cdot$$
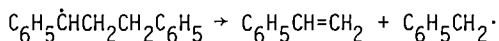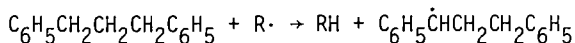
and the acid-catalyzed decomposition of a diphenylmethane with an electrophilic agent, E^+

69
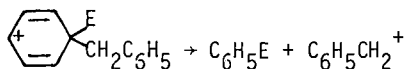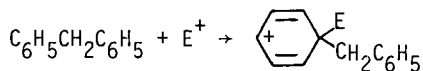
In the absence of a catalyst at 400°C, the free radical exchange reaction between the hydrogen atoms in the benzylic positions occurs much more readily than the exchange reactions of the hydrogen atoms bonded to the aromatic ring (3). Accordingly, we sought evidence for the acceleration of either process in the presence of inorganic compounds.

Results and Discussion

In each experiment, diphenylmethane (0.377 mole) and tetralin-d_{12} (0.377 mole) and a potential catalyst (0.045 mole) were sealed in a glass reactor at ambient temperature. The reactor was submerged in a fluid sand bath at 400°C for the desired reaction interval. After cooling, the organic contents of the reactor were separated from the inorganic reagents and analyzed by gas chromatography and nuclear magnetic resonance. The exchange reaction proceeds to give about 15% of the monodeuterio com-

$$C_6H_5CH_2C_6H_5 + \text{Tetralin-}d_{12} \xrightarrow[\text{30 min}]{400°C} C_6H_5CHDC_6H_5 + \text{Tetralin-}d_{11}$$
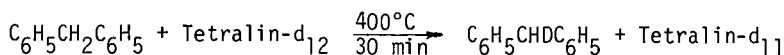
$$15\%$$

pound in 30 minutes in the absence of a catalyst. Lithium, sodium and potassium chloride are ineffectual as expected. Similarly, sodium fluoride, chloride, bromide and sulfate did not accelerate the exchange reactions. Sodium iodide enhanced the benzylic exchange reaction to a minor extent (22%). Iodine and hydrogen iodide accelerate the reaction to a much greater extent.

Lithium, sodium, and potassium carbonate and sodium and potassium bicarbonate do not enhance the exchange reactions. Thus, none of the alkali metal compounds exert any catalytic influence on this exchange reaction at the threshhold temperature of 400°C.

Somewhat similar results were realized with the alkaline earth compounds. Neither calcium oxide or carbonate or barium carbonate or oxide enhance the exchange reaction. Calcium and magnesium chloride are also ineffectual catalysts for the exchange reaction after a 30 minute reaction. However, our preliminary results for reactions carried out for 120 minutes suggest that magnesium chloride enhances the rate of the exchange of the hydrogen atoms of the aromatic nucleus but not the benzylic exchange reaction.

Zinc halides also exert an accelerating influence on the rate of exchange of both the aliphatic and aromatic hydrogen atoms.

Compound	%D in Recovered Diphenylmethane		%D in Recovered Tetralin		
	Ar	α	Ar	α	β
ZnCl$_2$	12	9	54	88	86
ZnI$_2$	37	40	40	28	52

Whereas cadmium chloride is inactive, compounds such as stannous chloride and stannic chloride selectively enhance the rate of exchange of the aromatic hydrogen atoms of diphenylmethane and tetralin-d$_{12}$ at 400°C. Anhydrous vanadium trichloride and ferric chloride and hydrated chromous chloride and hydrated cupric chloride exert a similar effect on the reaction.

Compound	%D in Recovered Diphenylmethane		%D in Recovered Tetralin		
	Ar	α	Ar	α	β
SnCl$_2$	19	0	28	91	91
CuCl$_2$·2H$_2$O	24	5	44	92	92

Other highly reactive compounds such as aluminum chloride and molybdenum (V) chloride cause extensive reactions of the diphenylmethane and the tetralin. Moreover, oxidizing agents, for example, the oxides of lead and iron convert diphenylmethane to benzophenone.

The results obtained at the threshhold temperature of 400°C strongly suggest that catalysts can selectively initiate free radical or electrophilic decomposition reactions of many coal molecules. The diverse character of the results will be emphasized in the presentation.

References

(1) Johnson, J.L., "Kinetics of Coal Gasification," John Wiley and Sons, New York, New York (1979).

(2) McKee, D.W., "Catalyzed Gasification Reactions of Carbon," in "Chem-
     istry and Physics of Carbon" edited by P.L. Walker, Jr. and P.A.
     Thrower. Volume 16, p. 1 (1981).

(3) H.-H. King and L.M. Stock, "Influence of Illinois No. 6 Coal and Coal-
     related Compounds on the Exchange Reaction Between Diphenylmethane
     and Perdeuteriotetralin," Fuel, 59, 447 (1980).

THE RATE AND THE MECHANISM OF CATALYTIC COAL LIQUEFACTION BY IRON SULFIDES: PART I. THE SYSTEM FeS$_x$: H$_2$: H$_2$S, RATES OF REACTION AND SURFACE CONVERSION

By: Attar, A. and Martin, J. B.
Dept. Chem., Eng., N.C.S.U., Raleigh, N.C. 27650

INTRODUCTION

The systems FeS$_2$-H$_2$-H$_2$S and FeS$_2$-hydrogen donor-H$_2$S play a critical role in the catalysis of coal liquefaction by naturally occurring minerals. Consequently, there is a tremendous incentive to understand the exact mechanism and rates of reaction which affect the catalysis of coal liquefaction by FeS$_x$.

Examination of the data available in the literature and studies from our own laboratory suggest that the dominant catalytic action is due to the formation of an intermediate compound, possibly [FeS$_{x+1}$H$_2$] which can react according to the scheme:

$$FeS_{x+1} + H_2 \rightleftharpoons [FeS_{x+1} H_2] \rightleftharpoons FeS_x + H_2S$$
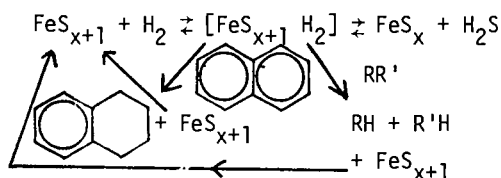
The main function of the FeS$_{x+1}$ is to permit conversion of molecular hydrogen to organically bound hydrogen, either in the form of donor molecules and/or coal derived molecules. The [H$_2$S]/[H$_2$] plays a critical role in this system since its value determines the equilibrium distribution of the active catalytic intermediate, FeS$_{x+1}$H$_2$, and the less active species FeS$_{x+1}$ and FeS$_x$.

This mechanism explains many of the observations in the system coal-solvent-FeS$_2$. The most important facts are:

1. Catalytic action by Fe salts is observed only when H$_2$S is present in the reactor. The level of the catalysis depends on the ratio [H$_2$S]/[H$_2$].
2. Regardless of the starting material, when the FeS$_x$ is allowed to catalyze the reaction long enough, a fixed ratio of Fe to S is achieved, typically of the order of Fe/S $\simeq$ 1/1.09. Such a ratio could be the result of the thermodynamic equilibrium achieved for the coal at the prevailing [H$_2$S]/[H$_2$].
3. The type of pyrite used to catalyze the reaction influences mainly the rate of the initial stages of the reaction but has little effect on the results of long time liquefaction.

Since the ratio [H$_2$S]/[H$_2$] (gas) and the ratio Fe/S (solid) play such a critical role in the liquefaction, it appeared useful to quantitize the rate of the individual reactions involved. To achieve reasonable data, it appeared essential that the same sample of FeS$_2$ be tested so that it would be possible to avoid questions related to the conversion of the surface and so that small differences in reactivity could be determined. In this paper preliminary results are presented on the system FeS$_x$-H$_2$-H$_2$S.

EXPERIMENTAL

In order to have more or less the same surface area and the same surface conditions, a pulsed differential reactor (PDR) was used, similar to that described by Attar (1979). The only difference was that a S.S.

packed bed reactor 1/4" ID x 1 ft packed with -100+120 mesh FeS_2 particles was used as the reactor. Helium was used as the carrier gas and pulses of H_2, H_2S or CO were used to investigate the effect of the surface conversion of the pyrite on its reactivity, the activation energies for the reaction, etc. Figure 1 is a schematic diagram of the reaction system.

In a typical experiment, a pulse of H_2 was injected into the He carrier and the product pulse, which consists of unreacted H_2 and H_2S + S_2 was separated on a Chromosorb 105 column and the components were determined by a TC detector.

ANALYSIS OF THE DATA

The relative rate of reaction, r_j, in the j-th pulse was determined from the consumption of the hydrogen, i.e.,

$$r_j = \frac{W^0_{H_2} - W_{H_2j}}{W^0_{H_2}} \qquad (1)$$

where $W^0_{H_2}$ is the number of moles of H_2 injected and W_{H_2j} are the number of moles of incorporated H_2. The temperature was programmed during most of the experiments, in order to allow the determination of the variations of r_j with the temperature. To a first order approximation, since the surface was barely converted in each pulse, one may write, assuming Arrhenius dependence of the rate constant on the temperature:

$$r_j = k_o \, s \, e^{-\frac{E}{RT}} [\overline{H_2}] \qquad (2)$$

or roughly:

$$\log r_j = \log [1 - \frac{W_{H_2j}}{W^0_{H_2}}] = \log k_o [\overline{H_2}] - \frac{E}{RT} \qquad (3)$$

$[\overline{H_2}]$ is the average concentration of H_2 near the surface and E is the activation energy. Figure 2 shows some of the data obtained. Curves A, B and C were done on the same pyrite sample by successive injection of H_2 pulses in three cycles of heating and cooling of degassed FeS_2. The data indicate that as the surface is being converted, the activation energy rises slightly, from 26.4 to 27.4 kcal/mole for about 1% surface conversion and that the preexponential factor decreases. This is due to the accumulation of FeS_{2-y} near the surface which resists to the diffusion of $S^=$ in the solid (see ref. 2).

Curve D was obtained using a different sample of iron pyrite while curve E was derived with a specially prepared sample of FeS_2. The last curve indicates that sample D is a much more reactive specimen, with an activation energy of 22.7 kcal/mole and a larger preexponential factor than the raw FeS_2.

SUMMARY

A new mechanism is proposed for catalytic coal liquefaction using FeS_x. The mechanism includes many of the observed facts on the role of Fe, S, H_2 and H_2S in such a system. Preliminary data are presented on one of the subsystems, i.e., FeS_2 + H_2 and the role of surface conversions in deactivation of the reaction of FeS_2 with pure H_2 is demonstrated. Specially prepared samples of FeS_2 appear to have a much larger activity toward H_2, and as will be shown in a future paper, much larger catalytic effect on the rate of coal liquefaction.

REFERENCES

1. Attar, A., Rev. Sci. Inst., 50 (1), 111 (1979).
2. Attar, A., Fuel, 58, 201 (1978).

FIGURE 1

75
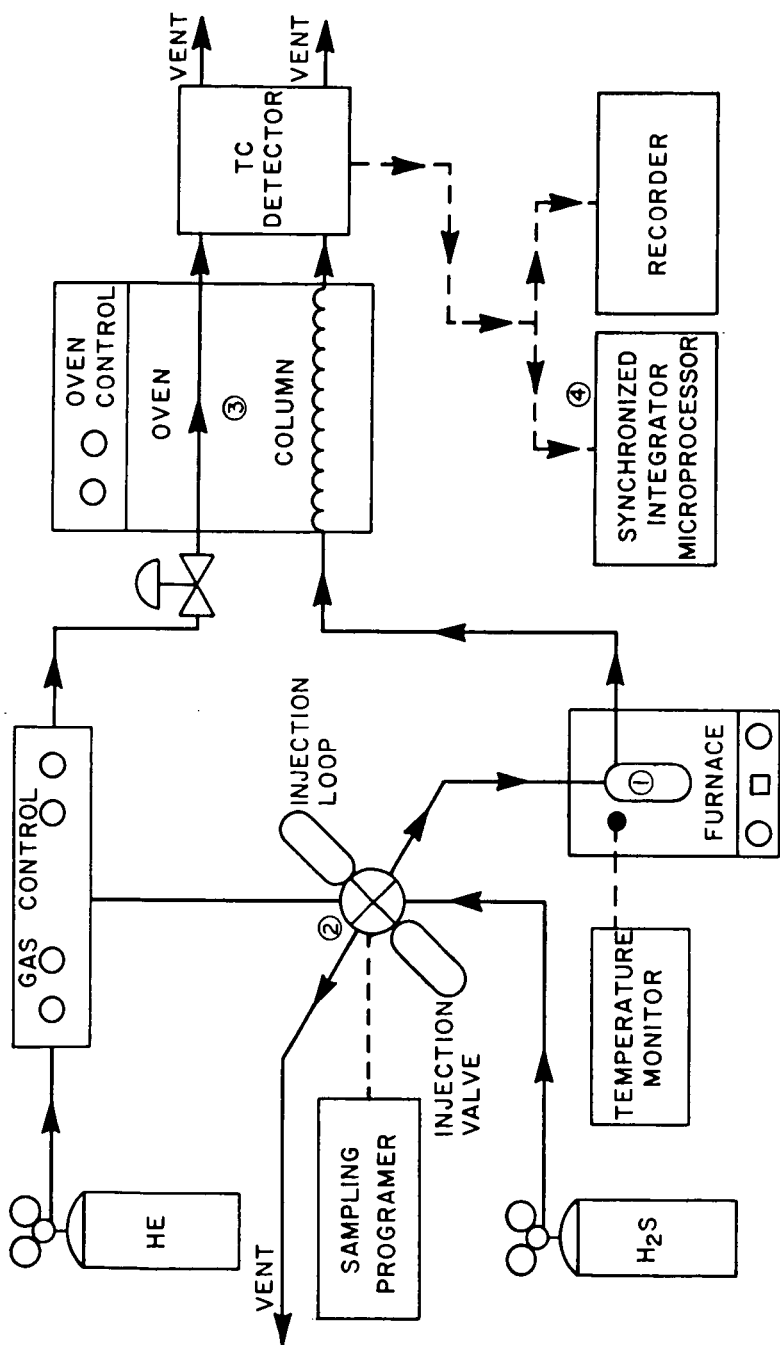
Figure 2

TEMPERATURE DEPENDENCY OF PYRITE REDUCTION
PULSE DIFFERENTIAL REACTOR SYSTEM

76
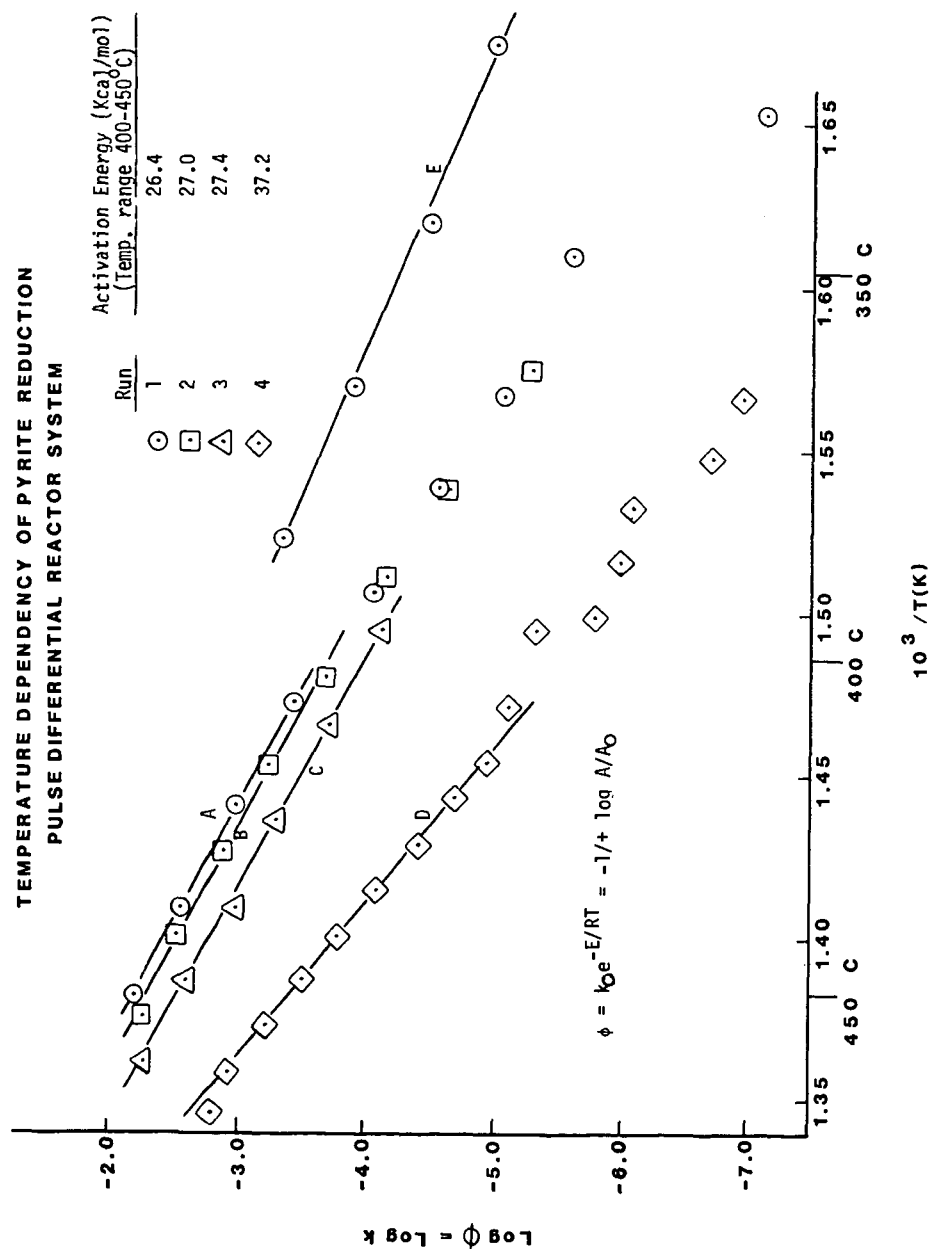
MODELLING OF LIGNIN THERMOLYSIS [+]

M.T. Klein* and P.S. Virk

Department of Chemical Engineering
Massachusetts Institute of Technology, Cambridge, MA 02139

Introduction

The object of the present work was to attempt a fundamental description of lignin
thermolysis. This was motivated by a recognition that the increased use of biomass
and low-rank coal resources must be accompanied by an enhanced understanding of the
factors which influence their thermal processing. Since lignin is a major component
of biomass, and has a direct evolutionary linkage to peat and lignitic coals,
insights into its thermolysis should prove relevant to the practical pyrolyses of
both biomass and coal.

Our investigation comprised three major components. First, a critical examination
of lignin structure and chemistry was undertaken to discern the most likely thermol-
ysis reaction pathways. Second, based on the foregoing, model compounds mimicking
the essential reactive moities in the lignin substrate were selected and pyrolysed.
Third, and finally, reaction pathways suggested by the model compound studies were
coupled with a structural analysis of lignin to formulate a mathematical model
which simulated the essential features of lignin thermolysis. The present paper
will focus on the modelling of lignin thermolysis; a special effort is made to
compare our model results with experimental data from lignin thermolyses previously
reported in the literature.

In outline of what follows, our approach to the problem is described first. This
includes an analysis of lignin structure; the choice of model compounds with a
summary of their experimentally-ascertained pyrolysis pathways; and the logic and
mathematics of the lignin thermolysis simulation. Representative results are
presented next, the simulated lignin thermolyses being described by the time-
evolution of products, including gases, aqueous liquids, phenolic tars, and residue
(char). We conclude with a discussion wherein the results of our simulation are
compared with experimental data reported in the literature for each of the fore-
going product fractions.

Lignin Structure

Lignin is a natural phenolic polymer formed by an enzyme-initiated random free-
radical co-polymerization of coniferyl, sinapyl and coumaryl alcohol monomers. The
available information concerning lignin structure is best summarized in Freudenberg's
(1) classic depiction of "a representative portion of spruce lignin", shown in
Figure 1, which was the starting point for the present investigation. Freudenberg's
formula should not be interpreted as a literal chemical structure for lignin but
rather as a schematic depiction of the bond types and proportions found therein by
experiments (1, 2, 3).

Analysis of Freudenberg's formula led to its characterization along the following
lines. Each aromatic unit, arising from a monomer, possesses in general a set of
propanoid (3-carbon-atom) and methoxy-phenol substituents. These aromatic units
are connected by eight types of interunit linkages. The most prevalent linkage is
the β-etherified guaiacyl glycerol moiety, as occurs between the methoxyphenol of

unit 6 in Figure 1. Other linkages found, in descending frequency of occurrence, are α-ether (units 3-4), diphenylmethane (units 2-3), diphenylether (units 6-7), biphenyl (units 9-10), pinoresinol (units 8-9), and phenylcoumaran (units 17-18). An essential feature of lignin structure is that the propanoid and methoxyphenol substituents on a given aromatic unit are essentially independent of one another since they are never involved in bonding with each other. Thus, the probability that an aromatic unit should contain a propanoid substituent of type k and a methoxyphenol of type j is the product of the individual probabilities of the occurrence of k and j, as given in Figure 1.

The foregoing probabilistic interpretation of Freudenberg's lignin formula is reduced to an aromatic unit matrix $\underline{A}$ in Figure 2. Each matrix element a_{jk} represents the number of aromatic units which possess type j methoxyphenol and type k propanoid substituents. Each row of the matrix represents a specific methoxyphenol found in lignin; these can originate from each of the three lignin monomers and within these the phenolic moiety may either be free or etherified in any of four forms, namely phenethylphenylether, benzylphenylether, phenylether and phenylcoumaran. Each column of the matrix represents a 3-carbon-atom propanoid side chain, respectively guaiacyl glycerol(β-ether, αβ-ether, α-phenyl β-ether), phenyl hydroxy acetone, cinnamaldehyde, pinoresinol, conidendrinoidlactone, and phenylcoumaran.

The matrix $\underline{A}$ of Figure 2 serves three purposes. First, the chemical moieties contained in its rows and columns are the basis for selection of model compounds relevant to lignin thermolysis. Second, the numerical values of each element offer a concise probabilistic description of the lignin substrate. (Note, incidentally, that the present A-matrix refers to the prototypical spruce lignin described by Freudenberg's formula; in the more general case, $\underline{A}$ will be a function of lignin origin.) Third, as we shall shortly find, lignin thermolysis generally leaves aromatic units intact while altering the substituents; a natural extension of the A-matrix to account for all possible products from thermolysis of the moieties in its rows and columns can then be used to unambiguously chronicle lignin thermolysis in terms of the substituents associated at any time with each of the original (conserved) aromatic units of the lignin substrate.

Model Pathways

Model compounds selected to mimic the thermal reactions of lignin are listed in Table 1. For each entry, the table lists an abbreviated name, chemical structure, the aspect of lignin structure modelled, and experimental pyrolysis conditions of temperature, holding time, and initial concentration. It can be verified that the entries in Table 1 model most of the interunit linkages (IL), methoxyphenol substituents (MP), and propanoid chains (PC) which appear in Figure 1. Specifically, PPE models the β-ether linkage most prevalent in lignin; guaiacol models the methoxyphenol substituent associated with coniferyl alcohol which is the dominant monomer in spruce lignin; veratrole models an etherified methoxyphenol; cinnamyl alcohol models a propanoid chain substituent, as do cinnamaldehyde, iso-eugenol, and acetophenone. Note also that some of the compounds in Table 1 were chosen to model moieties which, while not originally present in lignin, arise during its thermolysis; for example, saligenol models a propanoid enol moiety resulting from the primary reversion of a guaiacyl-glycerol β-ether. Still other compounds in Table 1, such as anisole, served as controls in the mechanistic interpretation of the model pyrolyses.

Results of the model compound pyrolyses are summarized in Table 2. For each substrate, the table delineates the observed pyrolysis pathways, their associated products, and reaction kinetics. Primary pathways are designated with an R while secondary pathways, involving reactions of a primary product, are designated with an S. Reaction kinetics are described by Arrhenius parameters ($\log_{10}A(s^{-1})$, $E*(kcal/mol)$) for pseudo-first order reaction; actual reaction orders, where experimentally ascertained, are quoted in the final column of the table. As an example, in entry 1, PPE decomposes by primary reaction R1 to phenol and styrene

products; the associated Arrhenius parameters are (11.1, 45.0) and the reaction was experimentally found to be first order in PPE; further, the styrene product of R1 undergoes secondary reaction S1 to form ethyl benzene, toluene, and benzene. The data presented in Table 2 now permit a quantitative description of reaction pathways and kinetics in lignin thermolysis.

Simulation of Lignin Thermolysis

The logic employed in our simulation of lignin thermolysis is depicted in Figure 3. Consider first some typical transformations experienced by a lignoid aromatic unit as shown in Figure 3a. Initially (time $t = 0$), this unit I will be recognized as element a_{11} of the spruce lignin matrix $\underline{A}$. During thermolysis, suppose the propanoid chain of I is sequentially subjected to β-ether reversion, pathway R1:PPE in Table 2, and enol product dehydration, by pathway R1:SAL in Table 2. At some time t_1, then, the substrate I will, in part, be transformed to the intermediate product II with concurrent evolution of water. However, II can further react by parallel pathways R1:CAD and R1:GUA, respectively leading to propanoid chain decarbonylation and methoxyphenol demethanation; thus at some further time t_2, II will, in part, be transformed to III, with concurrent evolution of carbon monoxide and methane. It should be noted that in Figure 3a, the original aromatic ring remains intact while its propanoid chain and methoxyphenol substituents are variously altered, chronicling the course of thermolysis. In mathematical terms, each substituent contained in the original $\underline{A}$ matrix gives rise to a new set of substituents that represent its thermolysis according to the pathways given in Table 2. At any time, the contents (aromatic units) of the original element a_{jk} of $\underline{A}$ are conserved while being redistributed into the elements p_{mn} of a new $\underline{P}$ (product)-matrix which represents all possible substituents that can arise from the original set. A little reflection will show that $\underline{A}$ is really a submatrix (the top left corner, say) of $\underline{P}$. Some further detail into the nature of the P-matrix, and the methods for product accounting, is given in Figure 3b. Consider the coniferaldehyde unit II in lignin, undergoing thermolysis. In Figure 3a, for simplicity, this was shown to react by two parallel pathways; however, in practice, it will undergo all possible reactions accessible to its methoxyphenol and propanoid chain substituents. Since these substituents are independent, the products will be formed by a superposition of the type shown in Figure 3b. The methoxyphenol in II is modelled by guaiacol A, which can pyrolyse by pathways R1: GUA and R2: GUA of Table 2 to catechol B and phenol C. The propanoid chain in II is modelled by cinnamaldehyde D which can pyrolyse by R1: CAD to styrene E. Thermolysis of II will then form all of the products shown in Figure 3b (and their associated gases), in amounts commensurate with the kinetics of the pathways involved.

The foregoing chemical logic was employed to mathematically simulate a constant volume batch pyrolysis of lignin. In this simulation, a set of differential equations, which described the time-variation of aromatic unit substituents, were solved numerically from an initial condition representing Freudenberg's spruce lignin. The rate of change of a given substituent was, in general, proportional to all other substituents, so that:

Differential Equations: $dX/dt = \underline{K}X$; $dY/dt = \underline{L}Y$ (1)

Initial Condition: $X = X_0$, $Y = Y_0$ at $t = 0$ (2)

In these the vector X represents all methoxyphenol-related substituents while vector Y represents propanoid chain-related substituents; these are, respectively, the rows and columns of the product matrix $\underline{P}$. The matrices K and L, derived in large part from Table 2, respectively contain the kinetic rate constants of those chemical reactions producing the components of vectors X and Y. The initial values X_0, Y_0 coincide with the sums of each row and column in the matrix $\underline{A}$, depicting the lignin substrate. Values of the vectors X and Y at any subsequent time t are a consequence of all possible chemical transformations embodied in the matrices $\underline{K}$ and $\underline{L}$. The contents of an element p_{mn} of the product matrix P then show the number of aromatic

units with methoxy-phenol related substituent m and propanoid chain-related sub-
stituent n. The nature of substituents m and n further permits the classification
of product p_{mn} as either tar (single-ring aromatic unit) or residue (multiple aromatic
rings). Details of the simulation logic, mathematics, and numerical evaluation are
available (4).

Results

Thermolysis of the prototypical spruce lignin of Figure 1 was simulated at temperatures
of 300, 400, 500, and 600C to holding times of 10^4, 10^4, 10^2, and 10^1 seconds,
respectively. Representative results at 500C are presented in Figure 4, an arith-
metic plot of product yield, expressed as weight percent of original lignin substrate,
versus time. Four product fractions, namely, gas, aqueous liquids, phenolic liquids
and carbonaceous residue, will be considered.

In regard to gas evolution, the simulation accounts for methane and carbon monoxide.
In the uppermost section of Figure 4 it can be seen that both gases evolve fast
initially and then more slowly, attaining asymptotic yields of circa 6 wt %, with
methane slightly exceeding CO. The methane arises primarily from guaiacy types of
methoxyphenol moieties, both those which are initially present with a free hydroxyl
and those which arise by reversion of etherified hydroxyls. The CO originates both
from the decarbonylation of carbonyl-containing propanoid chains and, to a lesser
extent, from the demethoxylation of methoxyphenols. An account of these dual sites
for CO release possessing quite different activation energies relative to the sites
for CH_4 release, the simulation predicts that the ratio of CO/CH_4 should be >1 at
low temperatures and conversions, <1 at moderate temperatures and conversions (as
in Figure 4), and then again >1 at high temperatures.

Among aqueous liquids, the simulation accounts for water and methanol. As seen in
the second (from top) section of Figure 4, the water yield increases monotonically,
but with decreasing slope, to an ultimate value of ~5 wt %. The water arises from
two sources; predominantly it is formed from dehydration of enol units which result
after β-ether reversion; minor amounts also arise from degradation of cinnamyl-
alcohol types of propanoid chains. The ultimate methanol yield predicted is only
about 0.1 wt %. This rather small value comes about because, in the simulation,
methanol arises solely from cinnamyl alcohol moieties, which are relatively rare in
lignin; further, the methanol-forming pathway is itself relatively minor amongst
cinnamylalcohol pyrolysis pathways.

The phenolic liquids fraction of our simulated lignin thermolysis included some
fifty individual phenolic compounds. The formation versus time for two sets of
phenolic products is shown in the two lowest sections of Figure 4. In the upper of
these two sections, it can be seen that the guaiacol production increases initially,
reaches a maximum, and then decreases towards zero at long times; the catechol
production increases slowly at low times but more strongly at longer times; phenol
production increases monotonically with increasing time but always remains less than
catechol. Qualitatively the same behavior is exhibited in the lowest section of
Figure 4 by methylguaicol, methylcatechol, and para-cresol products, each of which
is the methyl-substituted analogue of the preceding products; note however that
yields of the methyl-substituted phenols are almost an order of magnitude higher
than those of their unsubstituted homologues. Phenolic product trends seen in
Figure 4 arise from the following considerations. The guaiacyl moiety occurs
directly in lignin, and further arises from reversion of etherified methoxy-phenols;
associated with these guaiacyl units are various propanoid chains, also subject to
degradation. Thus coniferaldehyde and guaiacyl vinyl ketone are the most nearly
primary guaiacol products, degrading to vinyl guaiacol, and hence to ethyl-, methyl-,
and unsubstituted guaiacol. Further, each guaicyl moiety is capable of demethanation
and demethoxylation, which respectively yield the corresponding catechol and phenol.
Each guaiacol product thus possesses pathways for formation and destruction, resulting
in the characteristic yield maxima seen in Figure 4. From the foregoing, catechols

are seen to be secondary products, arising from guaiacyl moiety demethanation; this causes their initial production to be slow but at long times they become the dominant phenolic products. Finally, phenols arise from two major sources, namely guaiacyl demethoxylation, noted above, and coumaryl alcohol monomer units directly incorporated in the lignin; the former source being of greater import. Phenol substitution patterns parallel those of guaiacol, with alkyl side-chains ranging from coumaraldehyde to vinyl-, ethyl-, and unsubstituted phenol. Yields of phenols relative to catechols increase somewhat with increasing temperature, since guaiacyl demethoxylation is more highly activated than guaiacyl demethanation; however the absolute yields of phenols always remained lower than those of catechols.

According to our simulation, the carbonaceous residue is comprised of all aromatic units involved in interunit bonding. If the gas, aqueous liquid, and phenolic product fractions are designated as volatile, and all multiple ring aromatics as non volatile, then the simulated carbonaceous residue fraction can be related to the weight loss that would be observed during lignin thermolysis. Such simulated weight-loss versus time curves are shown by the dashed lines in Figure 5, which will be more fully discussed in the next section.

Discussion

The discussion will be confined to comparisons between the present results and previous literature, as embodied in the matrix of Table 3. In the rows of this matrix, the four major product fractions have been delineated in terms of overall and constituent component yields. The matrix has six columns, representing our model predictions and five sets of literature references. The latter includes the collected reports of several authors as summarized in reference 4, the data of Iatridis and Gavalas (5), of Kirshbaum (6), and of Domburg (7, 8). In each matrix element, a numerical value or comment indicates that information relevant to that row was reported, whereas an 'X' implies that it was not. The present simulation column 1, provides entries for each row save CO_2 yield. The overall gas fraction is the sum of CO and CH_4; these are by far the prevalent constituents of the lignin off-gas. The aqueous distillate was composed of water and methanol only; acetone, acetic acid and other minor liquid products were not included in the simulation. The phenolic fraction comprised the sum of all single ring phenols; this overall yield should correspond best to the overall tar yield reported in pyrolysis experiments. Finally, the carbonaceous residue fraction is composed of all multiple ring aromatic units. The investigations of collected authors (4), column 2, provide detailed accounts of gas and aqueous distillate yields, and overall tar and char yields. Because detailed temperature-time information is lacking for many of these investigations, entries in this column are best considered the asymptotic 'ultimate' yields of destructive distillations. The data of Iatridis and Gavalas (5) were obtained in a reactor designed to emphasize primary reactions, providing detailed temperature-time information and entries for all save water and overall aqueous distillate yields. Kirshbaum (6) provided overall gas, phenolics, and carbonaceous residue yields; detailed phenolic product spectra were provided also. Detailed description of phenolic product spectra and DTA/DTG weight loss data were given by Domburg (7, 8). The discussion to follow considers each row of Table 3; note that all yields are in weight percent of original lignin substrate.

The simulated overall gas fraction rose with increasing time and temperature and ultimately achieved a value of about 15% at 600 C. This compares favorably with the data of collected authors (4) in Table 3, where gas yields ranged from about 10-20%. Iatridis and Gavalas report an overall yield as high as 23% at 650 C, but this included 7.2% CO_2. As discussed below, this rather high CO_2 content may be due to their use of a Kraft lignin. Omitting CO_2, their overall gas yield is 16%, in good agreement both with the simulation and earlier literature. Additionally, Kirshbaum reports total gas (and losses) yield of ∿5% at 250 C and ∿18% at 600 C. The simulated (CH_4, CO) yields are respectively (6.0, 5.0) % at (500 C, 100s) and

81

(6.1, 9.0) % at (600 C, 7s); both these CH_4 and CO yields are in substantial agreement with the collected literature (4) which provides ultimate (CH_4, CO) yields of (7.0, 7.0) %. Simulated methane and $\overline{CO}$ yields both somewhat exceed those of reference 5, but, interestingly, these authors report that the experimental CO/CH_4 ratio varied from about 2.3 at 400 C to 0.88 at 500 C and 1.8 at 600 C, which closely accords with the behavior of this ratio in our simulation. This was earlier inter-preted in terms of dual sites for CO release from lignin.

The simulated overall yield of aqueous liquids, based on the sum of water and methanol yields, was about 6%, appreciably lower than the average yields of ~15% reported by the collected authors (4). Of the two individual components, the simulated water yields of 6% are about half of the values reported in the literature, although these latter are often unreliable on account of water being physically associated with the lignin or introduced during its isolation. Simulated methanol yields of 0.1% are also substantially lower than the yields of 0.28 to 1.5% reported by the collected authors (4). It would appear that further pathways for both water and methanol production need to be identified and incorporated into the present model of lignin thermolysis.

The simulated overall yield of phenolic liquids ranged from 7 to 80%. Experimental phenolic fraction yields typically range from 3 to 30% (4), although tar yields greater than 50% have been reported (9). The simulated phenolic fraction yields exceed experimental for two likely reasons. First, many complex phenols in the tar fraction are not experimentally identified and second, our simulation did not con-sider the condensation and polymerization reactions which might lower the yield of single ring phenols in practice. In regard to individual phenols, the present simulation predicts most of the thirty phenols which have been detected in the literature (6, 7, 8). In most cases, the simulated yields of individual phenols agree with experimental values to with a half an order of magnitude. It is particu-larly noteworthy that deviations between the present simulation and experiments are no greater than deviations between individual experiments.

The simulated carbonaceous residue yields of 91% at 300 C and 10^4s and 40% at 600 C and 7s compare favorably with the literature. In Table 3, ultimate tar yields from destructive distillation (4) were 40 to 60%. Iatridis and Gavalas (5) report weight losses of 20% and 53% at 400 and 600 C, respectively, corresponding to char yields of 80% and 47%. Kirshbaum (6) reports a char yield of 91% at 250 C and only 26% at 600 C. The present definition of residue as multiple ring aromatics evidently provides simulated carbonaceous residue yields that are in good accord with the experimental literature.

Finally, simulated weight-loss kinetics, derived from the carbonaceous residue yields as noted earlier, are compared with the experimental data reported by Iatridis and Gavalas (5) in Figure 5. It can be seen that the simulated weight loss curves (dashed), accord well with the experimental weight loss curves (solid), both in regard to shape and absolute magnitudes. The observed agreement is noteworthy in that the simulation was based entirely on our a priori description of lignin struc-ture, reaction pathways, and kinetics, and incorporated no information derived from actual lignin thermolyses. Furthermore, the modest deviations between simulated and experimental weight loss curves in Figure 5 can reasonably be attributed to differences between the respective lignin substrates. The authors (5) used a Douglas for precipitated Kraft lignin, whereas the present simulation was based on Freudenberg's unperturbed "protolignin." Kraft pulping alters the chemical nature of lignin, resulting in increased internal condensations, with the original reactive α- and β-ether linkages transformed into less reactive diphenyl-methane, ethane, and ethylene linkages; it also introduces carboxylic acid units into the lignin macro-molecule. The low temperature reactivity of a Kraft lignin might be expected to be greater than its protolignin counterpart because of facile CO_2 evolution from the carboxylic acid units. At higher temperatures and conversions, the reactivity of a Kraft lignin may well be lower than that of the protolignin since relatively re-

fractory diphenylmethane, ethane and ethylene units have replaced the original reactive α- and β-ethers. In the light of these assertions, it is interesting that Iatridis and Gavalas report CO_2 yields of 5.9% at 400 C and 120s, and 4.1% at 600 C and 10s. These suggest a constant number of easily decarboxylated acid sites in their substrate. Further, the authors' reported weight loss of 20% at 400 C and 120s exceeds our simulated weight loss of 13% by an amount substantially equal to their CO_2 yield. At 600 C and 10s the experimental weight loss corrected for CO_2 is $\sim$50%, somewhat lower than our simulated value of 60% on account of the reduced reactivity of their Kraft lignin.

<u>Summary and Conclusions</u>

Mathematical simulation of whole-lignin pyrolyses, at 300 to 600 C with holding times of 1 to 10^4s, was achieved by combining a statistical interpretation of lignin structure with experimental results of model compound pyrolyses. The outcome of these simulations, expressed in terms of product fractions as a percent of initial lignin was:

(i) Gas Fraction: Simulated overall gas, methane, and CO yields accorded with previous experimental lignin pyrolyses; respective ultimate yields typically 15%, 6%, and 9% were in quantitative agreement with the literature. The simulated variation of (CH_4/CO) ratio with time and temperature further agreed with that recently reported by Iatridis and Gavalas (<u>5</u>).

(ii) Aqueous Fraction: Simulated water yields were typically about half the reported experimental yields of 12%. Simulated methanol yields were half an order of magnitude lower than the literature yields of 0.3-1.5%.

(iii) Phenolic Fraction: Simulated overall phenolic liquids yields were generally higher than experimentally observed. The simulation accounted for more than thirty individual phenols reported in the literature. Simulated yields of simple individual guaiacols, cathechols, syringols, and phenols, each nominally 2%, were within the band of values reported in the literature.

(iv) Carbonaceous Residue: Simulated curves of weight loss versus time at 400, 500, and 600 C were nearly coincident with the experimental curves reported by Iatridis and Gavalas (<u>5</u>) for pyrolysis of a Kraft lignin. Also, the modest disagreements between these curves, at both low and high temperatures, were traced to structural differences between the respective lignin substrates.

<u>References</u>

1. Freudenberg, K., Neish, A.C., <u>Constitution and Biosynthesis of Lignin</u>, Springer-Verlag, New York (1968).
2. Harkin, J.M., in Battersby and Taylor, <u>Oxidative Coupling of Phenols</u>, Marcel-Dekker (1967).
3. Sarkanen, K.V., in Sarkanen, K.V., and Ludwig, C.H., eds., <u>Lignins: Occurrence, Formation, Structure and Reactions</u>, Wiley Interscience, New York, (1971).
4. Klein, M.T., <u>Model Pathways in Lignin Thermolysis</u>, Sc.D. Thesis, Department of Chemical Engineering, M.I.T., Cambridge, Mass. (1981).
5. Iatridis, B. and Gavalas, G.R., I & EC Prod. Res. Dev., <u>18</u> (2), 127 (1979).
6. Kirshbaum, I.Z., Domburg, G.E., Sergeeva, V.N., Khim. Dev. No. 4, 96 (1976).
7. Domburg, G.E., Sergeeva, V.N.,Kalnish, A.I., Thermal Analysis, Vol.3 (Proc. 3rd ICTA Davos (1971)) pp. 327-40, Burkhaeuser, Basel, (1972).
8. Domburg, G.E., Sergeeva, V.N., J. Thermal. Anal., <u>1</u>, 53 (1969).
9. Domburg, G.E., Kirshbaum, I., Sergeeva, V.N., Khim, Dev. <u>7</u>, 51 (1971).

TABLE 1. MODEL COMPOUNDS FOR LIGNIN THERMOLYSIS

	Compound	Abbr.	Structure	Model of	Pyrolysis T °C	Conditions t s	C_0 mol/ℓ
1	Phenethyl-phenyl ether	PPE	[structure]	IL	300-550	30-14400	0.083-1.68
2	Guaiacol	GUA	[structure]	MP	250-535	110-6000	0.46-3.07
3	Veratrole	VER	[structure]	MP	350-550	60-1500	0.33
4	Cinnamaldehyde	CAD	[structure]	PC	250-400	120-1500	0.38-1.3
5	Saligenol	SAL	[structure]	PC	175-350	60-1500	0.37
6	Cinnamyl-alcohol	CAL	[structure]	PC	300-500	50-1500	0.37-1.1
7	2,6 Dimethoxy-phenol	DMP	[structure]	NP	300-500	120-1800	0.32
8	Isoeugenol	IEG	[structure]	NP,PC	300-500	60-1560	0.33
9	Vanillin	VAN	[structure]	NP	300-500	120-1500	0.85
10	Acetophenone	APH	[structure]	PC	350-550	120-5000	0.14-1.4
11	α-hydroxy-diphenylmethane	OHD	[structure]	IL	400-550	120-6000	0.27
12	Phenylether	PET	[structure]	IL	500-587	240-9000	0.30
13	Cinnamic Acid	CIA	[structure]	PC	250-400	120-1500	0.20
14	Ferulic Acid	FEA	[structure]	PC,NP	200-350	120-1500	0.50
15	Anisole	ANI	[structure]	CON	344-550	180-1500	0.46-3.07
16	Benzaldehyde	BAD	[structure]	CON	300-500	120-3600	0.16-3.3

Note: Model codes are: IL - Interunit link, MP - Methoxyphenol, PC - Propanoid chain, CON - Control.

TABLE 2. MODEL PATHWAYS AND KINETICS IN LIGNIN THERMOLYSIS

	Substrate	Pathway: Products	$\log_{10}A(s^{-1})$	E^*(kcal/mol)	Order
1.	PPE	R1: [products]	11.1	45.0	1
		S1: [products]	5	22	(>1)
2.	GUA	R1: [products]	10.9	43.7	1
		R2: [products]	11.5	47.4	1
3.	VER	R1: [products]	13.9	55.9	1
		R1': [products]	14.1	58.4	
		R2: [products]	14.8	60.1	
		R3: [products]	11.2	49.2	
4.	CAD	R1: [products]	12.1	48.2	1
		R2: [products]	8.6	33.7	(2)
5.	SAL	R1: [products]	13.4	33.4	(1)
6.	CAL	R1: [products]	4.2	21.8	
7.	DMP	R1: [products]	10.4	42.2	
8.	IEG	R2: [products]	11.1	45.5	
		R1: [products]	10.8	42.9	
		R2: [products]	11.3	46.2	
9.	VAN	R1: [products]	12.2	47.3	
		R2: [products]	10.2	38.5	
10.	APH	R1: [products]	10.9	56.4	1
		R2: [products]	9.6	50.5	(1.5)
11.	OHD	R1: [products]	9.6	43.4	
12.	PE	R1: [products]	14.8	72.1	
13.	CAA	R1: [products]	8.0	31.0	(1)
14.	FEA	R1: [products]	5.2	19.8	
15.	ANI	R1: [products]	13.0	54.7	1
		R2: [products]	14.5	61.0	
16.	BAD	R3: [products]	7.9	40.5	(1)
		R1: [products]	9.5	41.5	1

Item	Model Prediction	Collected Authors: (4)	Iatridis and Gavalas (5)	Kirshbaum (6)	Domburg (7,8)
Gas Fraction					
Overall yields	15% @ 600C	10-20%, 15% mean	23% max including CO_2	5% @ 250C, 15% @ 600C gases and losses	5% @ 250C, 12% @ 600C gases and losses
CH_4	6% @ 500C	7% based on mean overall yield of 15%	4.8% @ 650C	X	X X
CO	9% @ 600C	7% based on overall mean of 15%	9.2% @ 650C	X	X
CO_2	X not included in simulation	1.5%	near 6%, all temperatures	X	X
Aqueous Fraction					
Overall	6% maximum	overall mean 15%	X	X	X
H_2O	6% maximum	12-15%	X	X	X
MeOH	0.1% maximum	0.2-1.0%	3% @ 650C	X	X
Phenolic Fraction					
Overall	Sum of single ring phenols as function of time 7-80%, include complex phenols	3-30%	0.3-3.0%, 400-650C	3.3-14.5%@475C	0.2%@250C, 14% @ 500C
Individual Phenols	Detailed yields of individual phenols as a function of time and temperature	X	only guaiacols and phenols	detailed yields of 20+ different phenols	detailed yields of 20+ different phenols
Carbonaceous Residue					
Overall	Ultimate residue yield from 0.014 @ 300C to 0.335 @ 600C	40-60% yield of char	weight loss of 20% @ 400C, 53% @ 600C	char yield of 91% @ 250C, 26% @ 600C	X
Kinetics	multiple ring aromatics as function of time, ultimate yields as function of temperature	X	weight loss for 400-600C as in function of time	X	DTA/DTG experiments yield E 26-30 kcal/mol

TABLE 3. COMPARISON BETWEEN LIGNIN THERMOLYSIS SIMULATION AND EXPERIMENTS.
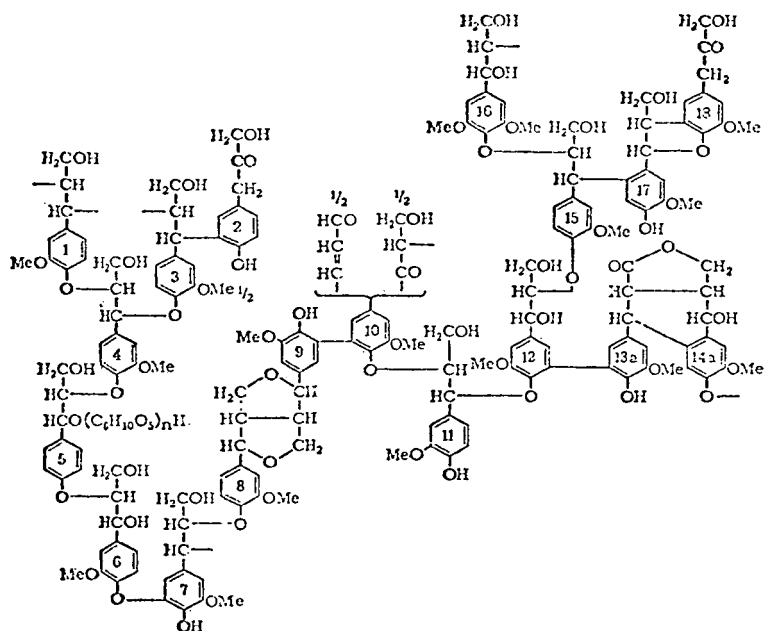
FIGURE 1. MODEL OF SPRUCE LIGNIN STRUCTURE (Freudenberg, 1)

		PC									∑ MP
MP											
	NORMALIZED DISTRIBUTION	(.33)	(.11)	(.11)	(.11)	(.06)	(.11)	(.11)	(.06)	(1)
CONIFERYL ALCOHOL	FREE (.28)	1.66	.55	.55	.55	.30	.55	.55	.30	5
	ETHERIFIED (.56)	3.33	1.11	1.11	1.11	.60	1.11	1.11	.60	10
COUMARYL ALCOHOL	FREE (.055)	.327	.11	.11	..11	.060	.11	.11	.060	1
	ETHERIFIED (.055)	.327	.11	.11	.11	.060	.11	.11	.060	1
SINAPYL ALCOHOL	FREE (0)	0	0	0	0	0	0	0	0	0
	ETHERIFIED (.055)	.327	.11	.11	.11	.060	.11	.11	.060	1
∑ PC	(1)	6	2	2	2	1	2	2	1	18

FIGURE 2. AROMATIC UNIT MATRIX A FOR SPRUCE LIGNIN

FIGURE 3. LOGIC OF LIGNIN THERMOLYSIS SIMULATION.

(a) Thermal Transformation of Lignin Moiety.
(b) Superposition of Model Pathways.

FIGURE 5. WEIGHT-LOSS KINETICS IN LIGNIN THERMOLYSIS.
—— Experimental (5)
- - - Present Simulation.
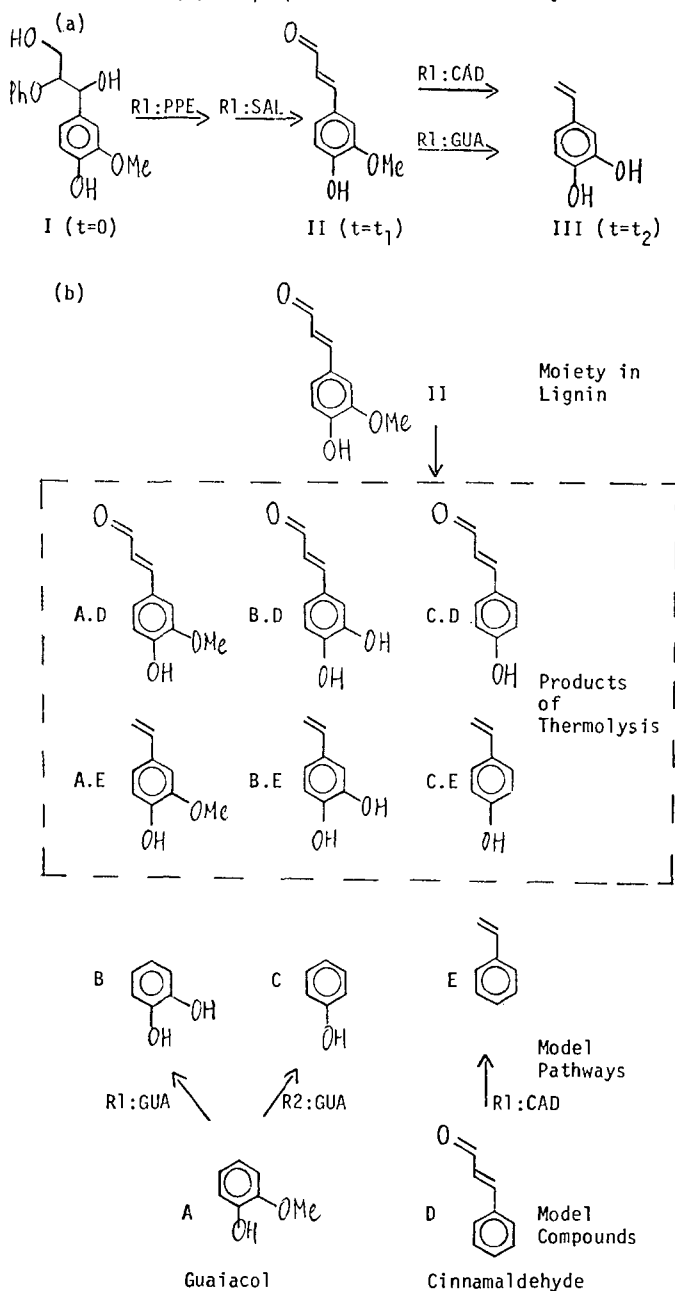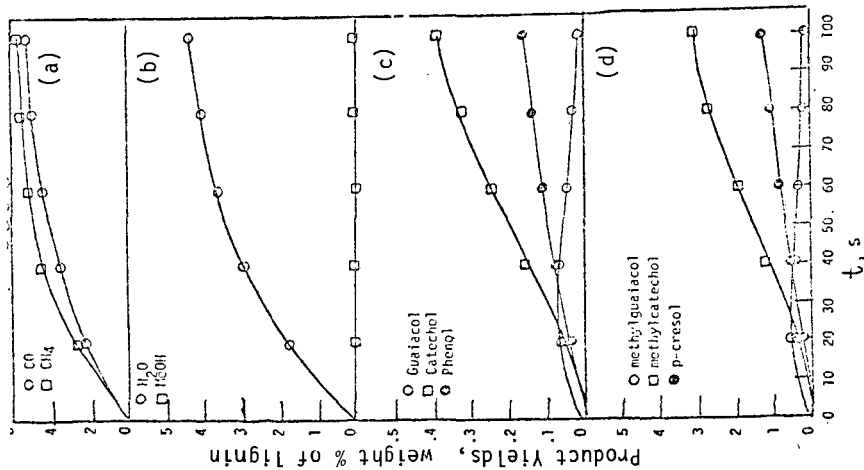
FIGURE 4. RESULTS OF LIGNIN THERMOLYSIS
SIMULATION AT T = 500 C.

ENHANCED COAL LIQUEFACTION WITH HIGH BOILING SOLVENTS. D. D. Whitehurst. Mobil
Research & Development Corp., P.O. Box 1025, Princeton NJ 08540

In the accelerated development of coal liquefaction since 1973, it has been the gen-
eral practice to use distillates as recycle solvents. This stems from the earlier German
experience where recycling asphaltenic products required more severe processing. Recent-
ly, it has been demonstrated that the inclusion of vacuum tower bottoms or of solvent
fractionated heavy products in a recycle loop can produce dramatic process improvements.

An investigation of the mechanisms of coal conversion in high boiling solvents has
been conducted using both model compounds, process derived materials, and fractions
thereof. These studies identified polycondensed aromatics as effective solvent com-
ponents. Due to their relative ease of hydrogenation and dehydrogenation they can
effectively interact with hydroaromatic species in the coal (H-shuttling), with less
active H donors or with hydrogen gas (H-transfer). Mineral matter catalysis can play
an important role in these reactions.

Polyfunctional components have a propensity for promoting char formation and can
produce adverse reactants. Information of this type can lead to identification and
generation of optimal recycle solvent composition.

These studies show that the mechanistic pathways discernible from the model com-
pound studies and the behavior of different chemical classes in heavy process solvents
can lead to improvements in coal liquefaction processes.

H-COAL SLURRY OIL COMPOSITION AND PROCESS PERFORMANCE

F. P. Burke and R. A. Winschel

Conoco Coal Development Company, Research Division, Library, PA 15129

INTRODUCTION

The H-Coal process, developed by Hydrocarbon Research, Inc., is a catalytic coal hydrogenation in which the coal is contacted with, usually, an alumina supported Co/Mo, or similar catalyst in an upflowing fluidized bed. The distinguishing features of the process are the reactor internals, which allow for fluidization of the catalyst bed, and catalyst addition and withdrawal systems to allow maintenance of the catalyst activity. The 3 TPD process development unit (PDU), operated by HRI at Trenton, NJ, has been used to study feed coal and space velocity effects, and to provide design data for scale-up of the process. A schematic of the unit (Figure 1) shows that the coal is fed to the reactor as a slurry with two recycle components. The hydroclone overflow (HO) contains distillate, non-distillate oils (resid), and solids. The clean oil tank (COT) is a surge vessel containing atmospheric still bottoms and vacuum still overhead. The amounts of these distillates in the clean oil tank can be independently varied.

An interest in the composition of these recycle oils, and how their composition is related to process performance, was the motivation for a recently completed program to analyze daily samples of recycle slurry oils from H-Coal PDU Runs 5, 8 and 9 by a variety of analytical techniques, and to relate the composition data to process performance in those PDU runs. PDU Runs 5 and 8 were made with Illinois 6 coal while PDU 9 used Kentucky 11 coal[1,2,3]. PDU Runs 5 and 9 were made in the Syncrude mode (space velocity = 31) while PDU Run 8 consisted of operations in both the Fuel Oil and Intermediate modes (Table 1). Daily samples of the clean oil tank and the hydroclone overflow were taken by HRI and shipped to CCDC for analysis. The analytical techniques used and the information desired from each are given in Table 2. The object of the study was to determine the relationship between slurry oil composition and process performance in eight specific areas:

1. Changes in the slurry recycle stream composition during startup.

2. The manner in which the process reaches steady state operation during startup.

3. The composition of the recycle stream during stable operation.

4. The changes in recycle composition in response to planned variations in process variables.

5. Changes in the recycle composition which cause or result from unplanned upsets in the process operation.

6. Changes in the recycle composition as evidence of changes in catalyst activity.

7. Differences in recycle composition as a function of space velocity (mode).

8. Differences in recycle composition as a function of feed coal (same space velocity).

In making interpretations of these data it is important to recognize that there are two ways in which the data can be expressed. The recycle slurry oil characterizations can be given as compositions, or intensive variables. For example, the weight percent

of benzene solubles in the recycle resid represents the nature of the material that is being recycled, without reference to the amount. Alternatively, the data can be expressed on a recycle rate, or extensive variable basis. Thus, the pounds of benzene insolubles recycled per pound of coal fed reflects both the composition of the recycle resid, and the total recycle rate of that resid. Both the composition and recycle rate data can be used to draw conclusions regarding steady state performance. In the work described here, all conclusions concerning steady state performance are based on a statistical treatment of the data which compares variations in the data with the experimental uncertainty of the measured variables. The mathematical basis of this treatment is described in the first topical report prepared under this contract[4]. The results presented below are abstracted from the much more extensive body of data included in the two topical reports and final report prepared under this contract[4,5,6].

The purpose of this paper is to illustrate the major conclusions reached in this study. Therefore, confirming results of other analyses are not generally presented.

COMPARISONS OF RECYCLE COMPOSISIONS

Because H-Coal is a hydrogenation process, ^{1}H-NMR was expected to provide a useful measure of recycle oil composition. Table 3 presents average ^{1}H-NMR distributions for PDU Runs 5 and 9 and for the two space velocity periods of PDU Run 8. The periods of Runs 5 and 9 used for averaging were chosen to represent the best approach to steady state in those runs. Because of a number of upsets over the first 16 days, we could not identify steady state periods for PDU Run 8, and all the data were used to calculate averages. Comparing first the results from Runs 5 and 8 (both Illinois 6 coal) we see that the higher space velocities produce a less aromatic recycle distillate. Since hydrogenation severity decreases with space velocity this was unexpected. The gain in aliphatics between the Syncrude, Fuel Oil and Intermediate space velocities is seen in the alkyl alpha and gamma protons, which measure long chain aliphatics, such as paraffins. These differences in distillate composition may reflect the fact that lower distillate yields at the higher space velocity mean that the recycle distillate will see more passes through the unit. Of course, the operability difficulties encountered in PDU Run 8, and the intentionally divided nature of that run, make firm conclusions unlikely.

PDU Run 9 (Kentucky 11 coal, Syncrude mode) gives a less aromatic recycle distillate than PDU Run 5 (Illinois 6 coal, Syncrude mode), though the difference is not as great as between PDU Run 5 and the Intermediate mode of PDU Run 8. Apparently, space velocity has more effect on recycle distillate composition than feed coal.

Selected samples of the recycle distillates from the three runs were used to extract Indiana V coal in a microautoclave at two standard conditions. The results (Table 4) show that all of the recycle distillates are good liquefaction solvents. The conversions to THF solubles are generally in the 70-80% range, and these results are indicative of good liquefaction solvents[7]. Differences which occur in a given run, and among the different runs, indicate that recycle distillates produced in the Syncrude mode are better liquefaction solvents than those from either the Intermediate or Fuel Oil modes. In PDU Run 5 there was a general tendency toward improved solvent quality as the run progressed. In PDU Run 9 the trend is reversed, although the conversions obtained with the PDU Run 9 distillates are equivalent to or better than those from PDU Run 5. For PDU Run 8 the two days shown compare conversions for distillates produced in the Fuel Oil mode with distillates produced in the Intermediate mode operation. The distillates from the Intermediate mode are consistently poorer, and in some cases by a large margin, than those from the Fuel Oil mode. This is consistent with data shown in Table 3 giving the average NMR distributions of these distillates, which show a surprisingly high concentration of alkyl beta and gamma protons for distillates produced at the Intermediate space velocity.

While the recycle distillates were qualitatively similar, the recycle resids (975°F[+], THF soluble) showed a much greater variation in composition, primarily as a function of

space velocity. Table 5 shows that the recycle resid from PDU Runs 5 and 9 (Syncrude) averaged around 49% oils (hexane solubles). The recycle resid in PDU Run 9 had a somewhat higher preasphaltene and lower asphaltene content than the recycle resid from PDU Run 5. However, the recycle resid in PDU Run 8 showed much lower oils content and much higher preasphaltenes content than for either of the Syncrude runs. This lower quality recycle resid in PDU Run 8 may have been related to (either as cause or effect) the operability problems which occurred in that run.

APPROACH TO STEADY STATE RECYCLE COMPOSITION

The data from PDU Runs 5 and 9 allow us to draw several conclusions concerning the approach to a steady state recycle slurry oil during those two runs. Because of the fragmented nature of PDU Run 8 we are not able to draw any conclusions concerning steady state operation from the data for that run. The majority of the data from PDU Runs 5 and 9 indicates that the recycle resid composition, but not the recycle rate, reached steady state between days 10 and 15. The recycle resid composition in PDU Run 5 does show some variation after day 20 of that run, when the hydrogen partial pressure was increased from an average of 1600 psig for the first 20 days of the run to an average of 1860 psig during the last 10 days. However, this appears to be an adjustment to a new equilibrium composition as opposed to a long term variation in the recycle resid composition. The plot of the ratio of benzene solubles to insolubles in the THF soluble recycle resid during PDU Runs 5, 8 and 9 (Figure 2) demonstrates this conclusion.

In contrast to the behavior of the recycle resid composition, the recycle rate of the resid did not reach steady state in PDU Run 9. This is illustrated in Figure 3, which shows the recycle rates of oils, asphaltenes and preasphaltenes on a lb/lb coal fed basis. Because the composition of the recycle resid reached steady state by about day 12, the plots are nearly parallel after that point. However, all three show steady increases throughout the 30-day run. A more rigorous treatment of the data[6] shows that the preasphaltene recycle rate reached an apparent steady state by about day 25. These results are important since a steadily increasing resid recycle rate tends to reduce the apparent resid yield from the unit. Therefore, the recycle composition can have a direct and immediate impact on the perceived unit performance.

Two measures of the recycle distillate composition, the ratio of aromatic to aliphatic protons, and the concentration of phenolic-OH in the clean oil tank, are shown in Figures 4 and 5, respectively. These data demonstrate that the recycle distillate composition did not reach steady state in PDU Run 9. The data on samples from PDU Run 5 indicate a steady state recycle distillate composition sometime near the midpoint of that run. However, the data from PDU Runs 5 and 9 are very similar up to about day 20 of those runs, and the behavior of the samples from PDU Run 5 after day 20 may have been influenced by increased hydrogen partial pressure, as discussed above. Note that an increase in hydrogen partial pressure would tend to decrease both the aromatic-to-aliphatic ratio and the concentration of phenolic-OH. This could compensate for declining catalyst activity at the end of PDU Run 5.

These data and others concerning the approach of the recycle resid and distillate compositions to steady state indicate that the rate of catalyst deactivation for the larger resid molecules is more rapid than the rate of catalyst deastivation for the smaller distillate molecules. In other words the catalyst has reached a steady state with respect to conversion of the resid to distillate range material by day 10-15 of both PDU Runs 5 and 9. However, the catalyst activity with respect to hydrogenation of the distillate is still declining at the end of the 30 day run.

CONCLUSIONS

The major conclusions drawn from this work are:

● Startup solvent is rapidly replaced in PDU operation. Any aromatic startup solvent of the appropriate boiling range should suffice if it is physically compatible.

- Aromaticity of recycle oil increases during run with declining catalyst activity. Distillate aromaticity reached steady state in PDU 5 but not in PDU 9, perhaps because of increased P_{H_2} after day 20 of PDU 5. Same is true for hydroxyl contents of recycle distillates.

- Composition of recycle resid reached steady state in PDU Runs 5 and 9, by about day 12, but changed in Run 5 coincident with increased P_{H_2}.

- Recycle rate of resid did not reach steady state in PDU 9, although composition did. Situation in PDU 5 was complicated by increased P_{H_2}.

- Recycle resid in PDU 8 was much higher in preasphaltenes than PDU 5 or 9, probably related to operability problems.

- Recycle distillates were qualitatively similar regardless of mode or coal. All are good liquefaction media.

- PDU 5 and 9 data indicate a fast catalyst deactivation for resid hydrogenation (10-15 days) and a slower catalyst deactivation for distillate hydrogenation (> 30 days).

- Kentucky 9 and Illinois 6 coals give similar slurry recycle oils at the Syncrude mode. Differences among Fuel Oil, Intermediate and Syncrude space velocities, with same coal, are greater.

This work was supported by U.S. DOE Contract DE-AC05-79ET14503.

REFERENCES

(1) Johanson, E. S. and Comolli, A. G., "PDU Run 9, Syncrude Mode Operation With Catalyst Addition and Withdrawal, Kentucky 11 Coal," U.S. DOE Contract EX-77-C-01-1547, Milestone Report (Draft), FE/2547-50, March 1980.

(2) Johanson, E. S. and Comolli, A. G., "PDU Run 5, Syncrude Mode Operation With Catalyst Addition and Withdrawal," U.S. DOE Contract EX-77-C-01-2547, Milestone Report, FE-2547-19, June 1978.

(3) Johanson, E. S. and Comolli, A. G., "PDU Run 8, Fuel Oil and Intermediate Mode Operation With Catalyst Replacement," U.S. DOE Contract EX-77-C-01-2547, Milestone Report, FE-2547-46, December 1979.

(4) Burke, F. P., Winschel, R. A. and Pochapsky, T. C., "Development of a Correlation Between Slurry Oil Composition and Process Performance," U.S. DOE Contract DE-AC05-79ET-14503, Topical Report No. 1, DOE/ET-14503-1, April 1980.

(5) Burke, F. P., Winschel, R. A. and Pochapsky, T. C., "Development of a Correlation Between Slurry Oil Composition and Process Performance," U.S. DOE Contract DE-AC05-79ET-14503, Topical Report No. 2, DOE/ET-14503-2, August 1980.

(6) Burke, F. P., Winschel, R. A. and Pochapsky, T. C., "Development of a Correlation Between Slurry Oil Composition and Process Performance," U.S. DOE Contract DE-AC05-79ET-14503-3, Final Report, DOE/ET-14503-3, January 1981.

(7) Kleinpeter, J. A., Burke, F. P., Dudt, P. J. and Jones, D. C., "Process Development for Improved SRC Options: Short Residence Time Studies," EPRI Project 1134-1, Final Report, EPRI AP-1425, June 1980.

Table 1

H-Coal PDU Runs Studied

PDU Run	Coal	Space Velocity $(lb/hr-ft^3)$ Mode	Operations Note
5	Illinois 6	31 (Syncrude)	Increased P_{H_2} after day 20.
8	Illinois 6	78 (Fuel Oil) 50-65 (Intermediate)	Operating problems caused by plugging.
9	Kentucky 11	31 (Syncrude)	Uneventful.

Table 2

Analytical Techniques

- ^{1}H-NMR (COT, HO Distillate, HO Resid)
  - Hydrogen Distributions
  - Donatable Hydrogen
- LIQUID CHROMATOGRAPHY (HO Resid)
  - Solvent Fractionation (Oils, Asphaltenes, Preasphaltenes)
  - Chemical Functionalities
  - Molecular Size Distribution
- GC/MS AND REVERSE PHASE LIQUID CHROMATOGRAPHY (COT and HO Distillates)
  - Detailed Compositional Analysis
  - Characteristic Parameters
- ^{19}F-DERIVATIZATION AND ^{19}F-NMR
  - Hydroxyl (OH) Content
- MICROAUTOCLAVE
  - Empirical Measure of Solvent Quality

Table 3

Average ^{1}H-NMR Distributions
of Hydroclone Overflow Distillates

PDU Run	Period	Mode	Average ^{1}H-NMR Distributions, Hydroclone Overflow Distillates						
			Cond. Ar	Uncond. Ar	Cyclic α	Alkyl α	Cyclic β	Alkyl β	γ
5	12-30	Syncrude	26.7	11.1	17.3	12.2	11.9	13.5	7.3
8	3-15	Fuel Oil	26.6	9.2	17.5	11.9	12.2	15.3	7.3
8	17-21	Intermediate	21.6	8.6	16.5	11.8	12.5	19.4	9.5
9	10-26	Syncrude	22.4	9.7	17.5	12.2	13.6	16.2	8.4

94

Table 4

Microautoclave Extractions of Indiana V Coal With H-Coal
Recycle Distillates - Conversion to THF Solubles, Wt % MAF Coal

PDU RUN		5			8			9	
Sample		HO	COT		HO	COT		HO	COT
	Day			Day			Day		
EQ Conditions	3	80.6	69.8	--	--	--	3	85.7	81.0
	12	79.6	76.5	13	73.8	72.3	19	79.9	76.8
	25	77.9	77.3	20	72.9	62.3	26	77.6	75.9
	Avg	79.4	74.5		73.4	67.3		81.1	77.9
KIN Conditions	3	76.3	74.8	--	--	--	2	78.2	75.3
	12	80.8	74.3	13	82.7	73.6	19	78.7	72.7
	25	83.3	75.0	20	70.4	68.9	26	79.8	73.9
	Avg	80.1	74.7		75.6	71.2		78.9	74.0

EQ - 750°F, 30 min, 2/1 solvent/coal
KIN - 750°F, 10 min, 8/1 solvent/coal

Table 5

Solubility Fractionation of Hydroclone Overflow THF Soluble Resids

PDU Run	Period	Mode	Average, wt % THF Soluble Resid		
			Oils	Asphaltenes	Preasphaltenes
5	12-30	Syncrude	49.0	32.9	18.1
8	11-15	Fuel Oil	28.4	32.8	38.8
8	17-23	Intermediate	33.7	33.6	32.7
9	10-30	Syncrude	48.5	27.4	24.1

95

Figure 1

H-Coal Process Simplified Flow Diagram
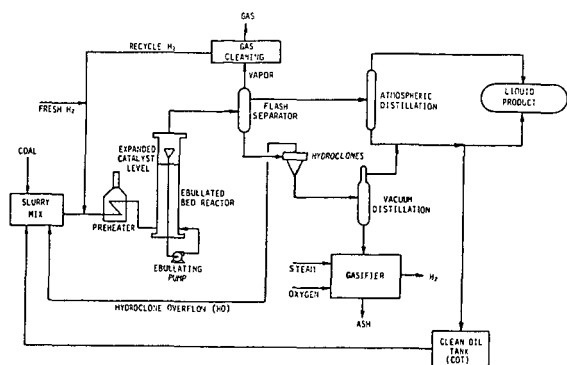
Figure 2

Comparison of Benzene Soluble/Insoluble Ratios
Recycle Resids - PDU Runs 5, 8 and 9
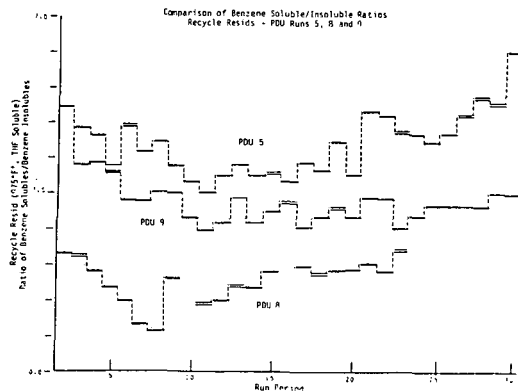
Figure 3

LCF Separation of HO THF Soluble Resid
H-Coal PDU Run 9
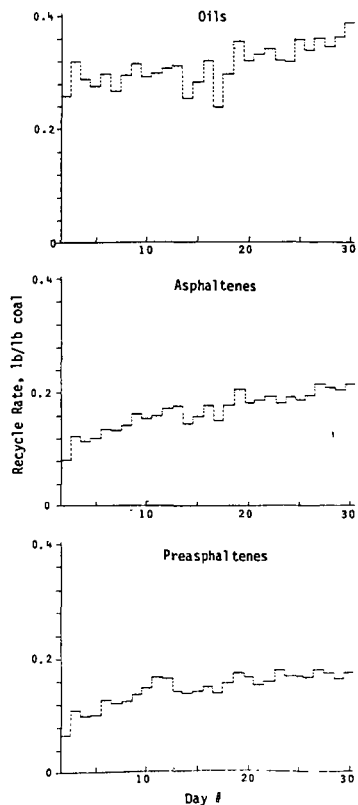
Figure 4

Ratio of Aromatic/Aliphatic Protons,
Total Recycle Distillate
H-Coal PDU Run 5 and 9
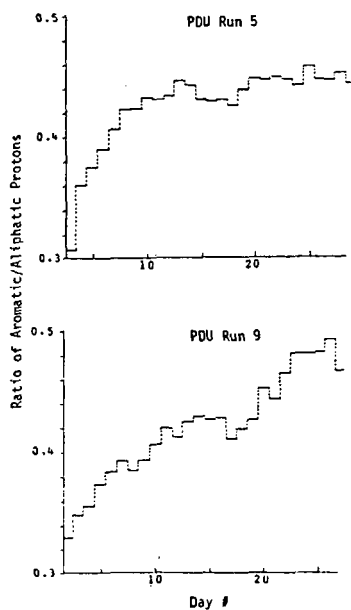
Figure 5

Concentration of Phenolic -OH by ^{19}F-NMR
COT Samples
H-Coal PDU Runs 5, 8 and 9

97
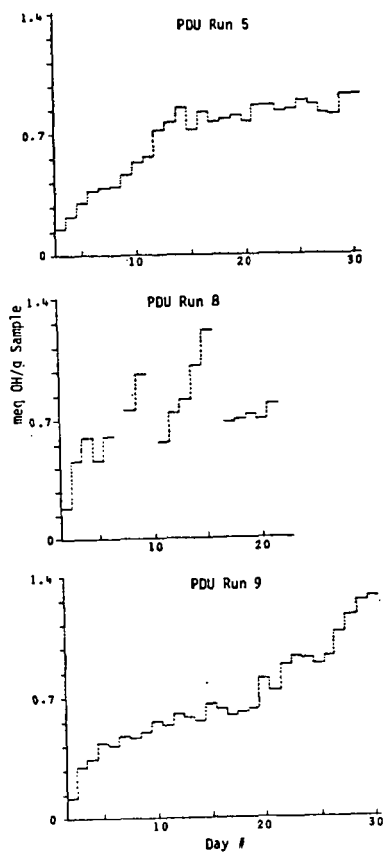
THE OCCURANCE OF AUTOGENIOUS WATER-GAS SHIFT REACTION ON HYDROGENATION OF SUB-
BITUMINOUS COALS. M. Gawlak, D. Carson, H. Wasylyk, B. Ignasiak, Alberta Research Council
11315 - 87 Avenue, Edmonton, Alberta, Canada, T5G 2C2.

Two subbituminous Alberta Coals (21-22% O, on daf matter) were liquefied in a
continuous unit, in a recycle mode, with hydrogen. Independently, autoclave lique-
faction tests were carried out in hydrogen using recycle solvent from continuous
liquefaction as a medium. The results revealed that in both cases from 10-30% of
the hydrogen consumed on liquefaction (4-6% by weight of daf coal) was used up for
generation of water. However, when the same coals were liquefied in autoclave under
similar conditions but in anthracene oil, a water-gas shift reaction occurred which
resulted in net consumption of water introduced with coal into autoclave. The results
are tentatively interpreted in terms of different acidity of solvents in relation to
metals contents of the treated coals.

SOLVENT EFFECTS IN EXXON DONOR SOLVENT COAL LIQUEFACTION. P. Maa, K. L. Trachte, and R. Williams. Exxon Research & Engineering Co., P.O. Box 45, Linden NJ 07036. Exxon Research & Engineering Co., P.O. Box 4265, Baytown TX 77520.

The Exxon Donor Solvent (EDS) coal liquefaction process utilizes a wide range of coal ranks, from lignitic to bituminous, and produces a variety of liquid product slates under moderate processing conditions. The recycle of hydrogenated, coal derived solvent is a key to the performance of the EDS Process.

The role of the recycle solvent in EDS is to provide a convenient vehicle for transporting coal into the process, to disperse the coal, and to donate hydrogen to free radicals produced by the thermal rupture of chemical bonds. The hydrogen donating capability of the recycle solvent allows a balanced utilization of both donor as well as molecular hydrogen under moderate processing conditions. In addition, through solvent conversion in the liquefaction reactor, product selectivity can be controlled to provide either predominantly naphtha or distillate product slates.

Liquefaction studies have been conducted in small batch autoclaves and integrated pilot units in order to better understand solvent-coal interactions in the EDS Process. Results of these studies will be discussed in this paper.

UPGRADING COAL LIQUEFACTION RECYCLE BOTTOMS

H. F. Silver, R. L. Miller and R. G. Corry
Chemical Engineering Department

R. J. Hurtubise
Chemistry Department

University of Wyoming, Laramie, Wyoming 82071

INTRODUCTION

In both the EDS and the SRC-II direct coal liquefaction processes, distillate yields have been increased significantly by including vacuum column bottoms product in the recycle solvent. While the distillable portion of the recycle solvent is upgraded in the EDS process, no specific effort is made to upgrade the non-distillable portion of the recycle solvent in either the EDS nor the SRC II processes. A study was therefore initiated at the University of Wyoming to determine the effect of upgrading coal liquefaction recycle bottoms.

EXPERIMENTAL PROCEDURE

Liquefaction of both subbituminous Wyodak and bituminous Kentucky coals has been studied in a two-liter Autoclave Magnedrive-II batch reactor. Samples of Wyodak coal, Wyodak coal derived recycle solvent, and solvent refined coal, SRC, were supplied by Catalytic, Inc. from the Southern Services Inc. pilot plant at Wilsonville, Alabama. Samples of Kentucky coal, Kentucky coal derived recycle solvent and SRC were supplied by the Pittsburg & Midway Coal Mining Co. from their pilot plant near Tacoma, Washington.

Portions of the recycle solvents boiling above 533K were used as received while other portions were mildly hydrogenated over a Co-Mo on Al_2O_3 catalyst (Nalcomo 477) for 60 minutes at 644K using an initial cold reactor hydrogen pressure of 13.8 MPa. Portions of the SRC were used as received while other portions were upgraded by solvent fractionation and by hydrogenation. The SRCs were solvent fractionated into cyclohexane soluble oils, cyclohexane insoluble - benzene soluble asphaltenes, benzene soluble oils plus asphaltenes and benzene insoluble-pyridine soluble preasphaltenes. Portions of the SRCs and their oil plus asphaltene fractions were mildly hydrogenated over catalyst at 644K for 60 minutes using an initial cold reactor hydrogen pressure of 13.8 MPa. Other portions were severely hydrogenated over catalyst at 700K for 60 minutes using an initial cold reactor hydrogen pressure of 20.7 MPa.

Coal liquefaction experiments were then conducted by charging the reactor with recycle solvent, SRC or SRC fraction and coal in a 1:1:1 weight ratio. The reaction was carried out at 714K for 60 minutes using an initial cold reactor hydrogen pressure of 13.8 MPa. Gaseous products were analyzed using an HP 5840 gas chromatograph. Liquid products were distilled using a modified ASTM-D 1160 apparatus. Unreacted coal and mineral matter were determined by soxhlet extractions using pyridine. All runs were duplicated.

DISCUSSION OF RESULTS

The extent of coal liquefaction in this work was measured using percent 700K+ conversion, X_{700}, defined by the relationship

$$X_{700} = \frac{W_{IN} - W_{OUT}}{W_{IN}} \times 100$$

where W_{IN} = grams of MAF coal plus grams of SRC or SRC fraction plus grams of 700K+ distillate charged to the reactor.

and W_{OUT} = grams of MAF 700K+ product recovered from the reactor.

A summary of the conversions obtained using different solvents is presented in Table I. The average reproducibility of conversions for duplicated runs was within $\pm$ 1.0% of the mean values reported in this table.

Examination of the results for solvents 1-6, containing Wyodak coal derived SRC, and solvents 12-16, containing Kentucky coal derived SRC, suggest that maximum conversions are obtained if the SRC is mildly hydrogenated. The data obtained from Wyodak solvents 4, 5 and 6, and for Kentucky solvents 13, 14 and 16 suggest that SRC component effectiveness may pass through a maximum as hydrogenation severity is increased. Comparison of solvent 3 with solvent 5 and solvent 15 with solvent 16 suggests that the observed increases in conversion relative to solvents 1 and 12 are due more to mildly hydrogenated SRC than mildly hydrogenated distillate.

While the relatively high conversion obtained from solvent 2 could be attributed to the catalytic activity of the ash in this sample of unfiltered SRC, ash found in Wyodak coal is generally not considered to be a catalyst for the coal liquefaction reaction. A more reasonable explanation for the high conversion observed when using solvent 2 is the lower initial boiling point of the high ash SRC as compared to the filtered SRCs. In the pilot plant, ash increases the viscosity of SRC. In order to reduce this viscosity, some of the normally distillable liquids were not removed from the high ash SRC during distillation.

The results shown in Table I also suggest that solvent fractionation may also improve the liquefaction effectiveness of SRCs. Results obtained using solvents 17-19 suggest that little, if any, improvement in Kentucky coal solvent effectiveness can be obtained by hydrogenating the benzene soluble oils plus asphaltenes obtained from Kentucky SRC.

Liquid yields and hydrogen consumption depend upon the extent of coal conversion. Net liquid yields of C_4-533K and 533-700K from Wyodak coal as a percent of the MF coal are presented in Figures 1 and 2 as a function of X_{700}. Points presented on these and the following figures are identified by the number in Table I identifying the solvent used in the experiment. As would be expected, liquid yields increase with increasing X_{700}. Similar plots of liquid yields for Kentucky coal are presented in Figures 3 and 4. For comparison purposes, the solid lines in Figures 1 and 2 have been reproduced as dashed lines in Figures 3 and 4, respectively, so that direct comparisons can be made between Wyodak and Kentucky coal yields. As can be seen in Figures 3 and 4, Kentucky coal produced greater liquid yields than Wyodak coal at low conversions. However, at high conversions, the liquid yields from the two coals are quite comparable.

Hydrogen consumptions for both Wyodak and Kentucky coal experiments are presented in Figures 5 and 6. The consumptions shown in these figures do not include the hydrogen consumed in upgrading either the distillable solvent nor the SRC or SRC fractions. It has been estimated that hydrogen consumed in this manner would be in the order of 1.0 to 2.0 wt% of the MAF coal charged to the reactor.

CONCLUSIONS

Results obtained from this work indicate the importance of solvent composition on the coal liquefaction reaction. Through the addition of mildly hydrygenated SRC to a recycle solvent, for example, net C_4-700K liquid yields approaching 60 wt% of the MF coal charged to a batch reactor were obtained from both Wyodak and Kentucky coals used in this study.

A certain amount of bottoms recycle upgrading may occur indirectly in processes such as the EDS process with bottoms recycle or the SRC-II process. However, it may be possible to obtain even further increases in distillate yields by direct upgrading of a bottoms recycle, either by hydrogenation or by solvent fractionation. It should be pointed out that these hypotheses are based on batch reactor runs, simulating continuous coal liquefaction operation. Deleterious compounds could build up in recycle streams in continuous plants that were not observed in this study. Further work in this area appears to be warranted.

ACKNOWLEDGEMENTS

TABLE I
X_{700} CONVERSION RELATED TO THE DEGREE OF SOLVENT HYDROGENATION

COAL	SOLVENT NO.	SOLVENT DISTILLABLE PORTION	NONDISTILLABLE PORTION	X_{700} (%)
WYODAK	1	UH[1]	SRC, UH	23.8
	2	UH	(SRC+Ash), UH	36.5
	3	UH	SRC, MH[2]	42.5
	4	MH	SRC, MH	35.8
	5	MH	SRC, UH	32.0
	6	MH	SRC, SH[3]	27.2
	7	UH	(O+A)[4], UH	28.4
	8	MH	(O+A), MH	37.4
	9	MH	(O+A), SH	29.0
	10	UH	A[5], UH	34.6
	11	UH	O[6], UH	35.9
KENTUCKY	12	UH	SRC, UH	28.5
	13	MH	SRC, MH	39.9
	14	MH	SRC, SH	36.4
	15	UH	SRC, MH	38.8
	16	MH	SRC, UH	30.5
	17	UH	(O+A), UH	35.5
	18	MH	(O+A), MH	37.0
	19	MH	(O+A), SH	37.0

NOTES: (1) UH = Unhydrogenated
       (2) MH = Mildly Hydrogenated
       (3) SH = Severely Hydrogenated
       (4) O+A= Oils plus Asphaltenes
       (5) A = Asphaltenes
       (6) O = Oils

Figure 3. C_4-533K Kentucky Coal Liquid Yields as a Function of X_{700}
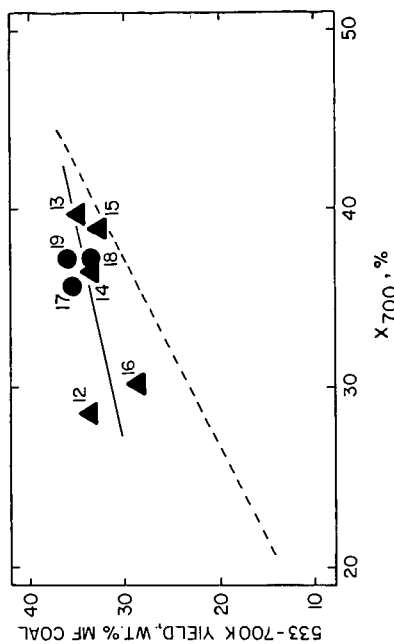
Figure 4. 533-700K Kentucky Coal Liquid Yields as a Function of X_{700}

Figure 1. C_4-533K Wyodak Coal Liquid Yields as a Function of X_{700}

Figure 2. 533-700K Wyodak Coal Liquid Yields as a Function of X_{700}

103
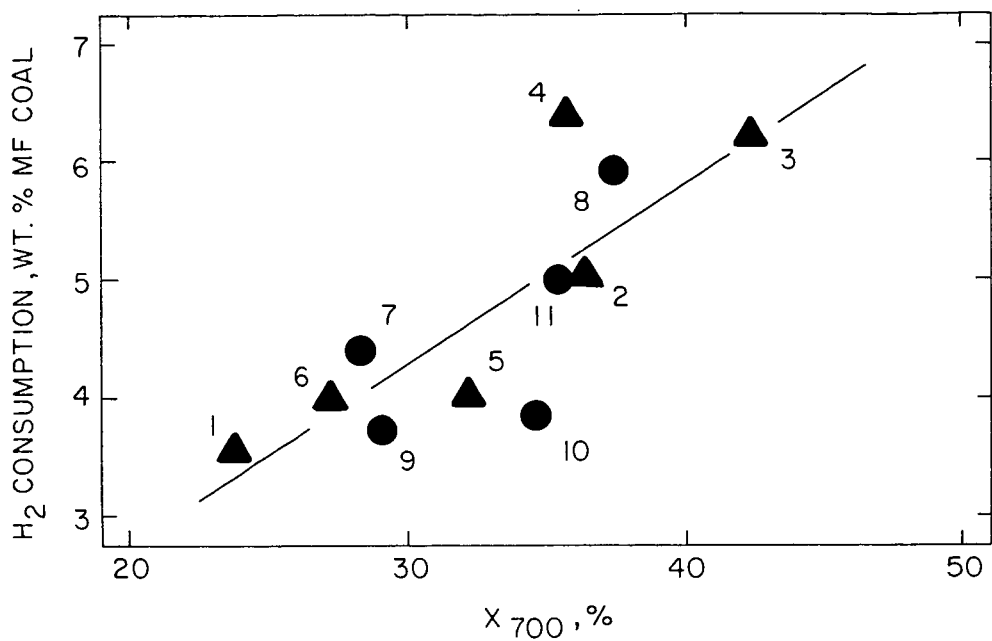
Figure 5. Hydrogen Consumption for Wyodak Coal as a Function of X_{700}
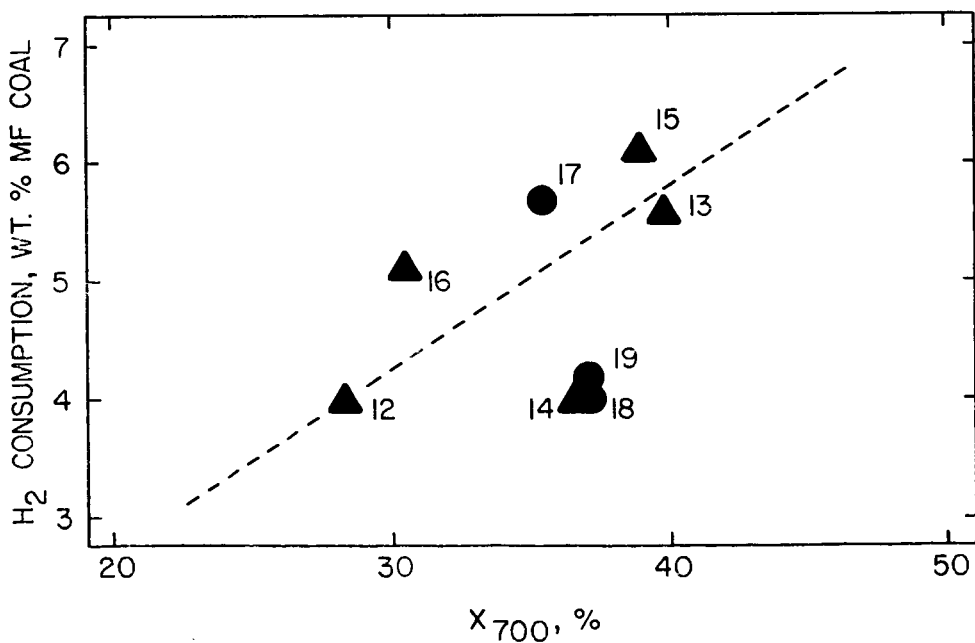
Figure 6. Hydrogen Consumption for Kentucky Coal as a Function of X_{700}

104

COAL LIQUEFACTION WITH SELECTIVE HEAVY RECYCLE. C. J. Kulik, H. E. Lebowitz, and
W. Weber. Electric Power Research Institute, 3412 Hillview Avenue, P.O. Box 10412,
Palo Alto CA 94303.

Earlier EPRI programs have shown the effects of recycling a light vacuum bottoms
(so called "Light SRC") stream as part of the solvent for coal liquefaction. The pre-
vious work showed that the Light SRC recycle resulted in improved performance, particu-
larly at relatively low temperatures, below 800°F. The previous work consisted of
comparatively short runs in which the recycle streams were not equilibrated; the ash
separation and vacuum bottoms fractionation were not integrated with the coal lique-
faction. The results were thus somewhat tentative.

Several runs have now been completed at the Wilsonville 6 ton per day coal lique-
faction pilot plant which substantially confirm the previous findings, and add interest-
ing data regarding the scale-up from semi-continuous to continuous operation. This
paper will discuss the pilot plant results and relationship between the two scales of
operation.

ROLE OF THE AROMATIC OXIDATIVE COUPLING
REACTION IN FUEL CHEMISTRY

J. B. Pierce *

Department of Chemistry
University of Lowell
Lowell, Massachusetts 01854

In the temperature range of $300°$ to $500°C$ bituminous coals pass through one or more plastic stages, but after each occurrence continued heating causes solidification (1). In the direct liquefaction of coals or processing of coal-derived liquids at pyrolytic temperatures catalytic surfaces become fouled with carbonaceous deposits (2,3,4). In jet fuels the presence of heterocyclic aromatic compounds containing nitrogen in the rings causes sludge to form (5). Carbazoles and related compounds tend to form carbonaceous electrode deposits at anodes in electrochemical cells.

Each of these effects is caused by an increase in molecular weight which might arise from a number of different chemical reactions. However, in these specific oxidation-reduction reactions a favored oxidation half reaction is the oxidative coupling of aromatic ring structures. The first clue to the operation of aromatic oxidative coupling as a route to products of higher molecular weight and lower solubility resulted from the observation of electrode film formation on anodes when coal-derived liquids were being examined electrochemically (6).

EXPERIMENTAL

The electrode films formed by anthracene oil and SRC-II type product oils derived from Blacksville No. 9 coal were studied by means of cyclic voltammetry and double potential step chronoamperometry. A Princeton Applied Research Model 170 Electrochemistry System was employed. The electrolyte was tetrabutyl ammonium fluoroborate, and solvents were acetonitrile for the anthracene oil and tetrahydrofuran for SRC-II type product oils.

DISCUSSION

Anthracene oil and many samples of SRC-II type product oil from the 1000 pound per day pilot plant at Pittsburgh Energy Technology Center (PETC) were examined electrochemically and found to form electrode deposits under oxidizing conditions. Successive voltammetric traces show the insulating effect of the film deposited by anthracene oil (Figure 1a). Progressive changing of the switching potential toward more cathodic potentials shows a decrease (Figure 1b) and elimination (Figure 1c) of the film-forming tendency.

In a different experiment the initial potential of an SRC-II
type solute was held at +1.000 volt for different lengths of
time, and the resulting films were reduced in the voltammetric
scan toward more cathodic potentials. The peak heights reflect
the currents used to reduce the films formed by oxidation at
+1.000 volt. A linear variation in peak height with time is
shown (Figure 2). In these samples the films are much more re-
active than those formed from anthracene oil.

The films formed on anodes proves the reaction to be an
oxidation. The formation of electrode films, which, depending on
conditions, varied from soft, brown, and soluble to hard, glossy,
black, and insoluble in pyridine, proves an increase in molecular
weight. The presence of reactive aromatic structures in coals and
coal-derived liquids (7) suggests the operation of the aromatic
oxidative coupling reaction. Table I comprises a list of selected
compounds that undergo oxidative coupling.

As reported by Dworkin and others(8) and illustrated with
anthracene, $C_{14}H_{10}$, aromatic oxidative coupling proceeds by way
of a radical cation intermediate.

Oxidations:

$$C_{14}H_{10} \longrightarrow C_{14}H_{10} + e^-$$

$$C_{14}H_{10} + C_{14}H_{10} \longrightarrow C_{28}H_{10} + 2H^+ + 2e^-$$

Reduction:

$$C_{14}H_{10} + 2H^+ + 2e^- \longrightarrow C_{14}H_{12}$$

Net Reaction:

$$3C_{14}H_{10} \longrightarrow C_{28}H_{18} + C_{14}H_{12}$$
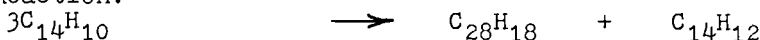
Many common reagents and catalysts cause radical cation formation
which initiate aromatic oxidative coupling. These include H_2SO_4
(9,10),oxidizing agents in acidic media (9,11,12,13), Lewis acids
(14-26), halogens (27), $Ag(ClO_4)$ and iodine (28,29), and metal
salts (30,31). Free radical cations are also formed by such solid
catalytic surfaces as gamma-alumina (32), silica alumina (33),
and zeolites (34). They may also be generated by photoionization
(35,36,37) and electrochemical oxidation(38). Both radical cat-
ions and radical anions were generated at PETC by electrolysis
of SRC-II type solutes in an ESR cavity (39).

In support of this information Ross and Blessing report,
"In the absence of an H-donor, then, oxidative crosslinking takes
place within the coal upon heating, yielding a product even less
soluble in solvents such as pyridine than was the starting coal"
(40). Others have reported the same behavior (41,42). Thus, one
may conclude that Lewis acids cause oxidative hydrogen transfer
from hydrogen donors or oxidative polymerization through a
sequence of coupling reactions. Other radical cation forming
catalysts and reagents may be expected to behave similarly.

CONCLUSIONS

Aromatic structures may polymerize by a stepwise, oxida-
tive coupling reaction, initiated by formation of radical cat-
ions. Common reagents and catalysts cause radical cations
to form.

REFERENCES

1. Davis, J.D., Reynolds, D.A., Naugle, B.W., Wolfson,D.E., and Birge, G.W., Technical Paper 726, U.S. Department of the Interior, U.S. Government Printing Office, 1949.

2. Kriz, J.F., and Ternan, M. A.C.S. Div. Fuel Chem. Preprints, Vol.25, No. 2, p 146, March 24-28, 1980.

3. Sivasubramanian, R., Olson, J.H., and Klatzer, J.R., A.C.S. Div. Fuel Chem. Preprints, Vol. 25, No. 1, p 86, March 24-28, 1980; ibid. p 149.

4. Shih, S.S., Angevine, P.J., Heck, R.H., and Sawruk, S., A.C.S. Div. Fuel Chem. Preprints, Vol. 25, No. 1, p 154, March 24-28, 1980.

5. Frankenheld, J.W., and Taylor, W.F., A.C.S. Div. Fuel Chem. Preprints, Vol. 23, No. 4, p 205, September 10-15, 1978.

6. Pierce, J.B., "New Approsches in Coal Chemistry", A.C.S. Symposium Series, Ed. by Blaustein, B.D., Bockrath, B.C., Friedman, S., and Retcofsky, H.L. (in press).

7. Philip, C.V., and Anthony, R.G., A.C.S. Div. Fuel Chem. Preprints, Vol.24, No. 3, p 204-14, September 10-14, 1979.

8. Dworkin, A.S., Poutsma, M.L., Brynestad, J., Brown, L.L., Gilpatric, L.O., and Smith, G.P., J. Am. Chem. Soc. 1979, 101, 5299.

9. Hoijtink, G.J., and Weijland, W.P., Rec. Trav. Chim., 1957, 76, 836.

10. Carrington, A., Dravnieks, F., and Symons, M.C.R., J. Chem. Soc., 1961, 905.

11. MacLean, C., and Van der Waals, J.H., J. Chem. Phys., 1957 27, 287.

12. Aalbersberg, W.I., Gaaf, J., and Mackor, E.L., J. Chem. Soc. 1961, 905.

13. Dallinga, G., Mackor, E.L., and Verrijn Stuart, A.A., Mol. Phys., 1958, 1, 123.

14. Weissman, S.I., de Boer, E., and Conradi, J.J., J. Chem, Phys. 1957, 26, 963.

15. Lewis, I.C., and Singer, L.S., J. Chem. Phys., 1965, 43, 2712.

16. Lewis, I.C., and Singer, L.S., J.Chem. Phys. 1966, 44, 2082.

17. Forbes, W.F., and Sullivan, P.D., J. Am. Chem. Soc., 1966, 88, 2862.

18. Shine, H.J., and Sullivan, P.D., J. Phys, Chem., 1968, 72, 1390.

19. Sullivan, P.D., J. Am. Chem. Soc., 1968, 90, 3628.

20. Buck, H.M., Bloemhoff, W., and Oosterhoff, L.J., Tetrahedron Lett. 1960, 5.

21. Rooney, J.J., and Pink, R.C., Proc. Chem. Soc., <u>1961</u>, 142.

22. Sato, H., and Aoyama, Y., Bull. Chem. Soc. Japan, 1973, <u>46</u>, 631.

23. Forbes, W.F., and Sullivan, P.D., J. Am. Chem. Soc., 1966, <u>88</u>, 2862.

24. Bell, F.A., Ledwith, A., and Sherrington, D.C., J, Chem. Soc. (B), <u>1969</u>, 2719.

25. Aalbersberg, W.I., Hoijtink, G.J., Mackor, E.L., Weijland, W.P., J. Chem. Soc., <u>1959</u>, 3055.

26 Buchanan, III, A.C., Dworkin, A.S., Brynstad, J., Gilpatrick, L.O., and Smith, G.P., J. Am. Chem. Soc. 1979, <u>101</u>, 5430.

27. Fitzgerald, Jr., E.A., Wuefling, Jr., P., and Richtol, H.H. J. Phys. Chem., 1971, <u>75</u>, 2737.

28. Sata, Y., Kinoshita, M. Sano, M., and Akamatu, H., Bull. Chem. Soc. Japan, 1969, <u>42</u>, 548, 3051.

29. Ristagno, C.V., and Shine, H.J., J. Org, Chem., 1971, <u>36</u>, 4050.

30. Heiba, E.I., Dessau, R.M., and Koehl, Jr., W.J., J. am. Chem. Soc. 1969, <u>91</u>, 6830.

31. Dessau, R.M., Shih, S., and Heiba, E.I., J. Am. Chem. Soc., 1970, <u>92</u>, 412.

32. Flockhart, B.D., Scott, J.A.N., and Pink, R.c., Trans. Faraday Soc., 1966, <u>62</u>, 730.

33. Rooney, and Pink, R.C., Trans. Faraday Soc. 1962, <u>58</u>, 1632.

34. Kurita, Y., Sonoda, T., and Sata, M. J. Catalysis, 1970, <u>19</u>, 82.

35. Lewis, G.N., and Lipkin, D., J. Am. Chem. Soc., 1942, <u>64</u>,2801.

36. Lewis, G.N., and Bigeleisen, J., J. Am. Chem. Soc. 1943, <u>65</u>, 2419.

37. Land, E.J., and Porter, G., Trans. Faraday Soc., 1963, <u>59</u>, 2016, 2027.

38. Bard, A.J., Ledwith, A., and Shine, H.J., "Advances in Physical Organic Chemistry", Vol. 13, Ed. bt V. Gold and D. Bethell, Academic Press, 1976, pp. 156-278.

39. Sprecher, R.S., and Pierce, J.B., Unpublished Work, 1980.

40. Ross, D.S., and Blessing, J.E., A.C.S., Div. Fuel Chem. Preprints, Vol. 24, No.2, p 130, April 2-6, 1979.

41. Low, J.Y., and Ross, D.S., A.C.S., Div. Fuel Chem. Preprints, Vol. 22, No. 7, p 121, August 29-September2, 1977.

42. Mobley, D.P., Salim, S., Tanner, K.I., Taylor, N.D,, and Bell, A.T., A.C.S., Div. Fuel Chem. Preprints, Vol. 23, No. 4, p 138, September 10-15, 1978.

43. Osa, T., Yildiz, A., and Kuwana, T., J. Am. Chem. Soc., 1969, 91, 3994.

44. Nyberg, K., Acta Chemica Scandinavica 1970, 24, 1609.

45. Bobbitt, J.M., Weisgraber, K.H., Steinfeld, A.S., and Weiss, S.G., J. Org. Chem., 1970, 35, 2884.

46. Bobbitt, J.M., Yagi, H., Shibuya, S., and Stock, J.T., J. Org. Chem., 1971, 36, 3006.

47. Bobbitt, J.M., Noguchi, I., Yagi, H., and Weissgraber, K.H., J.Am. Chem. Soc., 1971, 93, 3551.

48. Bechgaard, K., and Parker, V.D., J. Am. Chem. Soc., 1972, 94, 4749.

49. Nelson, R.F., and Adams, R.N., J. Am Chem. Soc., 1968, 90, 3925.

50. Marcoux, L.S., Adams, R.N., and Feldberg, S.N., J. Phys. Chem. 1969, 73, 2611.

51. Nelson, R.F., and Feldberg, S.W., J. Phys, Chem., 1969, 73, 2623.

52. Bacon, J. and Adams, R.N., J.Am. Chem. Soc. 1968, 90, 6596.

53. Ambrose, J.F., Carpenter, L.L., and Nelson, R.F., J. Electrochem. Soc., 1975, 122, 876.

54. Ambrose, J.F., and Nelson, R.F., J. Electrochem. Soc., 1968, 115, 1159.

55. Frank, S.N., Bard, A.J., and Ledwith, A., J. Electrochem. Soc. 1975, 122, 898.

56. Solis, V., Iwasita, T., and Giordano, M.C., J. Electroanal. Chem, 1975, 105, 169.

57. Jordan, J., Ankabrandt, S.J., Robat, A., and Stutts, J.D., Abstract No. 133, 12th Central Regional Meeting, Am. Chem. Soc., Pittsburgh, Pa., November 12-14, 1980.

Compounds Susceptible to Oxidative Coupling

Compounds	References	Compounds	
Benzene	43	Triphenylamines	49,50,51
p-Xylene	44	Anilines	52
Mesitylene	44	Carbazoles	53,54
Durene	44	Iminobibenzyls	55
Phenolic Tetrahydro-		o-Phenylenedianine	56
isoquinolines	45,46,47	Dibenzothiophene	57
Catechol Ethers	48		
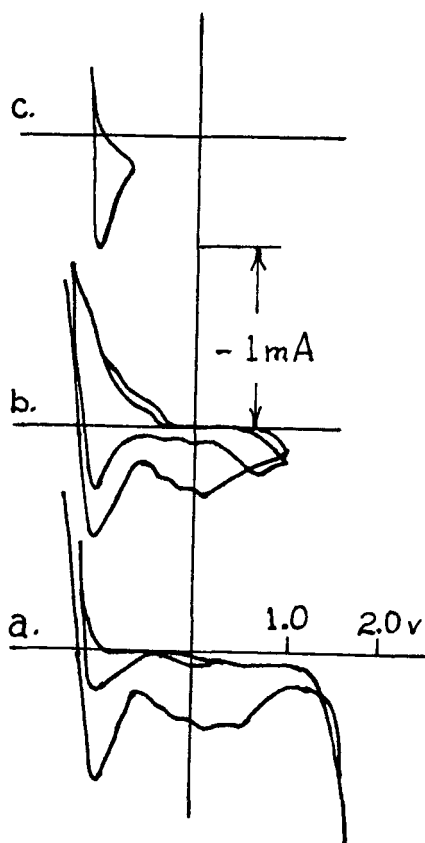
Figure 1. Effect of Film Formation on Voltammograms of Anthracene Oil.
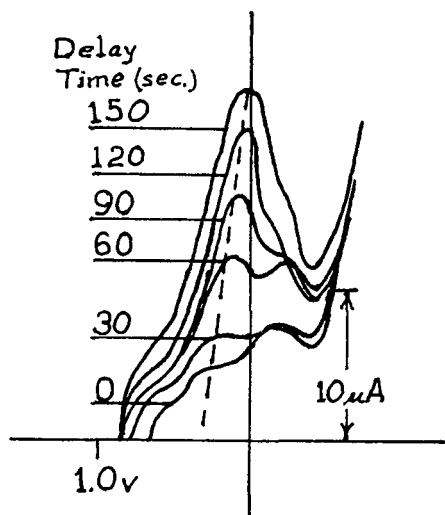
Figure 2. Effect of Film Formation on Voltammogram of SRC-II Type Liquids.

Low Temperature Hydrogenation of Polycyclic Aromatic Hydrocarbons (PAH's)
by Tetralin in a Molten Salt Catalyst*

A. C. Buchanan, III, A. S. Dworkin, L. L. Brown, and G. P. Smith

Chemistry Division, Oak Ridge National Laboratory
P. O. Box X, Oak Ridge, Tennessee   37830

Molten $SbCl_3$ has been shown to be an effective catalyst for the hydrocracking of coal with a high selectivity for the production of distillate hydrocarbons (1), analogous to the more extensively studied molten salt hydrocracking catalysts based on $ZnCl_2$ (2,3). Our research is aimed at a basic study of molten salt catalysis with recent studies examining the chemical behavior of PAH's (model compounds for some of the structural units of coal) in molten salts in which $SbCl_3$ is the primary constituent (4-7). We have observed reactions for PAH's in $SbCl_3$ based melts in which the anhydrous $SbCl_3$ solvent is involved catalytically (4) and stoichiometrically (5,6). Both types of chemistry have been explained by redox driven reactions in the melt in which Sb^{3+} is an oxidant.

Tetralin is often used as a hydrogen donor solvent for thermally generated neutral radicals in coal liquefaction and model compound studies. In the present work, we investigate the possibility that tetralin may act as a hydrogen donor to some PAH's under extremely mild (80°C, no H_2) molten salt catalytic conditions in which PAH radical cations are believed to be present as reactive intermediates.

We have studied the reaction behavior of phenanthrene, pyrene, anthracene, and naphthacene (tetracene) with tetralin at 80°C in neat aprotic $SbCl_3$ by in situ ^{1}H NMR, and by determining the reaction stoichiometry via product analysis following quench and separation procedures. All reagents were carefully purified (4,5), and material transfers were carried out in a controlled argon atmosphere dry box. ^{1}H NMR experiments (at 200 MH_z) were performed under argon in sealed 5mm OD tubes while larger scale reactions were performed under argon in Schlenk glassware. Following a 30 min reaction period, the reaction mixture was hydrolyzed with 6 M HCl and the organic products were extracted into CH_2Cl_2. $SbCl_3$ is a catalyst in these reactions, and no antimony metal was ever observed. The organic products from the reaction of anthracene with tetralin in $SbCl_3$ were analyzed by GC-MS using a 30 m x 0.25 mm ID glass capillary column with an OV-101 liquid phase. Quantitative results were obtained by GC using a 10' x 1/8" column packed with 3% Dexsil 300 and flame ionization detection. Hexamethylbenzene was used as an internal standard, and the results were corrected for differences in detector response.

Solutions of pyrene and phenanthrene with tetralin do not react in neat $SbCl_3$ at 80°C. Only the NMR spectra of the parent PAH and tetralin are observed even at temperatures up to 130°C. However, anthracene and naphthacene react rapidly with tetralin at 80°C, and are selectively hydrogenated to 9,10-dihydroanthracene (DHA) and 5,12-dihydronaphthacene (DHN) respectively. DHA and DHN were identified from a comparison of their ^{1}H NMR spectra with those of authentic samples (4).

The reaction of anthracene with tetralin in $SbCl_3$ is currently the most extensively studied. Tetralin itself is unreactive in $SbCl_3$ (80-130°C), and anthracene also does not show any reaction in $SbCl_3$ at 80°C for the 30 min reaction period. At longer reaction periods, anthracene slowly undergoes Scholl condensation reactions that we have previously reported (4). This Scholl reaction is believed to proceed through the anthracene radical cation. In the presence of tetralin, however, anthracene does not undergo Scholl condensation but instead is rapidly hydrogenated by tetralin. ^{1}H NMR experiments using fully deuterated anthracene demonstrate that the hydrogens added at the 9 and 10 positions of anthracene ($\delta 3.99$) are from the tetralin. This observation is supported by the quantitative analysis of tetralin, anthracene, and DHA in the organic products from larger scale reactions.

The product distribution and reaction stoichiometry are found to depend on the amount of tetralin initially present. We find that the yield of DHA increases with increasing amounts of tetralin and reaches a maximum of 39% at a 2:1 tetralin: anthracene mole ratio (Table 1). Furthermore, we find from GC-MS that the dehydrogenated tetralin does not produce naphthalene. Instead it forms principally two condensed products 1 (MW = 262) and 2 (MW = 308) whose relative amounts also depend on the initial amount of tetralin present as shown in Table 1. The overall reaction stoichiometry can be described as the sum of two limiting equations with Equation 1 predominating at high tetralin/anthracene mole ratios and Equation 2 predominating at low tetralin/anthracene mole ratios.
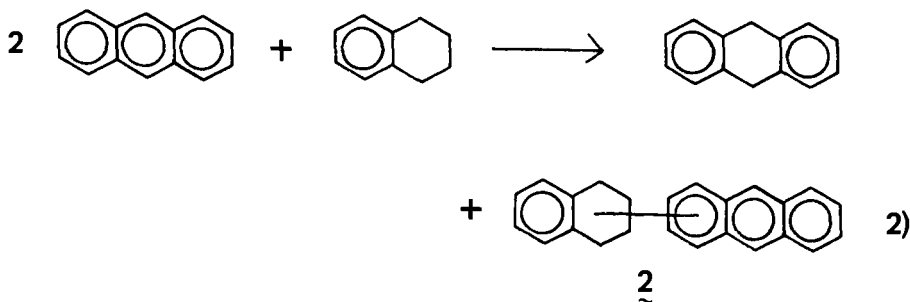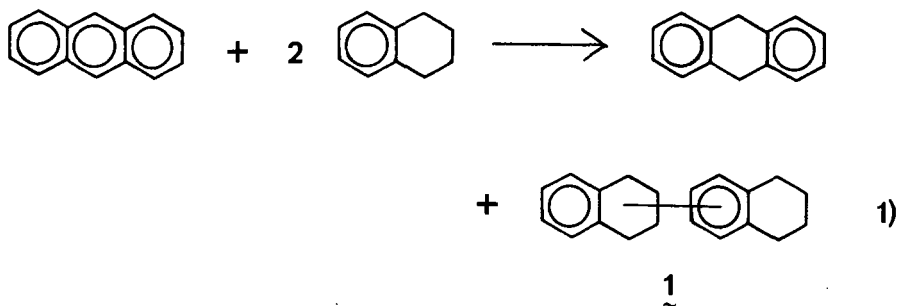
We are in the process of determining the structures of 1 and 2, and these results should provide useful clues towards understanding the reaction mechanism.

Although anthracene and naphthacene are hydrogenated by tetralin in $SbCl_3$, phenanthrene and pyrene are unreactive. From a previous ESR study (7) we know that phenanthrene and pyrene are not oxidized by $SbCl_3$ to radical cations, whereas the more easily oxidized PAH's, anthracene and naphthacene, do form radical cations in $SbCl_3$. These results, along with our previous observations of redox driven reactions in $SbCl_3$ in which Sb^{3+} acts as an oxidant (4-6), suggest that the unusual low temperature hydrogenation reactions reported here proceed via reaction of the PAH radical cation with tetralin. Research in this area is continuing in an effort to further elucidate the reaction mechanism.

REFERENCES

1. Wald, M. M.; U.S. Patent 3 542 665, 1970.
2. Zielke, C. W.; Struck, R. T.; Evans, J. M.; Costanza, C. P.; Gorin, E. Ind. Eng. Chem. Process. Des. Dev. 1966, 5, 151, 158; Zielke, C. W.; Klunder, E. B.; Maskew, J. T.; Struck, R. T. ibid. 1980, 19, 85.
3. Ida, T.; Nomura, M.; Nakatsuji, Y; Kikkawa, S. Fuel 1979, 58, 361.
4. Dworkin, A. S.; Poutsma, M. L.; Brynestad, J.; Brown, L. L.; Gilpatrick, L. O.; Smith, G. P. J. Am. Chem. Soc. 1979, 101, 5299.
5. Buchanan, A. C., III; Dworkin, A. S.; Smith, G. P. J. Am. Chem. Soc. 1980, 102, 5262.
6. Buchanan, A. C., III; Dworkin, A. S.; Smith, G. P. J. Org. Chem. 1981, 46, 471.
7. Buchanan, A. C., III; Livingston, R.; Dworkin, A. S.; Smith, G. P. J. Phys. Chem. 1980, 84, 423.

Table 1. Influence of Tetralin Concentration on the Anthracene-Tetralin-SbCl$_3$ Reaction[a]

Tetralin (mmol)	Anthracene (mmol)	DHA yield (%)[b]	1/2 mole ratio[c]
0	1.40	0	—
0.70	1.40	20	.15
1.40	1.40	30	.50
2.80	1.40	39	1.5
5.60	1.40	38	3.5

[a] Reactions were run in 34.2 mmol SbCl$_3$ at 80°C for 30 min.

[b] Based on original anthracene (±2%).

[c] Based only on gc area ratios.

Copper Catalyzed Aging Reactions of a SRC II Middle Distillate

Laudie Jones and Norman C. Li

Duquesne University, Pittsburgh, PA 15282

INTRODUCTION

Stability of synfuels is an important consideration in direct utilization
or upgrading processes. The tendency of synfuels to form gums and sedi-
ments and to increase in viscosity poses a serious detriment in handling
procedures and burning efficiency. Recently, investigators have studied
the aging characteristics of shale (1) and coal-derived liquids (2-5)
in an attempt to identify the reactive components and to postulate
mechanisms. In aging studies of a Synthoil product in an oxygen atmos-
phere, the viscosity increase was accompanied by a decrease in the con-
tent of oil components and in increase in the content of benzene-insol-
uble components (4). Similar results were observed in a study of a
SRC I/SRC II blend aged by bubbling oxygen directly into the sample (6).
These studies indicate that during oxidative degradation, the oil com-
ponents 'react' to form benzene-insoluble components which are primarily
responsible for the increased viscosity.

The oxidative degradation of a SRC-II middle distillate, which is an oil,
free of asphaltenes and benzene-insolubles was investigated in this
study. The objective was to determine the molecular types of compounds
responsible for the viscosity change and postulate mechanisms. Since
the middle distillate is relatively stable to oxidative degradation,
copper shavings were added to accelerate the process.

EXPERIMENTAL

SRC II middle distillate (b.p. range, 170-276°C) from Illinois no. 6
coal was obtained from Gulf R&D Co., and from a process run operated at
2000 psi hydrogen pressure at 454°C for 1 hr residence time. The coal
liquid was placed in a 3-necked flask, equipped with a gas bubbling
inlet and a condenser to minimize the loss of volatiles. Oxygen was
bubbled through the sample (1-2 ml/min) and copper shavings, 2 wt %,
were added to accelerate the degradation. The flask was immersed in a
thermostat bath at 62°C, and samples were withdrawn at time intervals,
for viscosity and other measurements.

Separation of Aged Coal Liquid into Pentane-Soluble and Pentane-Insol-
uble Components:

Pentane, 20-fold by volume, was added to the aged coal liquid, mixed
(magnetic stirring bar) for 1 hr at room temperature and then filtered
through a 0.5 micron millipore styrene membrane. The precipitate was
dried in a vacuum oven at 80° for 12 hr to remove pentane (94% of the
precipitate is soluble in benzene). Pentane from the pentane-soluble
fraction was removed by distillation at 40°C. The sample was then sub-
jected to rotary evaporation at 70° for 5 min to insure complete removal
of pentane.

INSTRUMENTATION

Viscosity data were obtained at 30° using a Brookfield Synchrolectric

viscometer with a small sample adaptor. Infrared spectra of CS_2 solu-
tions (5g/L) in a 5 mm KBr liquid cell were obtained with a Beckman
IR-20 spectrometer. NMR spectra were obtained with a 60-MHz or 600-
MHz spectrometer as CDCl3 solutions with TMS as internal reference.
Gel permeation chromatograms were obtained with a Waters HPLC and three
μ-styragel columns in series: 10^3, 500, and 100 A using THF as solvent
at a flow rate of 1 ml/min.

RESULTS AND DISCUSSION

Viscosity of the coal liquid increased exponentially with time when aged
at 62°C with oxygen and copper. Aging with copper or oxygen alone at
62° does not affect the viscosity in a 5-day period. Thus, the loss of
volatiles which undoubtedly occurs with oxygen bubbling through the
sample does not contribute to the observed viscosity change.

Infrared spectra of dilute solutions of the coal liquid before and after
aging 5 days at 62° were obtained. The unaged coal liquid shows a prom-
inent free hydroxyl stretching band at 3600 cm^{-1}. The intensity of this
band is not significantly affected by aging with copper or oxygen alone.
Aging with both copper and oxygen, however, reduces the intensity of
this band. This indicates that the hydroxyl group is modified during
aging.

The unaged coal liquid is completely soluble in pentane. After aging
5 days, 30% of the aged coal liquid becomes insoluble in pentane.
Therefore, pentane was used to separate the aged material into two frac-
tions: the pentane-soluble and pentane-insoluble fractions.

Comparison of the 60 MHz NMR spectra of the coal liquid before and after
aging 4 days shows that for the aged pentane-soluble fraction: (a) there
is a decrease in the intensity of the signal at 2.3 ppm attributed to the
methyl protons attached to benzylic groups, (b) the hydroxyl signal at
5 ppm is absent, and (c) the higher-field aromatic signals from 6.3 to
6.8 ppm are also absent. The 600-MHz spectra of the unaged coal liquid
and its acid-free fraction (obtained by ion exchange chromatography) are
presented in Fig. 1. The acid-free spectrum is identical to that of the
aged pentane-soluble fraction (not shown). Obviously, during aging,
acidic methyl substituted phenols are modified and are no longer soluble
in pentane.

The gel permeation chromatography of the unaged coal liquid shows three
peaks (retention times of ~28, 29 and 30 min.) After aging for three
days, profiles of the pentane-separated fractions (Fig. 2) show that the
aged pentane-soluble fraction (top), which constitutes 70 wt % of the
aged coal liquid, contains components which elute at 29 and 30 min. Com-
ponents of the unaged coal liquid which elute at 28 min are no longer
present after aging. As comparison, the acidic and basic components of
the unaged coal liquid (isolated by ion-exchange chromatography) also
elute at 28 min. The profile of the pentane-insoluble fraction (Fig. 2
bottom) shows that this fraction is composed of large molecular size
components. These results suggest that the polar constituents of the
coal liquid are reacting during aging to form large molecular aggregates
which are pentane-insoluble.

The coal liquid was also enriched 10 wt % with acidic and basic frac-
tions which were isolated by ion-exchange chromatography. The effect of
these additives on the formation of pentane-insoluble material is shown
in Table 1. The enriched coal liquids were aged at 62°C for 1 day with
oxygen and 1% copper. Clearly, enrichment with the acid II fraction

116

yields the largest amount of pentane-insoluble material (46 wt %). The acid-II fraction consists of alkyl substituted phenols, the base II fraction contains quinoline type compounds and tne acid I fraction contains carbazoles, indoles, anilines and xylenols (5).

The elemental composition of the coal-liquid before and after aging 4 days is presented in Table 2. The aged pentane-soluble fraction contains 23% less oxygen and 50% less nitrogen than the unaged coal liquid. The decrease in oxygen content is consistent with IR, NMR, and GPC results showing a reduction in the amount of phenolic compounds during aging. The large amount of oxygen contained in the pentane-insoluble fraction indicates: (a) oxygen containing compounds of the coal liquid have been concentrated in this fraction and (b) the oxygen bubbled into the coal liquid has been incorporated into the structure of this fraction. This is confirmed in FTIR spectra (not shown). The increased nitrogen content of the pentane-insoluble fraction indicates that nitrogen containing compounds are involved in the aging reaction.

Significant characteristics of the aged pentane-soluble fraction are that the viscosity and the atomic H/C ratio are similar to those of the unaged coal liquid, but the oxygen and nitrogen contents are less (Table 2). A low heteroatom content is required in syncrude upgrading procedures to prevent fouling of the catalyst. Our experiments have shown that a reduction in heteroatom content can be achieved with metallic copper under mild conditions.

The results of this study suggest that at least one of the aging reactions is the selective polymerization of phenolic compounds. Incorporation of oxygen and polymerization of nitrogen compounds also occur. In oxidative coupling of phenols, -OH groups give way to ether linkages, in the formation of polymers. The distinctly smaller retention time of the pentane-insolubles in the GPC profiles and the increased VPO molecular weight of the pentane-insolubles are consistent with the formation of polymers.

REFERENCES

(1) C.J. Nowack, R.J. Del Fosse, G. Speck, J. Solash and R.N. Hazlett, Preprint, Div. Fuel Chem., Am. Chem. Soc., 25 (3), 40 (1980).
(2) Y.Y. Lin, L.L. Anderson, and W.H. Wiser, Preprint, Div. Fuel Chem., Am. Chem. Soc., 19 (5), 2 (1974).
(3) D. Finseth, M. Hough, J.A. Queiser, and H.L. Retcofsky, Preprint, Div. Petrol. Chem. Am. Chem. Soc., 24 (4), 979 (1979).
(4) F.R. Brown and F.S. Karn, Fuel, 59, 431 (1980).
(5) D.W. Brinkman, J.N. Bowden, J.W. Frankenfeld, and W.F. Taylor, Preprint, Div. Fuel Chem., Am. Chem. Soc., 25 (3), 110 (1980).
(6) T. Hara, L. Jones, N.C. Li, and K.C. Tewari, unpublished results.

Table 1. Aging of Enriched Coal Liquids

(62°C, 1% Cu, O_2, 1 Day)

	Pentane Insolubles
Ill #6	14%
10% Acid-Free Enriched	10
10 Acid I Enriched	11
10% Acid II Enriched	46
10% Base II Enriched	12

Table 2. Elemental Composition and Characterization of SRC II Middle Distillate, Before and After Aging 4 days, 2 wt % Copper and Oxygen at 62°C

	Unaged	Aged Pentane-Soluble	Aged Pentane-Insolubles
C	85.58	86.67	75.48
H	9.12	9.33	6.00
N	0.85	0.43	1.80
O	4.29	3.31	12.78
S	0.19	0.27	0.27
	100.03	100.00	96.29
Copper			2.7
MW	172*	170**	570***
Viscosity+	4.3	3.6	
Atomic H/C	1.28	1.28	0.96

*VPO method, toluene, 37°C 2-15 g/l
**VPO method, methylene chloride, 28°C, 4-7 g/l
***VPO method, pyridine, 86°C, 4-7 g/l
+Centipoise at 30°C

FIG. 2

GPC PROFILES AGED ILL NO. 6

AGED
PENTANE SOLUBLES

UV 254

20 24 28 32
MIN

AGED
PENTANE INSOLUBLES

UV 254

20 24 28 32
MIN

FIG. 1

600 MHZ ^{1}H NMR SPECTRA
ILL NO. 6

ORIGINAL

7.5 PPM 2.5

ACID FREE

7.5 PPM 2.5

119
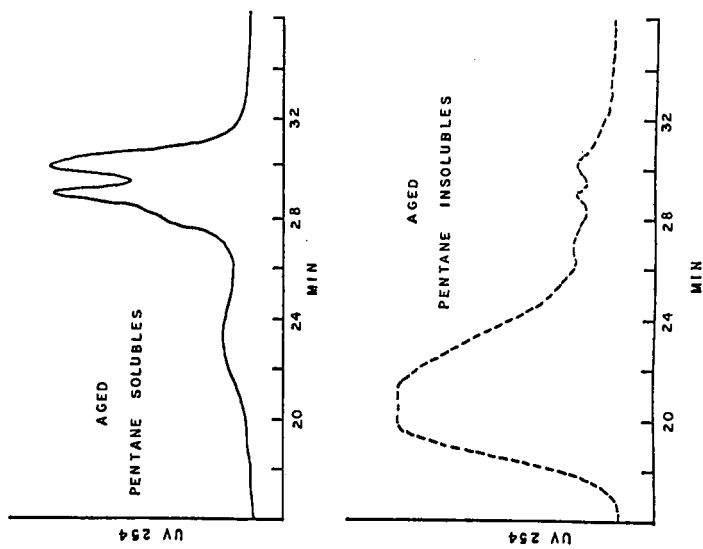
THE OXIDATION OF FUEL OIL #6 STUDIED BY DIFFERENTIAL SCANNING CALORIMETRY

By

J.A. Ayala and M.E. Rincón

Instituto de Investigaciones Eléctricas,

Departamento de Combustibles Fósiles,

Apdo. Postal 475, Cuernavaca, Mor.,

México.

INTRODUCTION

The studies on combustion of heavy fuel oil are important because of the extended use of this fuel as an energy source for the production of electricity. With the continuous increase in the extraction of products from crude oil, there exists a continuous degradation in the quality of the residue that is to be burned in a utility boiler. The degradation of the quality in the residual oil, means a higher sulfur content in the fuel, higher aromaticity, and higher asphaltene and metallic content. Some of these species, yield products of combustion which are aggressive to both the environment, and some of the components within the boiler. It is believed (1) that an understanding of why and how pollutants form, must come from an understanding of the chemical kinetics in the flame. That is, in order to protect the environment, and increase the availability of a large boiler more research is needed to understand the chemistry of oxidation of complex fuel mixtures.

Various authors (2-6) have pointed out the potentiality of the different techniques in thermal analysis for the characterization of petrolum products and coal. However, very little kinetic information has been extracted from the studies which involve the use of thermoanalytical techniques. The chemical kinetics of thermo-oxidative processes in fuels, may contribute to a large extent to the understanding of the chemistry

of oxidation of such mixtures. Weber (2), has reported the
potencial utilization of differencial thermal analysis (DTA)
to obtain kinetic parameters for the oxidation of hydrocarbons.
He concluded, though, that for the kinetics of oxidation of
heavy fuel oil no theory for DTA could yet be used, because of
the complexity of the thermograms. Adonyi (3), has shown that
kinetics may be obtained for petroleum products by means of DTA,
and thermogravimetric techniques (TG). More recently, Noel and
Cranton (4), have measured the activation energy, Ea, for the
oxidation of lube oil by differential scanning calorimetry (DSC).
These authors make the observation that more research is necessary
in order to have a better understanding of the results observed by
DSC. Smith et al. (7), have used TG to measure the rate, and the
Ea for the oxidation of sixty-six coal samples. Valayavin et al.
(8), utilized TG to study the thermolysis of high molecular weight
petroleum residues, and established a reaction rate law as a function
of the viscosity of the medium and a diffusion parameter.

In the present work, we have utilized DSC to study the
thermal oxidation of four samples of mexican fuel oil. We have also
obtained kinetic parameters such as the overall activation energy
for the oxidation of the fuel at low temperature (200 - 550°C).

EXPERIMENTAL

The experimentation was carried out by means of a DuPont
Thermal Analyzer Model 990 with its standard DSC attachment. The
instrument was calibrated with Indium. The temperature was varied
from 20 to 550°C with a scanning rate of 10°C/min. The sensitivities
used were 20 and 50 mV/cm. The sample and reference pans were made
of aluminum, and the sample weight was kept at around 2 mg. Four
different samples of mexican fuel oil # 6 were analyzed, and the
experiments were performed with a constant flow of nitrogen, oxygen
or a mixture of both. The flow rates, and the O_2/N_2 ratios utilized

throughout the experiments are shown in Table 1.

RESULTS AND DISCUSSION

Experiments with pure nitrogen flow did not show any endothermic reaction, but a gradual displacement from the base line, especially above 300°C. This displacement indicates that the evaporation of some compounds in the fuel has ocurred. A residue was observed in the sample pan after the run was completed. Figure 1 shows a typical thermogram obtained with pure oxygen flow. This thermogram es very similar to those shown in the literature for tar sands (2), or high asphaltene crude oil (9), which may show the quality or the characteristics of the fuel. Indeed, the fuel studied here has a > 10% asphaltene content, and > 3% sulfur. In figure 1, it is observed a small exothermic reaction zone (zone 1) at ~ 300°C, and a larger zone (zone 2), also exothermic, which starts at ~ 400°C. Several small peaks are shown at the low temperature side of the second zone. It is also observed a rapid fall-off of the signal after the maximum has been reached. All the sample was consumed during the experiments with high oxygen concentration in the gas flow. Figure 2, presents a thermogram obtained with a low oxygen concentration in the gas flow. It is observed that the reaction zone is shifted towards higher temperatures.

From the calibration of the instrument with In, it was calculated that the sensitivity of 20 mV/cm corresponded to 43.5 mcal/min-cm. Table 2 shows the results for the heat of reaction measured for both exothermic zones in the thermograms. The values in Table 2 range from as high as 3.3 Kcal/g for the experiments with pure O_2, to as low as 1.4 Kcal/g for the experiments with a 1:9 O_2/N_2 ratio. These values for the heat of reaction, are low if they are compared with the usual heat content of these fuels, which is ~ 10 Kcal/g. Other reports (4), have also measured similar heats of reaction to those reported here, and utilizing a similar

122

technique. The difference between our values, and the value
of 10 Kcal/g for the heat content of the fuel are explained
as follows: 1) First, we have a flow system in which we are
continuously carrying away heat from the reaction envelope.
2) Second, most probably, we do not have a complete oxidation
of the fuel. That is, we do not have a complete adiabatic
combustion-type of experiment from which the heat content of
the fuel is normally evaluated. It must be observed, that the
extreme values for the heat of reaction in table 2 were obtained
for experiments with approximately the same total flow. The only
difference among both experiments is the oxygen concentration.
Similar features were observed in other investigations where
TG and DTA were used (2,9), and in which the pressure of air
inside the reaction device was varied. That is, the actual
oxygen concentration, and availability for the fuel was varied.
We may conclude that different reaction channels are being
followed according to the oxygen concentration. Hence, different
heats of reaction are measured for the experiments with pure O_2,
and for experiments with a 1:9 O_2/N_2 ratio.

      In order to obtain kinetics parameters from the
thermograms, we utilized the theory of Borchardt and Daniels
(10). The zones I and II in the thermograms were treated indepen
dently, and it was assumed a reaction of pseudo-first order. A
pseudo-first order kinetics implies a first order reaction with
respect to the fuel, and a constant oxygen concentration. The
latter assumption is clearly justified for the experiments with
a high oxygen content in the gas flow. A first order reaction
with respect to the fuel may be justified through the results .
Figure 3 and 4 show the Arrhenius plot for the zone I of the
thermograms. The results in figure 3 are for the experiments
with pure oxygen; whereas those in figure 4 present the experiments
with low concentrations of O_2 in the gas flow. For the data in
figure 3 it is possible to draw two different straight lines.
Thus, two different activation energies are obtained, one of
12 ± 1 Kcal/mol, and a higher one of 22 ± 1 Kcal/mol. From the data

in figure 4, only one activation energy has been obtained with a value of 16 ± 1 Kcal/mol. The lower value for Ea in the experiments with pure O_2 occurs at the higher temperatures of zone I in the thermograms. Thus, it is possible that diffusion controlled reactions occur at these temperatures. In fact, it has been found (8) that, the thermolysis of petroleum residues in a TG experiment is highly influenced by diffusion processes. The results in figure 4, along with the results of the heat of reaction for the experiments with a poor oxygen concentration, indicate that a different reaction scheme is being followed. This last statment should be supported by the identification of the reaction products.

Figures 5 and 6 show the results for zone II in the thermograms. Figure 5 presents the results for the pure O_2 experiments, and figure 6 presents the data for the experiments with a low oxygen concentration. In this case, we only obtain one activation energy for the pure oxygen data (figure 5) $Ea=36\pm1$ Kcal/mol. In figure 6 we observe a straight line only for the experiments with a 1:3 O_2/N_2 ratio, and gas flows of 41 ml/min and 87 ml/min. The rest of the data points in figure 6 show large deviations from a straight line. These deviations in the experiments, with the lowest oxy gen concentration in the gas flow, seem to indicate that we may no longer assume a pseudo-first order kinetics.

The various techniques in thermal analysis, may be very useful to obtain an overall view of the oxidation reactions for mixtures as complex as the heavy fuel oil. This overall picture, may include quantitative information such as activation energies. In general, we believe that these studies may serve as a basis to understand more complex oxidation reactions such as those occuring within a flame.

ACKNOWLEDGMENTS

REFERENCES

1) I. Glassman, "The Homogeneous Oxidation Kinetics of Hydrocarbons: Concisely and With Application", Annual Meeting of The Combustion Institute. Sezione Italiana, Torino, June 1979.

2) L. Weber, "Application of DTA to Petroleum Chemistry", Chem. Inst. Can.,Proc. 1st. Toronto Symp. on Thermal Analysis, Feb. 8 1965, p.141-62.

3) Z. Adonyi, "Thermoanalysis of Petroleum products criticism to the Conradson number and a possibility to determine the flash point", Period Polytech, Chem. Eng. v 16 n 3, 1972, p.285-298.

4) F. Noel and G.E. Cranton, Anal. Calorimetry, 3, 305 (1974).

5) R.L. Blaine, American Laboratory, January 1974, 18.

6) E.J. Gallegos, "Analysis of Five U.S. Coals", Adv. in Chem. Ser., No. 170, p. 13 (1979).

7) S.E. Smith, R.C. Neavel, R.N. Miller and E.J. Hippo, "DTGA Combustion of Coals in the Exxon Coal Library", The Combustion Institute, Spring Meeting, Central States Section, Baton Rouge, March 1980.

8) G.G. Valayavin. V.V. Fryazinov, M. Yu. Dolomatov, and E.V. Artamonova, Khim. Tekh. Toplivi Masel, March 1980, p. 54.

9) J.H. Bae, Soc. Petr. Eng. J., June 1977, p.211.

10) H.J. Borchardt and F. Daniels, J.Phys.Chem., 61, 917(1957).

TABLE 2

HEAT OF REACTION

SAMPLE	FLOW (ml/min)	RATIO $O_2:N_2$	ZONE I (Kcal/g)	ZONE II (Kcal/g)
#1	90	1:0	0.4	1.9
#2	90	1:0	0.6	2.5
#3	90	1:0	0.5	2.5
#4	98	1:0	0.5	2.7
#4	89	1:1	0.3	1.8
#4	87	1:3	0.2	1.6
#4	91	1:9	0.2	1.2
#4	41	1:3	0.3	1.6
#4	24	1:3	0.2	1.4

TABLE 1

EXPERIMENTAL FLOW CONDITIONS

FLOW (ML /MIN)	GAS	RATIO $O_2:N_2$
90–100	N_2	0:1
90–100	O_2	1:0
85–90	O_2/N_2	1:1
85–90	O_2/N_2	1:3
40	O_2/N_2	1:3
24	O_2/N_2	1:3
11	O_2/N_2	1:3
90	O_2/N_2	1:9
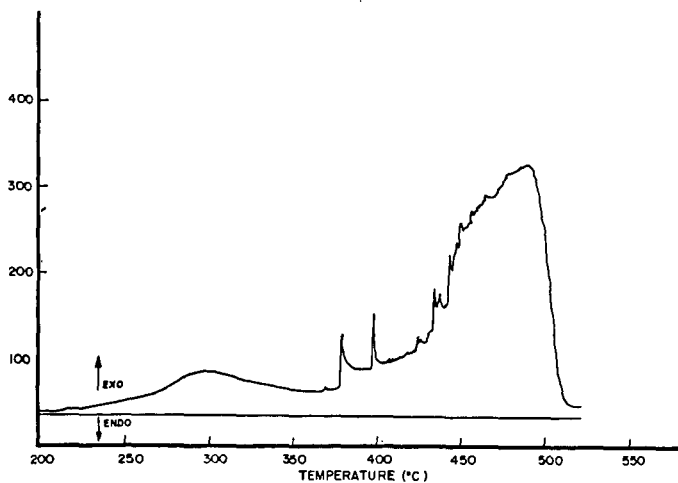
Figure 1. Sample #4. Atmosphere: pure oxygen.
Total flux: 98 ml/min.
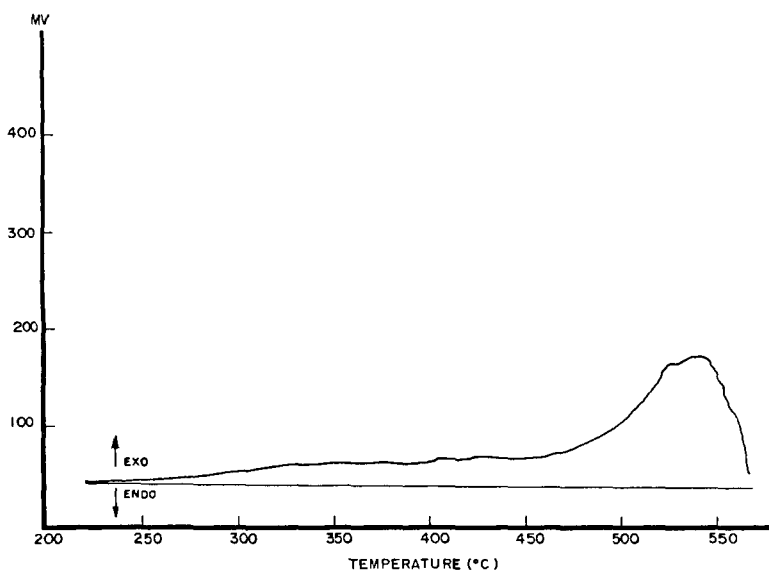
Figure 2. Sample #4. Atmosphere: O_2/N_2 (1:9).
Total flux: 91 ml/min.

128

Figure 4. Arrhenius plot for experiment with low oxygen concentration Zona I. Sample #4.

χ 1:3 O₂/N₂ (87 ml/min)
† 1:3 O₂/N₂ (41 ml/min)
Φ 1:3 O₂/N₂ (24 ml/min)
Δ 1:9 O₂/N₂ (91 ml/min)

Figure 3. Arrhenius plot for experiments with pure oxygen. Zone I.

Δ Sample #1 (O₂= 90 ml/min)
Φ Sample #2 (O₂= 90 ml/min)
† Sample #3 (O₂= 90 ml/min)
χ Sample #4 (O₂= 98 ml/min)

129
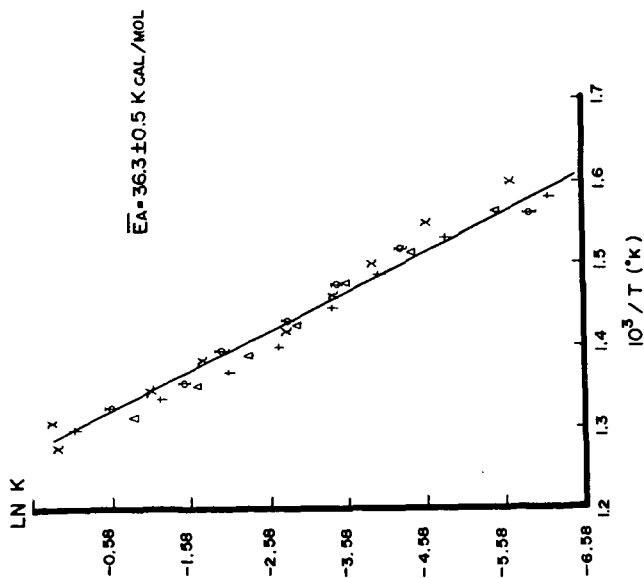
Figure 5. Arrhenius plot for experiments with pure oxygen. Zone II.
△ Sample #1 (O_2= 90 ml/min)
φ Sample #2 (O_2= 90 ml/min)
+ Sample #3 (O_2= 90 ml/min)
χ Sample #4 (O_2= 98 ml/min)
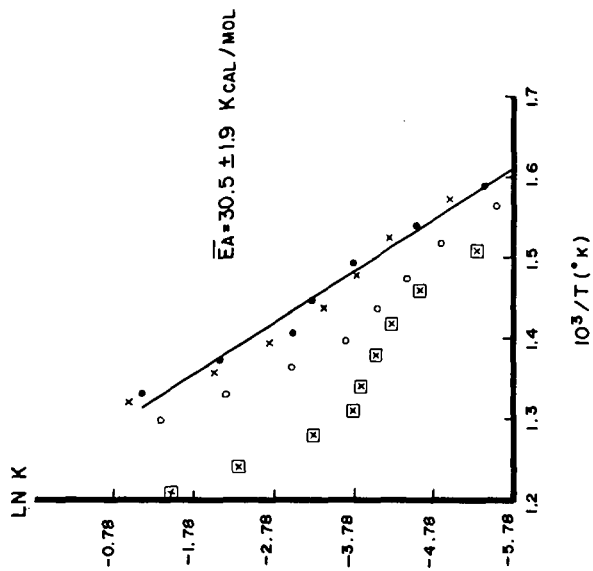
Figure 6. Arrhenius plot for experiments with low oxygen concentration. Zone II. Sample #4.
χ 1:3 O_2/N_2 (87 ml/min)
● 1:3 O_2/N_2 (41 ml/min)
⊠ 1:3 O_2/N_2 (24 ml/min)
○ 1:9 O_2/N_2 (91 ml/min)

INVESTIGATION IN THE USE OF HEAVY OILS
(AND DERIVATIVES) TO PROCESS COAL

SPEROS E. MOSCHOPEDIS[1], RANDALL W. HAWKINS[1] and
JAMES G. SPEIGHT[2]

1. Coal Research Department
    Alberta Research Council
    11315 - 87th Avenue
    Edmonton, Alberta, Canada
    T5G 2C2

2. Corporate Research Science Laboratories
    Exxon Research and Engineering Company
    P.O. Box 45, Linden, N.S.   07036

INTRODUCTION

The use of oil as an energy source started from the beginning of this century,
and for many years has been regarded as the cheapest source of liquid fuels.
However, the recent dramatic escalation in work oil consumption and price, and
the concern over future supplies, which are expected to fall short of demand
by the end of this century, have forced the energy industry to consider other
sources for the production of liquid fuels. The sources which can provide
liquid fuels are coal and lignite, oil sands, oil shales, peat, and biomass.

Coal is the largest source of hydrocarbons in the world which can be con-
verted to liquid fuels, but requires enormous amounts of expensive hydrogen.
In an attempt to reduce the cost of hydrogen required to convert coal to liquid
fuels, the use of oil sands bitumens, Lloydminster heavy oil, and other liquids
derived therefrom, have been reported (1,2) as potential low cost hydrogen
donor solvents. The present study is a continuation of the work reported
elsewhere (1,2) and reports the effect of process parameters (i.e. temperature,
pressure and time) on the extent of the coal conversion and on product dis-
tribution.

EXPERIMENTAL

Oil sands bitumen (dry) and coker gas oil were obtained from Great Canadian
Oil Sands Ltd. (GCOS)*. Cold Lake bitumen and Lloydminster heavy oil were
obtained from the Alberta Research Council sample bank. All samples were used
as received.

The experimental conditions for the solvation and catalytic hydrogenation
of coal, and the procedure for the fractionation of the bitumen and various
liquid derivatives are described elsewhere (2,3).

Elemental compositions were determined by the micro-analysis laboratories
of the Alberta Research Council and the University of Alberta. Molecular
weights were measured osmotically in pyridine, and the nmr spectra were recorded
(carbon tetrachloride solutions) by means of a Varian E-60B spectrometer. Gas
analysis were obtained by means of a Hewlett Packard gas chromatograph fitted
with a Poropak N column and a molecular sieve.

* Now Suncor, Oil Sands Division.

The aromatics content, f_a, of the bitumen and derived liquids has been defined elsewhere (2).

RESULTS AND DISCUSSION

The current communication is a continuation of the previous investigations (1,2) whereby coal can be converted to soluble products using oil sands bitumen, Lloydminster heavy oil and liquids derived therefrom as solvents.

The data (Figure 1) indicate that it is, indeed, possible to solubilize part of the coal by using the Athabasca bitumen, and related liquids as solvents, and as previously reported (1,2) the extent of solubilization varies depending upon the type of solvent used. Nevertheless conversion yields using these solvents compared favorably to the results obtained when tetralin (a well-known hydrogen donor for coal liquefaction) was used as a solvent, particularly in the presence of hydrogen. It is note worthy that when tetralin was used as solvent, coal conversion yields from the solvation and noncatalytic and catalytic hydrogenation show little variation (i.e. from 47-50%) and practically remain constant. On the other hand, the percent conversion yields of the other solvents have shown a substantial increase in the presence of hydrogen, for example, from 10 to 24% in coal solvation to 30 to 40% in the catalytic hydrogenation (Figure 1).

CONTROL EXPERIMENTS

Control experiments were performed in the manner described elsewhere (2), in order to determine the degree of coke (toluene insolubles) formation during the thermal treatment of the solvents. Briefly, when these liquids are heated with or without hydrogen (in the absence of catalyst) for 60 minutes at 400°C, an overall increase in the aromatic contents is evident as their H/C atomic ratios decrease and their f_a values increase when compared with the parent solvents (Table 1). In contrast, when the solvents are heated in the presences of hydrogen and catalyst, an overall increase in the aliphatic content is evident. The API gravities of the solvents are generally increased by the heat treatment but surprisingly the API gravities of CGOS bitumen and coker gas oil are drastically reduced (Table 2) when these solvents are heated at 450°C, although liquid products of high fluidity were obtained. In addition, changes in the hetero-atom contents in these solvents (Table 1). For example oxygen and sulphur contents are decreased, particularly during the catalytic hydrogenation of the solvent, while nitrogen contents in general remained unchanged or increased supporting the concept of thermal stability due to its inclusion in hetero-aromatic systems (4). Compositional differences of the solvents as a result of heat treatment also occur (Table 2) and there are variations in the distribution of products--coke (toluene insolubles), liquids (toluene solubles), and gases (Table 3). Coke formation under these conditions (temperature 400°C and 450°C) was anticipated since oil sands bitumen and heavy oil are susceptible to heat (5,6). Composition of gases from the thermal treatment of solvents (Table 4) shows that the gas products mainly consist of hydrocarbons and hydrogen sulfide.

132

PROCESS CONDITIONS

EFFECT OF TEMPERATURE

a) Coal Solvation

Comparison of the conversion yields of coal solvation, using GCOS bitumen
and coker gas oil as solvents (Table 5), shows that the conversion yield is
constantly increased with increasing temperature for coal/bitumen processing
whilst the conversion yield reaches a maximum value at 400°C, and then drast-
ically drops to almost zero for coal/coker gas oil processing. Trends in the
distribution of the reaction products (solids, liquids, and volatiles,(Table
5) using these two solvents were similar.

The toluene insoluble products (solids, undissolved coal plus coke) has a
minimum value at 400°C, which coincides with the optimum conditions for the
liquid and volatile products, and then drastically increases at 450°C due to
coke formation as determined from blank experiments (Table 3). Because coke
formation occurs simultaneously while coal is converted to liquid and gaseous
products, greater amounts of toluene insolubles are obtained than the initial
coal charge at 450°C. Furthermore, the liquid (toluene solubles) and volatile
products follow opposite paths; as the reaction temperature increases, the
maximum yield of volatiles (at 450°C) correspond to the lowest yield of liquids,
suggesting that solids and volatiles are produced at the expense of liquid
products.

b) Catalytic Hydrogenation

It is apparent from the data (Table 5) presented that the trends due to
increase of reaction temperatures are similar for both solvents with the only
difference in the yields of solid products. Thus, the conversion yields for
both solvents are increased with temperature but when bitumen is used as sol-
vent coal conversion yields reaches a maximum (at about 400-450°C) while coal
conversion yields with coker gas oil continue to increase with temperature.

The percent distribution of the various products derived by processing coal
with the two types of solvents show (Table 5) that the yields of liquids are
high at lower temperatures (i.e., decrease with increasing temperature) while
the yields of volatiles increase with increasing temperature indicating again,
that the volatiles are produced at the expense of liquid products. On the
other hand, the yield of solids produced using coker gas oil as solvent con-
tinuously decreases as temperature increases; the solids decrease and then
appear to increase as the temperature exceed 400°C.

EFFECT OF TIME

a) Coal Solvation

The data demonstrate (Table 6) that coal solvation yield with both solvents
reaches a maximum value after 60 minutes at 400°C, and then drastically drops.
The product distribution (solids, liquids, and volatiles) is similar for both
the coker gas oil and bitumen and resembles the product distribution for coal
solvation with both solvents (Table 6). It is apparent that a reaction time
of 60 minutes at 400°C coincides with the optimum conditions for the most
efficient production of liquid products.

133

b) Catalytic Hydrogenation

Conversion yields using bitumen as solvent reach a maximum after 60 minutes reaction time, and then levels off, while with coker gas oil continues to increase linearly (Table 6). The relationship between time and product distribution by processing coal with bitumen show that there is not a drastic effect as the time exceeds 60 minutes. However, when coker gas oil is used as solvent, the liquid products are steadily increased and solids decrease without a substantial increase of gases indicating that under these conditions, longer periods are beneficial.

EFFECT OF PRESSURE

The limited data available (Table 7) show that conversion yields reach a maximum at a pressure of approximately 1000 psig. There is a pronounced effect on the yields of liquid products which are constantly increased with increasing pressure; volatiles decrease with increasing reaction pressure, while there is a small variation of the solids at pressure over 1000 psig.

Tables 8, 9, and 10 show the relative composition of gases derived from processing coal under various conditions using bitumen and coker gas oil as solvents. As previously discussed, the evolution of oxygen and sulphur from coal as carbon monoxide and dioxide, and as hydrogen sulphide particularly in the catalytic hydrogenation of coal are the most noticeable features.

ACKNOWLEDGEMENT

REFERENCES

1. Moschopedis, S.E.: "The use of oil sands bitumen and its derivatives as hydrogen donors to coal", Fuel, 59, 67, 1980.

2. Moschopedis, S.E., Hawkins, R.W., Fryer, J.F., and Speight, J.G.: "The use of heavy oils (and derivatives) to process coal". Fuel, 59, 647, 1980.

3. Moschopedis, S.E., Fryer, J.F., and Speight, J.G.: "Investigation of the carbonyl functions in a resin fraction". Fuel, 55, 187, 1976.

4. Moschopedis, S.E, and Speight, J.G. "Investigation of nitrogen types in Athabasca bitumen". Preprints, Am. Chem. Soc., Div. Fuel Chem., 24, (4), 1007, 1979.

5. Speight, J.G. "Thermal cracking of Athabasca bitumen, Athabasca asphaltenes, and Athabasca deasphalted heavy oil", Fuel, 40, 134, 1970.

6. Speight, J.G., and Moschopedis, S.E., "The production of low-sulfur liquids and coke from Athabasca bitumen", Fuel Processing Technology 2, 295, 1979.

Table 1 — Analyses of bitumens and derived liquids
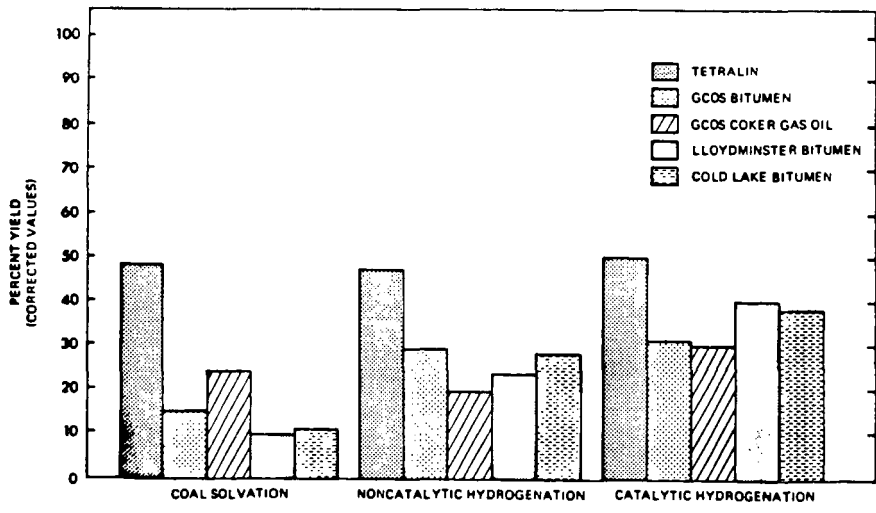
Material description	% Composition					MW	H/C	Haros %	fₐ
	C	H	N	O	S				
a) Parent material									
GCOS bitumen Athabasca deposit	84.18	10.31	0.40	0.78	4.33	532	1.47	5.8	29.9
GCOS coker gas oil	84.65	10.95	0.40	0.64	3.34	296	1.55	8.2	28.7
Lloydminster heavy oil	83.75	10.94	0.27	1.47	3.55	410	1.57	7.0	27.1
Cold Lake bitumen	83.68	10.66	0.39	1.13	4.13	508	1.53	7.3	29.1
b) Heated for 60 min at 400° C									
GCOS bitumen Athabasca deposit	84.96	9.98	0.67	0.68	3.41	394	1.41	6.8	34.3
GCOS coker gas oil	85.61	10.73	0.30	0.60	3.32	311	1.50	9.4	31.8
Lloydminster heavy oil	84.77	10.80	0.30	0.81	3.04	335	1.52	9.7	31.0
Cold Lake bitumen	84.54	10.67	0.41	0.90	3.58	468	1.51	9.5	31.5
c) Heated for 60 min at 400° C, H₂ – 1000 psig									
GCOS bitumen Athabasca deposit	85.64	9.90	0.45	0.85	3.13	420	1.39	11.5	38.6
GCOS coker gas oil	84.74	10.52	0.28	0.80	3.65	350	1.49	10.9	33.6
Lloydminster heavy oil	86.08	10.25	0.26	0.83	2.56	410	1.43	12.0	37.1
Cold Lake bitumen	84.84	9.78	0.42	1.24	3.69	374	1.38	9.5	37.4
d) Heated for 60 min at 400° C, H₂ – 1000 psig + catalyst									
GCOS bitumen Athabasca deposit	84.88	10.93	0.33	0.69	3.16	551	1.54	4.7	32.8
GCOS coker gas oil	87.81	11.26	0.15	0.11	0.67	341	1.54	5.4	27.1
Lloydminster heavy oil	85.52	11.86	0.19	0.40	2.01	425	1.66	5.0	20.9
Cold Lake bitumen	85.61	11.63	0.30	0.63	1.81	440	1.63	8.8	25.6

FIGURE 1.

Table 2. *Composition and properties of bitumens and liquids derived from bitumen heated under various conditions*

Material description	% Asphaltenes	% Resins	% Oils	API gravity
a) Parent material				
GCOS bitumen Athabasca deposit	15.4	22.3	62.3	7.5
GCOS coker gas oil	0.5	5.6	93.9	17.3
Lloydminster heavy oil	11.9	20.5	67.6	14.8
Cold Lake bitumen	16.1	18.9	64.9	7.5
b) Heated for 60 min at 400° C				
GCOS bitumen Athabasca deposit	15.0	20.1	64.9	9.8
GCOS coker gas oil	0.2	10.2	89.6	16.0
Lloydminster heavy oil	12.5	13.5	74.0	14.3
Cold Lake bitumen	14.5	12.0	73.5	11.4
c) Heated for 60 min at 450° C				
GCOS bitumen Athabasca deposit	7.8	11.4	80.8	3.8*
GCOS coker gas oil	11.2	17.9	70.9	3.6*
d) Heated for 60 min at 400° C, H_2 - 1000 psig				
GCOS bitumen Athabasca deposit	8.7	16.5	74.8	17.7
GCOS coker gas oil	0.2	10.3	89.5	21.9
Lloydminster heavy oil	6.3	27.0	66.7	16.8
Cold Lake bitumen	11.2	12.2	76.6	12.9
e) Heated for 60 min at 400° C, H_2 - 1000 psig + catalyst				
GCOS bitumen Athabasca deposit	8.4	12.1	79.5	12.5
GCOS coker gas oil	0	7.9	92.1	23.7
Lloydminster heavy oil	7.3	15.5	77.2	18.4
Cold Lake bitumen	7.4	13.3	79.3	17.4
f) Heated for 60 min at 400° C, H_2 - 2000 psig + catalyst				
GCOS bitumen Athabasca deposit	8.4	–	91.6 –	13.7
GCOS coker gas oil	0.3	–	97.7 –	16.2
g) Heated for 60 min at 450° C, H_2 - 1000 psig + catalyst				
GCOS bitumen Athabasca deposit	4.7	10.1	85.2	10.3
GCOS coker gas oil	0	7.0	93.0	20.6

Table 3. Product distribution of bitumen and liquids derived from bitumen heated under various conditions.

Material description	Volume insolubles %	Toluene solubles %	Volatiles plus Ar. %
a) Heated for 60 min at 400°C			
GCOS bitumen Athabasca deposit	2.6	90.2	7.2
GCOS coker gas oil	1.4	90.7	7.9
Lloydminster heavy oil	0.2	92.0	7.8
Cold Lake bitumen	2.0	89.8	8.2
b) Heated for 60 min at 450°C			
GCOS bitumen Athabasca deposit	26.2	28.7	45.1
GCOS coker gas oil	11.6	47.6	40.8
c) Heated for 60 min at 400°C, H$_2$-1000 psig			
GCOS bitumen Athabasca deposit	1.3	91.2	7.7
GCOS coker gas oil	nil	97.0	3.0
Lloydminster heavy oil	1.5	86.6	11.9
Cold Lake bitumen	1.7	90.6	7.7
d) Heated for 60 min at 400°C, H$_2$-1000 psig + catalyst			
GCOS bitumen Athabasca deposit	1.2	91.7	7.1
GCOS coker gas oil	nil	94.0	6.0
Lloydminster heavy oil	0.8	95.9	3.3
Cold Lake bitumen	1.1	94.4	4.5
e) Heated for 60 min at 400°C, H$_2$-2000 psig + catalyst			
GCOS bitumen Athabasca deposit	1.0	89.6	9.4
GCOS coker gas oil	nil	96.4	3.6
f) Heated for 60 min at 450°C, H$_2$-1000 psig + catalyst			
GCOS bitumen Athabasca deposit	4.3	36.7	59.0
GCOS coker gas oil	0.5	49.5	50.0

Table 4. Gas product distribution derived from bitumens and liquids derived from bitumen heated under various conditions.

Material description	CO	CO$_2$	H$_2$S	CH$_4$	C$_2$H$_6$	C$_3$H$_6$	C$_2$H$_2$	C$_3$	C$_4$	C$_5$ isc apt
a) 60 min, 400°C										
GCOS bitumen Athabasca deposit		N.D.								
GCOS coker gas oil		N.D.								
Lloydminster heavy oil			14.3	37.6	0.9	26.2	-	17.1	1.5	4.4
Cold Lake bitumen		1.0	18.4	31.0	0.7	23.9	-	16.3	2.0	3.9
b) 60 min, 450°C										
GCOS bitumen Athabasca deposit		0.8	6.6	50.9	0.2	24.5	-	12.9	1.7	2.6
GCOS coker gas oil		0.2	2.5	54.9	0.1	26.2	-	12.7	1.7	2.7
c) In presence of H$_2$-1000 psig (60 min, 400°C)										
GCOS bitumen Athabasca deposit		0.8	14.6	26.0	0.3	14.0	-	13.4—26.6		
GCOS coker gas oil		N.D.								
Lloydminster heavy oil			11.9	29.5	0.3	14.8	-	13.8—29.6		
Cold Lake bitumen		0.5	12.7	27.3	0.3	14.0	-	11.2—34.5		
d) In presence of H$_2$-1000 psig + catalyst (60 min, 400°C)										
GCOS bitumen Athabasca deposit		N.D.								
GCOS coker gas oil		N.D.								
Lloydminster heavy oil		31.0	27.0	13.9	1.8	14.5	1.8	7.0	1.0	2.0
Cold Lake bitumen		1.6	32.8	17.0	-	33.4	-	8.1	1.6	3.6
e) In presence of H$_2$-2000 psig + catalyst (60 min, 400°C)										
GCOS bitumen Athabasca deposit		-	63.3	18.6	-	8.2	-	6.8	0.8	2.3
GCOS coker gas oil		-	17.5	45.2	-	17.3	-	13.6	-	4.3
f) In presence of H$_2$-1000 psig + catalyst (60 min, 450°C)										
GCOS bitumen Athabasca deposit		-	14.8	47.1	-	22.4	-	12.3	1.7	2.2
GCOS coker gas oil		-	12.9	41.6	-	27.0	-	14.3	1.5	2.8
N.D. Not determined										

Table 5. Temperature effect on coal conversion yields and product distribution (60 minutes, H_2 - 1000 psig)

Conditions	% Yield[+]	%Toluene insolubles	% Toluene solubles	%Volatile plus gas	Toluene solubles fraction		
					% Pentane insolubles	% Pentane solubles	API gravity
Coal solvation							
GCOS bitumen Athabasca deposit							
300° C	2	28.8	69.8	1.4	16.1	83.9	7.9
350° C	5	28.0	69.4	2.6	19.5	80.5	12.8
400°C	15	26.1	65.4	8.5	19.0	81.0	10.7
450°C	27	40.1	20.9	39.0	15.3	84.7	4.4
GCOS coker gas oil							
300°C	0	27.1	71.9	1	0.4	99.6	17.4
350°C	7	29.1	68.9	2	2.0	98.0	15.
400°C	24	23.6	68.2	8.2	3.1	96.9	18.9
450°C	0	39.2	27.7	33.1	3.0	97.0	8.1
Catalytic hydrogenation							
GCOS bitumen Athabasca deposit							
350°C	8	26.2	70.7	3.1	17.0	83.0	13.7
400°C	32	20.8	69.1	10.1	12.5	87.5	12.4
450°C	34	22.6	25.4	52.0	11.8	88.2	1.8
GCOS coker gas oil							
300°C	0	29.6	69.4	1	0.3	99.7	17.4
350°C	7	26.7	71.3	2	1.6	98.4	17.0
400°C	30	20.6	73.9	5.5	1.8	98.2	17.3
450°C	45	16.3	42.3	41.4	4.5	95.5	8.5

+ Calculate yield after subtraction of coke formed from the solvent in blank determinations.

Table 6. Time effect on coal conversion yields and product distribution (400° C, H_2 - 1000 psig)

Reaction time	% Yield[+]	% Toluene Insolubles	% Toluene solubles	%Volatile plus gas	Toluene solubles fraction		
					%Pentane Insolubles	%Pentane solubles	API gravity
Coal solvation							
GCOS bitumen Athabasca deposit							
1/4 hour	10	26.3	68.4	5.3	21.7	78.3	9.2
1 hour	15	26.1	65.4	8.5	19.0	80.9	10.7
2 hours	0	31.6	51.3	17.1	16.1	83.9	9.9
GCOS coker gas oil							
1/4 hour	10	26.8	70.1	3.1	4.2	95.8	15.8
1 hour	24	23.6	68.2	8.2	3.1	96.9	18.9
2 hours	12	25.6	55.7	18.7	6.4	93.6	12.7
Catalytic hydrogenation							
GCOS bitumen Athabasca deposit							
1/4	17	24.2	69.2	6.6	17.8	82.2	10.1
1 hour	32	20.8	69.1	10.1	12.5	87.5	12.4
2 hours	31	20.1	66.5	13.4	11.5	88.5	13.1
GCOS coker gas oil							
1/4 hour	17	24.2	72.8	3.0	3.5	96.5	17.9
1 hour	30	20.6	73.9	5.5	1.8	98.2	17.3
2 hours	41	17.4	75.5	7.1	3.8	96.2	18.5

+ Calculated yield after subtraction of coke formed from the solvent in blank determinations.

138

Table 7. Pressure effect on coal conversion yields and product distribution (60 minutes, 400 C°)

	% Yield[a]	% Toluene Insolubles	% Toluene Solubles	% Volatile plus gas	Toluene solubles fraction		
					% Pentane Insolubles	% Pentane Solubles	API gravity
Catalytic hydrogenation							
GCOS bitumen Athabasca deposit							
500	16	24.5	63.3	12.2	17.8	82.2	9.6
1,000	32	20.8	69.1	10.1	12.5	77.5	12.4
1,500	30	21.7	68.3	10.0	15.0	85.0	11.4
2,000	30	21.8	75.0	3.2	14.7	85.3	12.1

Table 8. Gas product distribution derived from processing coal for 60 min. at various temperatures

Temperature	% Relative Composition									
	CO	CO_2	H_2S	CH_4	C_2H_4	C_2H_6	C_2H_2	C_3	C_4 iso	C_4 norm
Coal solvation										
GCOS bitumen Athabasca deposit										
300°C	-	97.8	-	-	-	1.7	-	0.5	-	-
350°C	2.1	74.5	3.6	10.5	-	5.9	-	2.7	-	0.6
400°C	0.6	31.9	7.5	31.6	-	15.4	-	9.8	1.1	2.0
450°C				insufficient sample						
GCOS coker gas oil										
300°C	-	94.0	1.5	-	-	3.8	-	0.6	-	-
350°C	1.6	64.8	2.3	12.7	-	14.6	-	2.9	0.2	0.9
400°C		N.D.								
450°C		N.D.								
Catalytic hydrogenation										
GCOS bitumen Athabasca deposit										
350°C	1.4	55.1	10.3	12.0	-	17.0	-	3.5	-	0.9
400°C	0.7	22.8	24.4	26.0	1.3	13.8	-	8.0	0.9	1.9
450°C	0.3	7.4	7.9	51.9	0.1	19.9	-	9.7	0.9	1.9
GCOS coker gas oil										
300°C	-	95.4	3.7	-	-	-	-	0.9	-	-
350°C	1.7	62.0	17.1	10.9	1.7	2.6	-	3.2	-	0.9
400°C		N.D.								
450°C	0.1	6.1	4.0	56.9	-	20.8	-	9.4	0.9	1.7
N.D:		Not Determined								

139

Table 9. Gas product distribution derived from processing coal at 400 C° for various times

Reaction Time	CO	CO_2	H_2S	CH_4	C_2H_4	C_2H_6	C_2H_2	C_3	C_4 iso	C_4 norm
Coal solvation										
GCOS bitumen Athabasca deposit										
1/4 hour	1.0	44.7	9.9	24.0	–	9.6	–	7.9	0.7	2.1
1 hour	0.6	31.9	7.5	31.6	–	15.4	–	9.8	1.1	2.0
2 hours	2.8	37.7	13.7	24.2	–	10.5	–	8.0	1.0	2.1
GCOS coker gas oil										
1/4 hour	2.9	56.5	3.1	19.8	–	10.1	–	6.2	0.4	1.1
1 hour		N.D.								
2 hours	2.8	23.8	3.4	39.2	0.1	15.7	–	11.0	1.4	1.1
Catalytic hydrogenation										
GCOS bitumen Athabasca deposit										
1/4 hour	0.2	17.0	19.5	27.6	0.4	13.6	–	16.6	2.4	2.9
1 hour	0.7	22.8	24.4	26.0	1.3	13.8	–	8.0	0.9	1.9
2 hours	1.5	23.7	18.4	32.2	–	12.0	–	8.5	1.3	2.3
GCOS coker gas oil										
1/4 hour	4.4	44.4	15.6	22.0	–	7.2	–	5.0	0.3	1.0
1 hour		N.D.								
2 hours	2.6	23.5	17.7	34.9	–	12.0	–	7.1	0.7	1.5

Table 10. Gas product distribution derived from processing coal for 60 min. at 400°C under various pressures

Pressure psig	CO	CO_2	H_2S	CH_4	C_2H_4	C_2H_6	C_2H_2	C_3	C_4 iso	C_4 norm
Catalytic hydrogenation										
GCOS bitumen Athabasca deposit										
500	0.9	33.7	17.6	26.1	–	10.2	–	8.1	1.1	1.3
1,000	0.7	22.8	24.4	26.0	1.3	13.8	–	8.0	0.9	1.9
1,500	3.5	26.2	22.4	26.9	–	10.2	–	7.7	1.0	2.1
2,000	1.2	23.9	21.6	31.5	–	11.1	–	7.6	0.9	0.3